TEMPERATURE DISTRIBUTION WITHIN A COMPRESSED GAS CYLINDER DURING FILLING

by

CHRISTOPHER JOHN BRUCE DICKEN

B.Eng. University of Victoria, 2001

A THESIS SUBMITTED IN PARTIAL FULFILLMENT OF
THE REQUIREMENTS FOR THE DEGREE OF

MASTER OF APPLIED SCIENCE

in

THE FACULTY OF GRADUATE STUDIES

(Mechanical Engineering)

THE UNIVERSITY OF BRITISH COLUMBIA

December 2006

ABSTRACT

The minimum refuelling time of compressed gas cylinders and the metering of the dispensed fuel are important factors for the commercialization of hydrogen-powered vehicles.

The temperature field within a compressed gas cylinder is investigated using modeling and experimental techniques.

A simplified 2-dimensional axisymmetric model is developed for predicting the gas temperature and pressure rise in a hydrogen cylinder during the fill process. The model is then validated by comparison with *in-situ* measurements of the average temperature rise and temperature distribution inside a working compressed hydrogen cylinder during the process of filling. The model is able to predict the average temperature rise within the cylinder to within 4K. Both experimental and model results show a large conical temperature gradient extending out from the cylinder inlet.

The effects of the initial mass and the total fill time on the temperature rise and the temperature distribution within a compressed hydrogen cylinder during refuelling have been measured.

A type 3, 74 L hydrogen cylinder was instrumented internally with 63 thermocouples distributed along the vertical plane. The experimental fills were performed from initial pressures of 50, 75, 100, 150, and 200 bar at fill rates corresponding to nominal fill times of 1, 3, and 6 minutes. The experimental conditions with larger ratios of final to initial mass produced larger temperature changes. However, the lower ratios generated the largest rates of temperature rise. Longer fill times produced lower final average gas temperatures (compared

to shorter fills), and a temperature field with significant vertical stratification due to buoyancy forces at lower gas inlet velocities.

The modeling and experimental results show that a sensor located along the centreline at the non fill end of the cylinder would best represent the average gas temperature within the cylinder.

TABLE OF CONTENTS

LIST OF TABLES

LIST OF FIGURES

ACKNOWLEDGEMENTS

I would like to thank my supervisor, Dr. Walter Mérida for his encouragement, support, and guidance throughout this project.

I gratefully acknowledge General Hydrogen Corporation for their technical support and Western Economic Diversification Canada for the funding of this work and the projects associated with it. The author would also like to thank Mark Rossetto of the National Research Council of Canada, Institute for Fuel Cell Innovation and Karin Garandza of General Hydrogen for their assistance in performing the experimental fills.

Finally I would like to thank my wife Alison for all the sacrifices she made so that I could pursue this work.

CO-AUTHORSHIP STATEMENT

Chapters 2 and 3 of this thesis were co-authored with Dr. Walter Mérida.

The topic of research was identified by the author in conjunction with General Hydrogen and the Institute for Fuel Cell Innovation. The design of the research program was performed by the author with guidance and input from Dr. Walter Mérida. All funding for the project was handled by Dr. Walter Mérida.

All literature review, experimental and modeling research was performed by the author with guidance and suggestions from Dr. Walter Mérida.

All data analysis was performed by the author.

The initial draft of the manuscripts presented in Chapters 2 and 3 where written by the author. The subsequent edits to the draft were performed by both the author and Dr. Walter Mérida.

CHAPTER 1: INTRODUCTION

The advent of hydrogen powered fuel cell and internal combustion vehicles have highlighted the need for hydrogen infrastructure. At present, pressurized gas is the leading technology for on-board hydrogen storage. For the range of a hydrogen-powered vehicle to be comparable to that of a gasoline-powered engine, and to meet vehicle packaging requirements, hydrogen must be stored at a pressure of 350 or 700 bar. Currently, most hydrogen-powered vehicles use cylinders designed for a service pressure of 350 bar, however the commercialization of cylinders capable of 700 bar has just begun.

Re-fuelling of a compressed gas hydrogen vehicle requires a fuelling station capable of storing pressurized hydrogen in excess of 350 bar. Upon fuelling, the hydrogen is expanded from the high-pressure station storage, into the "empty" vehicle cylinder. The station dispensing system controls the rate of hydrogen passed into the cylinder and hence the rate of pressure rise within the cylinder.

The time required to fill a vehicle's hydrogen cylinder is an important factor for consumer acceptability. "Fast filling" is a term often used in industry to identify the speed with which a compressed gas cylinder is filled. Cylinders are limited to a maximum gas temperature of 85 °C and a maximum fill pressure of 125% of their rated service pressure, as defined by standards [1,2]. Thus in an attempt to define the term "fast", a gas cylinder can be filled, as fast as possible to its rated capacity of gas, without exceeding these two requirements [3]. Minimizing the fill time requires minimizing the maximum temperature during the fill.

There have been many studies that directly or indirectly relate to the fast filling of compressed gas cylinders. These studies generally fall into three categories: experimental studies, numerical modeling studies and a combination of the two. The majority of studies are

undertaken by companies or research groups with experience in the natural gas or hydrogen dispensing and storage fields. Further studies undertaken by the chemical and nuclear industries address the "blowdown" of pressure vessels. The blowdown of a pressure vessel is a rapid emergency evacuation of the vessel. This process is essentially the reverse of the fast fill process and hence relevant for review.

1.1 HYDROGEN AS A FUEL

A definition of a sustainable energy system is one, which meets our current energy needs without sacrificing cultural and economic growth, the environment or the ability of future generations to live even better than we do today [4]. Climate change, environmental degradation and the use of non-renewable energy sources are in direct conflict with this definition of a sustainable energy system. This provides the motivation for the use of hydrogen as an energy carrier. In order to transition from our current energy system to a sustainable energy system, we require an energy carrier that can significantly reduce greenhouse gas emissions, improve air quality and will allow renewable energy sources to infiltrate all energy service applications. Hydrogen can meet these criteria as it is the only energy carrier that can be stored for use in the transportation sector (which accounts for a significant portion of greenhouse gas, NO_x, SO_x, and particulate emissions) and can be cleanly and efficiently converted to energy services (through the use of fuel cells). The use of hydrogen as an energy carrier will free up the use of renewable energy sources for transportation applications [5]. Other motivating factors for hydrogen include energy security for oil importing countries, and ever increasing oil prices.

While the most abundant element in the universe, hydrogen is not found in its natural state (H_2) on earth. To utilize hydrogen we must "mine it" by way of reforming or electrolysis

of existing chemicals such as natural gas, methanol or water. Hydrogen has the highest specific energy (J/kg) content of any fuel, however due to its extremely low triple point temperature, hydrogen has one of the lowest volumetric energy densities of all fuels.

The suitability of hydrogen powered vehicles as a replacement to present day internal combustion engines must be determined based on a comparison of energy efficiency, greenhouse gas emissions, and cost. The assessment of these factors must take into account the full energy system cycle. For vehicles the term "well to wheel" (WTW) is used to describe the energy efficiency or greenhouse gas (GHG) emissions from the energy source (the well) to the transportation service (the wheel). The cost is assessed based on a comparison of operating and capital costs of each vehicle and supply technology.

For a gasoline-powered vehicle, the majority of GHG emissions occur during the combustion of the fuel inside the vehicle engine. Approximately 15% of well to wheel GHG emissions occur in the reforming, processing, transportation and distribution of gasoline. Conversely, ~85% of well to wheel greenhouse gas emissions occur from the vehicle itself. The same relationship is true for energy efficiency [6]. The energy losses that occur between from the well to the vehicle tank for gasoline production only account for 15% of the total well to wheel energy losses [7]. The large energy loss that result between the tank and the wheels is due to the inefficiency of internal combustion engines at their current operating temperatures.

Life cycle assessment of energy efficiency and GHG emissions for fuel cell powered vehicles are dependent on: the energy source used to produce the energy carrier, and the choice of energy carrier. Currently the majority of hydrogen produced in North America is the

product of natural gas reforming. Looking forward towards a sustainable energy system, hydrogen will need to be produce from renewable energy sources.

Since fuel cell vehicles (FCV) run on hydrogen, they emit no GHGs, the tank to wheel emissions are zero for both FCV cases. For the case of hydrogen derived from wind energy the well to tank emissions are approximately zero. For the case of hydrogen reformed from natural gas, the GHG emissions are ~115 g/km. One of the great drivers for fuel cell vehicles is their energy efficiency. The total energy losses are split equally as 50% of the total energy loss occurs between the well and the tank and 50% occurs between the tank and the wheel.

A comparison between the gasoline case and the two fuel cell cases can be seen graphically in Figure 1-1 and Figure 1-2. The data in these figures is adapted from Choudhury et. al. [6]. Analysis of the graphs leads to the following conclusions. Producing gasoline is more energy efficient than producing hydrogen. Gasoline powered internal combustion engines is much less energy efficient than fuel cell engines. An elimination of WTW GHG emissions can be achieved when FCVs are fuelled with hydrogen provided by the best renewable pathways [6]. Hydrogen FCV from natural gas offer reduced emissions relative to gasoline internal combustion engines.

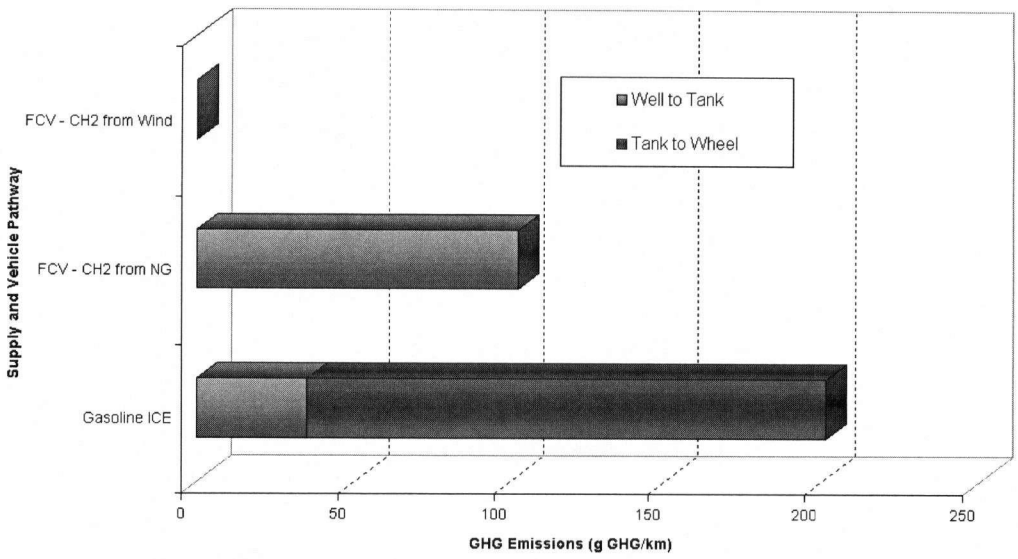

Figure 1-1: GHG Emissions for different fuel supply and vehicle pathways [6]

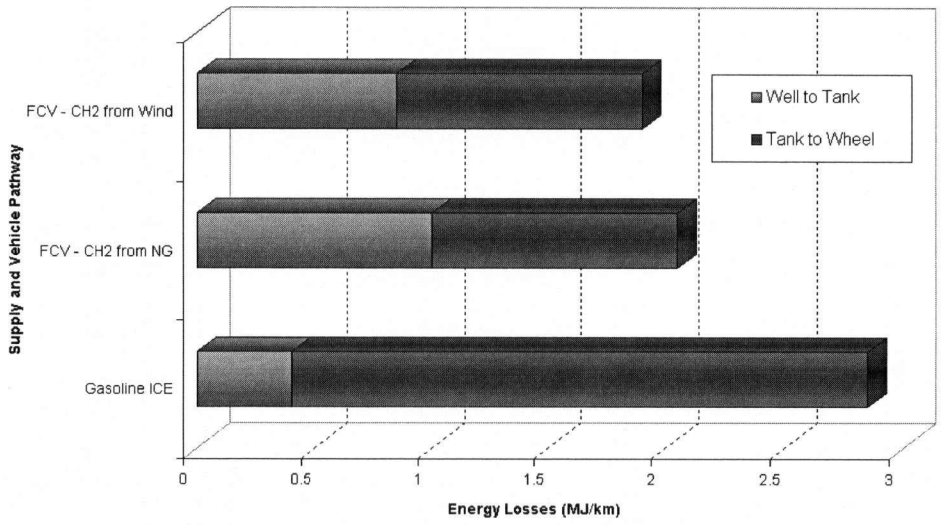

Figure 1-2: Energy Losses for different fuel supply and vehicle pathways [6]

The majority of GHG emissions for gasoline vehicles occur at the tail pipes of the vehicles. In contrast all GHG emissions for fuel cell powered vehicles occur at a central electrolyser or NG reformer. This localization of GHG emissions is beneficial for capturing and sequestering GHGs and other pollutants.

The major barriers to adoption of hydrogen as an energy carrier are: the development of infrastructure for the production, transportation and distribution of hydrogen, storage on-board vehicles, and the need for further development in the cost, reliability and freeze start of fuel cell vehicles.

1.2 REVIEW OF HYDROGEN INFRASTRUCTURE

1.2.1 Hydrogen Storage

When discussing various methods for hydrogen storage it is important to outline the application. Hydrogen can be stored on different scales. It can be stored on a large scale for stationary and production applications, on an intermediate scale for industrial and buffering applications and on small scale for on-board vehicle storage. A review of three of the most promising methods for storing hydrogen for vehicle applications is presented in this section. To evaluate the various methods of hydrogen storage it is important to review the desired characteristics for an on-board storage system [8].

Safety

Safety is always of paramount importance. There is considerable fear (be it justifiable or not) within the public over the safety of hydrogen. Nowhere will this fear be manifested more than in reluctance to accept hydrogen powered passenger vehicle as safe or safer than gasoline powered vehicles. Safety is related to two factors, the probability of a safety related incident and the magnitude of the resulting safety incident. The probability of an incident can be mitigated through design, where the magnitude of the incident will likely depend on the type of storage system used.

Mass

Mass of the system is important as it affects the acceleration and handling of the vehicle. The mass of the storage system will also affect where it is located within the vehicle. The US Department of Energy has outlined a goal of 9wt% H_2 gravimetric storage efficiency and 81 kg/m^3 volumetric storage efficiency [9].

Volume

Volume of the system is an important parameter. Fuel cell vehicles are being designed to fit the body and chassis of existing gasoline powered vehicles. Thus, the hydrogen storage system must fit within the confines of existing car bodies and must not impinge on the passenger and storage compartments. The US Department of Energy has outlined a goal of 81 kg/m^3 volumetric storage efficiency [9].

Response Time

Response times of the storage system to the demand for hydrogen must not affect the acceleration of the vehicle. The maximum rate of hydrogen supply must be sufficient to meet the acceleration specifications of today's gasoline powered vehicles.

Parasitic Loads

The parasitic loads of a storage system are the energy loads required for pumping, compressing, liquefying, heating or refrigeration. A second form of parasitic load is heat load. All heat in a vehicle must be transferred to the environment by way of a radiator. In general, larger heat loads require a larger radiator and larger cooling system, consequently affecting the volume, mass and efficiency of the vehicle.

Tank Geometry

The tank geometry is a significant variable for packaging the storage system in a vehicle. A flexible tank geometry such as those found in gasoline vehicles, makes packaging easier and more efficient.

Lifetime

The lifetime of the storage system is important as it affects the warranty costs that are built in to the price of a vehicle. It is not essential that the storage system last for extremely long periods of time, it is more important that the system lifetime match the design lifetime of the rest of the vehicle. Both an under-designed and over-designed system will increase the total costs of the vehicle.

Reliability

The reliability of the storage system will directly affect the price of the vehicle as manufacturers build in warranty costs. Reliability is also a crucial factor for sales and customer satisfaction.

Refuelling

The refuelling time and ease of refuelling is essential as the user expects refuelling to be as easy, or easier than refuelling a gasoline-powered car. Furthermore the ease of handling and safety of refuelling needs to be similar to today's refuelling stations.

Freeze Start

Freeze start is a growing issue for fuel cell vehicles and will have implication for certain types of storage systems. Simply defined the system must be able to start-up and operate in freezing temperatures.

Cost

Cost is essential. Initially fuel cell powered vehicles may be subsidized or cost slightly more than gasoline cars but to be widely accepted in the transportation market, for the same service, the overall cost of the vehicle must be similar or lower than gasoline powered vehicles.

1.2.1.1 Pressurized Gas

Hydrogen can be stored on board vehicles in the form of a compressed gas. This method of storage is the simplest and most mature technology for hydrogen storage.

The gas is compressed at a fuelling station and dispensed into the on-board tank. The on-board tank is shaped in the form of a cylinder and is usually comprised of either all metal, carbon fibre hoop wrapped with an aluminum liner, fully carbon fibre wrapped with an aluminum liner, or fully wrapped with a plastic liner. These four types of cylinders are labelled type 1, 2, 3, and 4 respectively. Thin metalized polymers are being investigated as a possible liner for compressed gas cylinders. The liner would be so thin that it's weight would be negligible and hence the mass of the cylinder would be determined solely by the type and amount of carbon fibre wrap [10]. The liner provides the gas tight seal and the wrap, usually a carbon fibre, provides the structural integrity. Figure 1-3 gives a comparison of compressed gas storage cylinder performance factor. The performance factor is defined as:

$$PF = \frac{P_{op} N_{SF} V}{W} \tag{1-1}$$

Where P_{op} is the operating pressure measured in psi, N_{SF} is the tank safety factor, V is the tank volume, and W the tank weight in lbs [10].

Type 3 and type 4 cylinders are predominant for high-pressure gas storage in the transportation sector where weight minimization is crucial. Currently, most demonstration vehicles employ cylinders capable of storing hydrogen up to 350 bar, while new lightweight composite type 3 and type 4 gas cylinders have been developed to withstand pressures up to 800 bar [11].

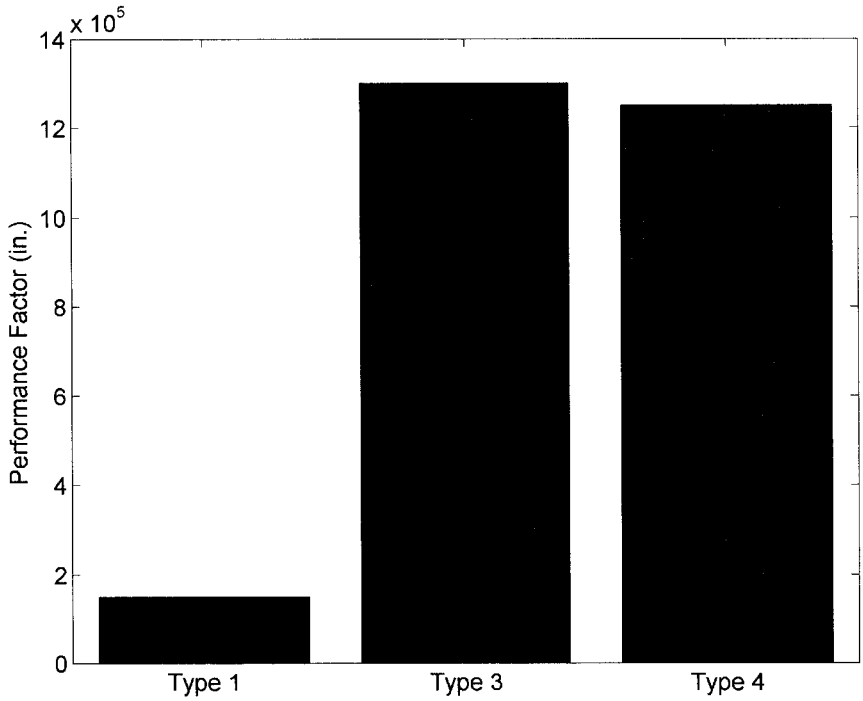

Figure 1-3: Comparison of compressed gas storage tank performance factors [6].

While a compressed gas on-board storage system has no significant energy requirements, the compression of the hydrogen taking place at the fuelling station must be taken into account. Figure 1-4 plots the amount of work required to compress hydrogen isentropically from 0.1 MPa and 295K up to the desired fill pressure. The initial stages of

compression from 0.1 MPa to 10MPa account for the greatest amount of required work. It is this phenomenon that makes high-pressure electrolysis such an attractive means of production.

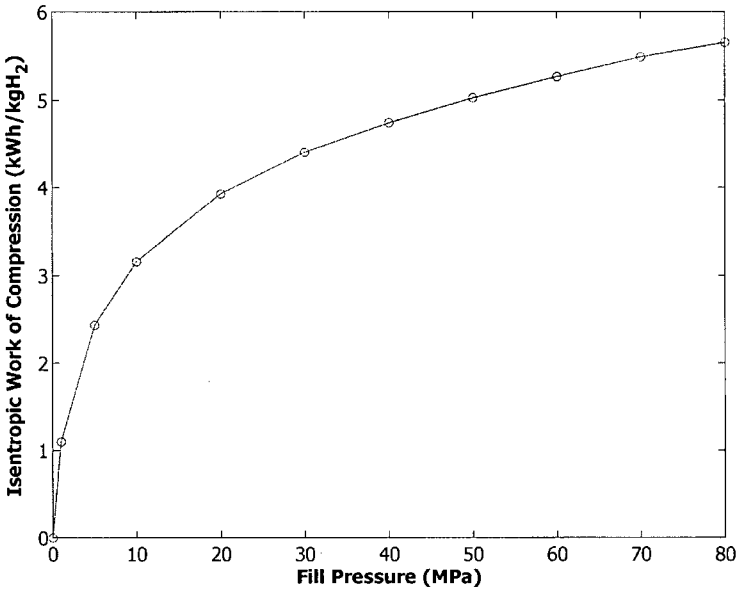

Figure 1-4: Isentropic Work of Compression for 1 kg of H2 initially at 0.1 MPa and 295K

Due to the increasing compressibility factor of hydrogen at high pressure there exists a trade-off between volumetric and gravimetric storage efficiency. As cylinders are fabricated for higher pressures the volumetric storage efficiency increases as more hydrogen is compressed into the same volume. However, to provide the extra strength, the cylinder wall thickness must be increased. The relationship between cylinder wall thickness and the burst pressure is given by the equation:

$$\frac{d_w}{d_o} = \frac{\Delta p}{2\sigma_t + \Delta p} \tag{1-2}$$

Where, d_w is the wall thickness, d_o the outer diameter of the cylinder, σ_t the tensile strength of the material and Δp the overpressure [11]. From this equation the thickness of the tank, and hence the mass of the tank increases linearly with design pressure. However, due to

real gas effects (hydrogen has a compressibility factor greater than unity at high pressures) the mass of hydrogen stored does not increase linearly. Instead, as the design pressure is increased, the corresponding increase in density diminishes. This phenomenon is shown in Figure 1-5. While volumetric efficiency increases with cylinders designed for greater pressures, the gravimetric efficiency decreases.

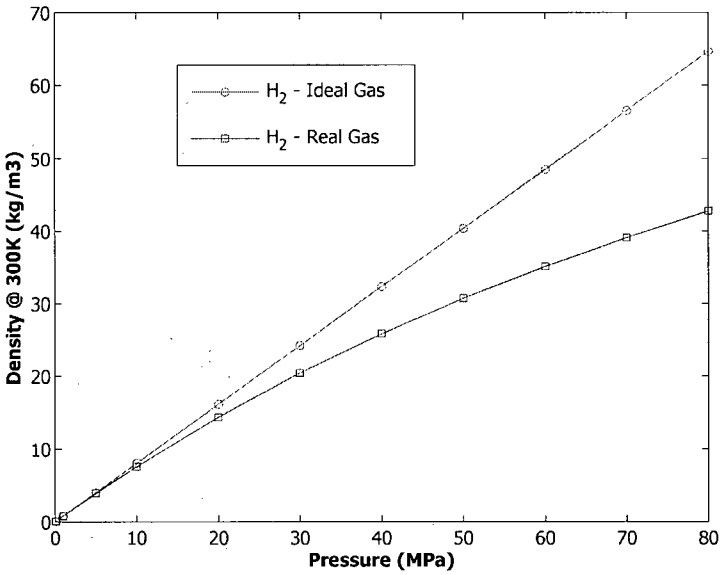

Figure 1-5: Hydrogen density vs. pressure at 300K for both ideal gas and real gas.

The benefits of compressed gas storage are: simplicity, lightweight, no issues with dormancy, ease of refuelling, comparative low cost and a good safety record. As a result, the storage of hydrogen as a compressed gas is the current direction that most automotive manufacturers are pursuing for both fuel cell and internal combustion vehicles [12]. The major issue confronting this storage method is the volume the system occupies in the vehicle [10].

The challenge facing the compressed gas technology is to continue to develop lightweight cylinders capable of high-pressure gas storage in order to further increase the

volumetric efficiency. With the increasing compressibility factor of hydrogen at high pressure it is unlikely that compressed gas storage will ever meet the volume of today's gasoline tanks.

1.2.1.2 Liquid Hydrogen

Hydrogen has a normal boiling point of 20.3 K. Since hydrogen is produced at or above ambient temperature, liquefaction cycles are used to cool hydrogen below its boiling point. The storage of hydrogen in liquid form requires heavily insulated vessels to minimize the heat leak to ambient. At 20.3 K and normal pressure, the density of liquid hydrogen is 70.79 kg/m^3 [13]. This is the maximum storage density attainable with liquid hydrogen at the normal boiling point, as the volume of the vessel and peripheral equipment are not included.

Unlike most gases, hydrogen has a maximum inversion temperature which is below ambient temperature. For this reason, hydrogen liquefaction cannot be achieved using a simple Linde-Hampson cycle. During the isenthalpic expansion phase, the hydrogen temperature will actually increase due to its negative joule-Thomson coefficient at ambient temperature. Thus, hydrogen must be pre-cooled below its inversion temperature before undergoing isenthalpic expansion. Pre-cooling is commonly achieved using liquid nitrogen which has a triple point temperature below that of the maximum inversion temperature of hydrogen. The pre-cooled Linde-Hampson, precooled Claude and the helium – hydrogen condensing cycle are commonly used for liquefaction of hydrogen [14].

The ideal work required to liquefy hydrogen is 12.92 MJ/kg of H_2. The lower heating value (LHV) for hydrogen is 119.95 MJ/kg [15]. Thus even for an ideal case, the energy required to liquefy hydrogen is 11% of the LHV. Table 1-1 provides a comparison of the figure of merit and work of liquefaction for the precooled Linde-Hampson, precooled Claude and helium-hydrogen condensing cycles. The Claude cycle requires the least amount of work

for liquefaction with 100-140 MJ/kg required depending on the efficiency of the heat exchanger used. Thus, 83-117% of the LHV is required to liquefy hydrogen. From a commercial perspective, this provides a major barrier to liquid hydrogen storage systems on-board vehicles.

Table 1-1: Comparison of Work of Liquefaction for different hydrogen liquefaction cycles from different studies [14].

Cycle	Liquid hydrogen %para	Work of Liquefaction (MJ/kgH_2)
Precooled Linde-Hampson	99.8	260-285
Precooled Claude	99.8	100-140
He – H2 condensing	99.8	120-200

A major problem affecting liquid storage of hydrogen on-board vehicles is the issue of dormancy and lock-up. Liquid hydrogen within a storage vessel will undergo boil-off due to: heat of conversion from ortho to parahydrogen, heat leak to the environment, sloshing within the tank, and stratification. This boil off will increase the pressure within the vessel to a point where it must be vented. The time between when the vehicle is stored to the time when hydrogen gas must be vented (to prevent over-pressure) is referred to as the lock-up time. Thus when a vehicle powered by liquid hydrogen is dormant (not in operation) the storage vessel will slowly lose hydrogen which leads to a loss of fuel economy (efficiency) and there are specific safety issues with venting hydrogen gas in enclosed spaces (such as a garage).

Hydrogen at normal temperature and pressure is named normal hydrogen and is composed of 75% orthohydrogen and 25% parahydrogen. The equilibrium concentration of ortho and parahydrogen varies with temperature only. In its liquid form, at equilibrium, hydrogen is almost entirely parahydrogen. The variation of the parahydrogen concentration

with temperature is shown in Figure 1-6. The conversion from ortho to para is exothermic and the heat of conversion varies with temperature as shown in Figure 1-7. The heat of conversion is greatest at low temperatures, for this reason, during liquefaction multiple ortho to para catalytic converters are used at various temperatures to minimize the overall heat of conversion.

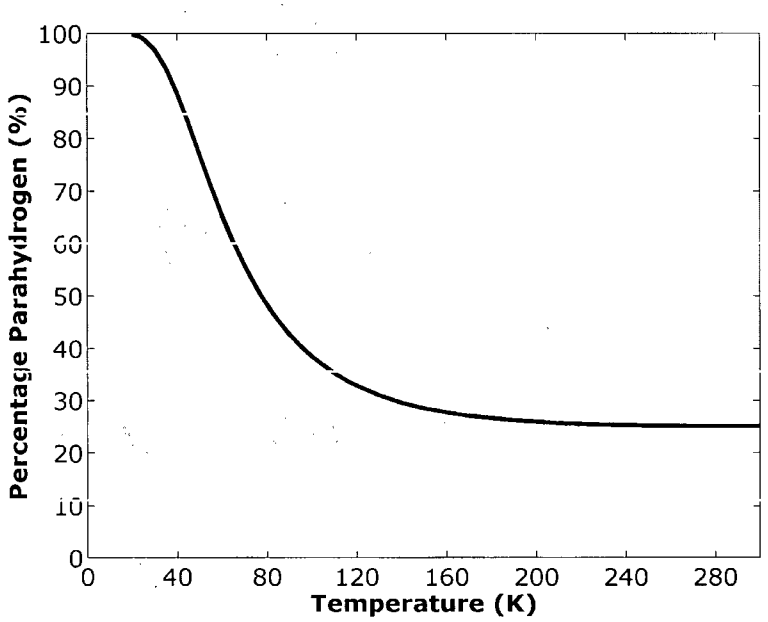

Figure 1-6: Percentage parahydrogen as a function of temperature. [16]

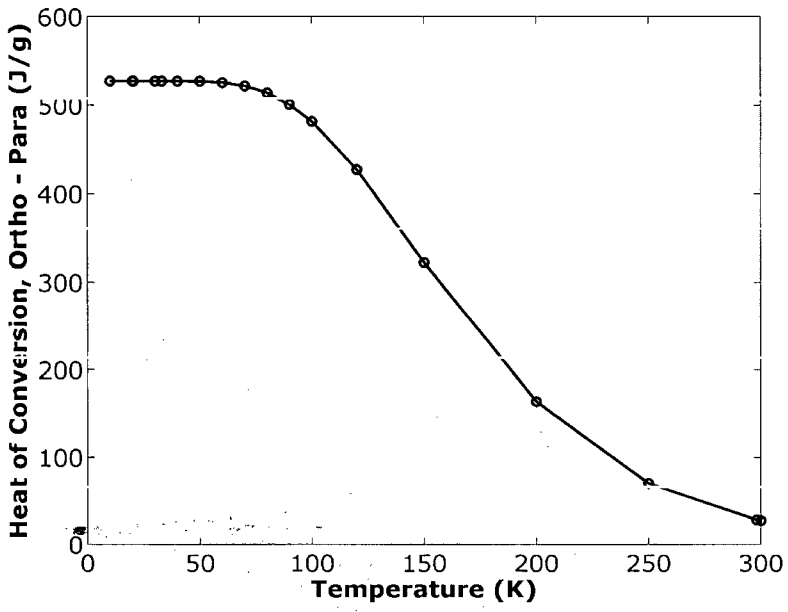

Figure 1-7: Heat of conversion from ortho to para hydrogen. [17]

When normal hydrogen is liquefied without undergoing catalytic conversion from ortho to parahydrogen, the concentrations of 75% ortho and 25% parahydrogen will become the initial concentration of the liquid hydrogen. Without the presence of a catalyst the ortho to para conversion is a second order reaction with a rate of conversion defined by [13]:

$$\frac{dx_{ortho}}{dt} = -K_1 x_{ortho}^2 \tag{1-3}$$

Where K_1 is the second order reaction rate constant (0.0114 hr^{-1}) and x_{ortho} is the mole fraction of orthohydrogen.

Following the analysis of Gursu et al. [18] the mass of liquid hydrogen as a function of time and initial mole fraction of orthohydrogen is given by the following equation:

$$m_L(t, x_o) = \exp\left[\frac{\Delta H_c}{\Delta H_v} x_o \left(\frac{1}{K_1 x_o t + 1}\right) - 1\right] \tag{1-4}$$

Where ΔH_c is the heat of conversion from ortho to parahydrogen and ΔH_v is the heat of vaporization both evaluated at the normal boiling point. x_o is the initial mass fraction of the orthohydrogen and t is time (hrs). Figure 1-8 shows the boil off of liquid hydrogen due to the heat of conversion of orthohydrogen into parahydrogen for various initial concentrations of parahydrogen. The plot shows the dramatic affect of the ortho-para heat of conversion. A typical storage time for an automobile can vary from a few hours up to a few weeks. For liquid hydrogen stored on-board a vehicle it is essential that the initial mass fraction of parahydrogen be greater than 90% to avoid excessive boil off due to ortho to para conversion.

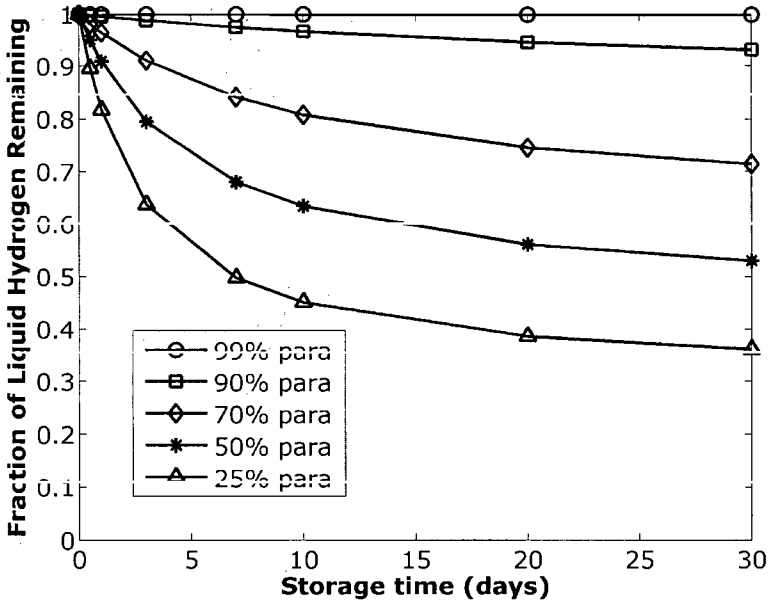

Figure 1-8: Liquid Hydrogen remaining in storage due to ortho to para conversion for various initial concentrations of parahydrogen.

Boil off will also occur due to heat leak into the liquid hydrogen storage vessel. Due to the large difference in temperature between the normal boiling point of liquid hydrogen (20.8 K) and normal ambient temperature, all three forms of heat transfer are significant.

The main advantages of liquid hydrogen storage are its high volumetric and gravimetric storage densities. Some of the major technological barriers that liquid hydrogen technology must overcome include the current high cost, the problem of hydrogen boil-off, and the large energy input required for liquefaction.

1.2.1.3 Chemical Hydride

Chemical hydrides store hydrogen within a compound that can then be released via a hydrolysis reaction with water. While there exists a multitude of compounds which can be used for this purpose, some of the most suitable candidates include: Sodium borohydride ($NaBH_4$), Lithium borohydride ($LiBH_4$), ($NaAlH_4$), (Mg_2FeH_6), ($Al(BH_4)_3$) [19]. $LiBH_4$ has the highest gravimetric hydrogen density at room temperature, containing 18% hydrogen by mass. This makes it an ideal choice for hydrogen storage. However, at present the absorption and desorption of hydrogen remains a challenge and more research is needed before the compound can be used as a practical hydrogen storage method. Among the other hydrides, $NaBH_4$ seems to be the most suitable compound for hydrogen storage as it releases more hydrogen at lower reaction temperatures and has a higher density of hydrogen than other hydrides.

$NaBH_4$ has reached the highest technological progress to date and has been used in multiple fuel cell demonstration vehicles. In 2001, Daimler Chrysler produced a prototype Chrysler "Town and Country" minivan that incorporates a hydrogen storage system that produces H_2 from the hydrolysis of $NaBH_4$. The manufacturer claims the vehicle has a range of 500 km and acceleration from 0 to 100 km/h in 16 seconds. Furthermore, the hydrogen storage system and fuel cell system are stored under the vehicle floor and thus, do not take away any room from the passenger and storage compartments [20].

The hydrolysis reaction of $NaBH_4$ is described below:

$$NaBH_4(aq) + 4H_2O(l) \rightarrow 4H_2(g) + NaBO_2(aq) \quad (1\text{-}5)$$

One mole $NaBH_4$ is reacted with four moles of water to produce 4 moles of hydrogen and one mole of the by-product $NaBO_2$. The reaction is exothermic, releasing 75 kJ/mol of H_2 generated [21]. The reaction occurs at room temperature and pressure and will occur spontaneously within the aqueous solution. For this reason, NaOH is added to the aqueous solution to increase the pH which in turn increases the half life of $NaBH_4$. The relationship between solution pH and half-life is outlined in equation:

$$Log(t_{1/2}) = pH - (0.034T - 1.92) \quad (1\text{-}6)$$

Where $t_{1/2}$ is the half-life and represents the time it takes to decompose a half of the solution in minutes [21].

A schematic of a typical $NaBH_4$ hydrogen storage system is shown in Figure 1-9. The sodium borohydride is stored in an aqueous solution in the tank and pumped into the catalyst chamber. The presence of the catalyst increases the reaction rate and hence the hydrogen generation rate. The gaseous hydrogen is then separated from the by-product solution and sent on to the vehicle engine.

The unique attributes of sodium borohydride storage systems present opportunities for system integration within a fuel cell vehicle. The hydrolysis of sodium borohydride requires water. Carrying water on-board within the aqueous solution to react with the sodium borohydride is inefficient. Fuel cell vehicles produce water as a by-product of the overall reaction. This water can be condensed out of the exhaust gas and used for the hydrolysis of sodium borohydride. In the fuel cell reaction, for every mole of hydrogen consumed, one mole of water is produced. The hydrolysis of $NaBH_4$ to produce one mole of hydrogen requires 1

mole of H_2O. Thus, the potential exists that the fuel cell reaction can supply just enough water for the hydrolysis reaction. However, in practice fuel cell vehicles require humidification and the product water of the fuel cell reaction is used for this purpose. Furthermore not all the product water can be recovered from the reactant gases exiting the fuel cell. The hydrogen generated from the hydrolysis of $NaBH_4$ is partially humidified at the temperature of the reactor. This partial humidification reduces the humidification requirements of fuel cell balance of plant. This in turn allows for the possibility of an increased amount of the product water that could be used for onboard dilution of the $NaBH_4$ solution.

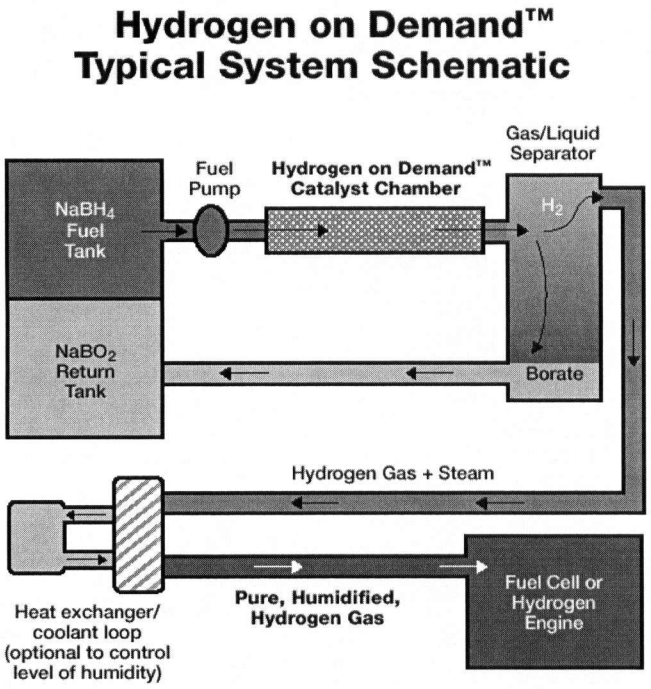

Figure 1-9: Millenium Cell - Hydrogen on Demand Storage System Schematic

The Millenium cell "Hydrogen on Demand" Hydrogen storage system is claimed to have a volumetric storage efficiency of 63g H_2/L for a 30%wt sodium borohydride solution. The gravimetric storage density of a 25wt% $NaBH_4$ solution is 5.3%H_2 by weight. Assuming

the balance of plant (catalyst chamber, separator, piping, tank, etc) components are 30% of the weight of the solution, the gravimetric storage density of the entire system drops to 4.1% H_2 by weight.

The major challenges facing sodium borohydride and other chemical hydride storage systems and the areas for future research include: Cost of production of $NaBH_4$. At present the cost of $NaBH_4$ is ~ $80/kg. Cost reduction can be achieved by further research into effective methods of recycling $NaBO_2$ [21]. Systematic studies of the factors affecting H_2 generation rate are required to determine the optimal parameter selection. Methods to obtain high H_2 yields using stoichiometric amounts of H_2O. Further catalyst studies focusing on enhanced kinetics and durability. Means of increasing volumetric and gravimetric storage efficiencies via increasing the $NaBH_4$ solution concentration. Methods to increase the solubility limits of the by-product $NaBO_2$ will allow for an increase in the initial $NaBH_4$ concentration.

1.2.2 Dispensing Gaseous Hydrogen

The filling of compressed gas cylinders involves dispensing high-pressure gas from a large station reservoir into the smaller vehicle cylinder. The rate of gas transfer and safety of filling are controlled by the station dispenser. Most dispensers use an adjustable pressure regulator to control the rate of pressure rise within the cylinder. As will be discussed later in this review, during transfer the gas inside the vehicle cylinder undergoes a significant increase in temperature. Thus, when a cylinder is filled to the rated design pressure the resultant increase in temperature means less mass of gas is stored. As the temperature of the gas cools to ambient, correspondingly the pressure also decreases such that the cylinder is no longer filled to design pressure. This is termed under filling. In order to avoid this situation, cylinders

are filled to rated mass, which due to the temperature increase during filling, the cylinder is filled beyond the rated service pressure.

The goal of the dispenser is to fill the cylinder to the rated mass of gas without exceeding the pressure and temperature limits of the cylinder. In order to complete the filling, the dispenser must employ a method for calculating the mass of gas present inside the cylinder since filling is based on the mass of gas within, rather than pressure.

1.2.2.1 Metering

Dispensing systems use a mass flow meter to measure and totalize the mass flow rate in order to determine the mass of gas dispensed. The mass flow measurement of high-pressure gases is not a standard application and as such limited choice exists for metering high-pressure gas [22]. Coriolis meters, sonic nozzle meters and turbine meters have been investigated as choices for metering high-pressure gas [23]. The cost of meters currently used in natural gas fuelling stations contributes up to 50% of the cost of the entire dispenser [23]. At present, the most accurate and currently best-suited meter for high-pressure applications is the coriolis type flow meter. These units can cost in excess of $10,000. This provides impetus for a low-cost and accurate method of measuring the mass of gas dispensed.

1.2.2.2 Filling to Rated Capacity

Dispensers used in the natural gas and hydrogen industry to date can be separated into two categories: dispensers that communicate with the vehicle being filled, and those without communication.

Dispensers which communicate with the vehicle being filled use either: a hardwired electrical connector from the dispenser which plugs into a vehicle receptacle or a method of

infrared or wireless communication between the fuelling station nozzle and the vehicle gas receptacle [24]. Communication allows the dispenser to monitor the pressure and gas temperature sensors mounted within the vehicle cylinder throughout the fill. Communication also provides the dispenser the exact internal volume of the vehicle cylinder, the rated mass of gas and the type of cylinder. With the knowledge of the internal volume and rated mass of gas these dispensers totalize their mass flow meter reading throughout the fill and compare it to the desired rated mass of gas to determine when the cylinder has been filled to capacity. The pressure and temperature sensors also serve to ensure the cylinder pressure does not exceed 1.25 times the design pressure and that the temperature of the gas does not exceed 85 °C as required by the ISO standard for compressed hydrogen fuel tanks [1,2].

Dispensers without communication must either fill the vehicle cylinder to the rated pressure (which it must know before hand), provide temperature compensation based on the ambient temperature (thus assuming the gas temperature within the cylinder is equal to the ambient temperature, which leads to inaccurate fills) or they must employ a method to determine the vehicle cylinder volume. The volume is required to determine the mass of the gas in the cylinder before fuelling and for determination of the rated mass of gas desired at the end of fill. The Gas Technology Institute through numerous empirical test fills at various conditions have come up with a control algorithm called Accufill [25,26] for Natural Gas and HydroFill [27] for Hydrogen. The crux of these patents is a method for determining the volume of the vehicle cylinder by dispensing a small amount of gas at the beginning of the fill and approximating the volume of the cylinder based upon the amount of hydrogen required to achieve a predetermined rated fill condition in the vehicle cylinder.

Table 1-2: Comparison of filling with and without communication with the vehicle

Fueling strategy	Advantages	Disadvantages
With Communication	Direct knowledge of the cylinder volume provides a more accurate fill. Monitoring of temperature allows for faster filling and a more accurate temperature compensated fill.	Added expense for dispenser and vehicle Added complexity to the refuelling process
Without Communication	Cheaper Less complexity	Uncertainties in temperature result in a less accurate fill Slower fill rate imposed to ensure the vehicle cylinder temperature does not exceed 85 °C

The fuelling strategies described above all rely on totalizing the reading of the mass flow meter in order to determine when the cylinder has been filled to rated capacity. The accuracy of the fill is then directly related to the accuracy of the mass flow meter.

A proposed technique for determining when the cylinder has reached the rated mass of gas is for the dispenser to calculate the mass of gas inside the cylinder based upon the volume of the cylinder, and the continuous measurements of pressure and temperature during the fill. This method, hereby termed the PVT method, requires the cylinder to be outfitted with a temperature and pressure sensor (which is standard in transportation instances). For this method to be accurate the temperature and pressure measured by the sole temperature and pressure sensors must represent the average temperature and pressure of the gas within the cylinder. The pressure within the cylinder during filling can be considered uniform. The temperature distribution within the cylinder during filling will be discussed further in the following sections.

1.2.3 Refueling of Gas Cylinders – Survey of Previous Work

1.2.3.1 Modeling Studies

Reynolds et al. [28] first studied the charging and blowdown of gas reservoirs in 1958. The authors perform a thermodynamic analysis of the pressure vessel as a control volume, outlining the energy balance equations for charging and blowdown and deriving the differential equations governing the temperature rise. Due to their assumptions, the equations they derive are limited to the following conditions: the cylinder mass, volume and specific heat remain constant, the mass flow rate into the cylinder is constant, the gas in the cylinder is mixed and is uniform in temperature, pressure, and density, the gas is ideal with $k=1.405$, the convective heat transfer coefficients on the inside and outside of the cylinder are constant, and the gas within the cylinder is stagnant.

Analytical solutions are presented for constant mass flow rate of gas entering the reservoir coupled with the special cases of: adiabatic reservoir walls, heat transfer to an isothermal sink (assumes the thermal capacitance of the reservoir walls far exceed the thermal capacitance of the gas), and heat transfer with negligible inside resistance (infinite convective heat transfer coefficient).

Further to the Reynolds study, there have been numerous studies of gas flow exiting a pressure vessel. This "blowdown" phenomenon has been modeled in various forms to predict the temperature and pressure decay within the vessel. Xia et al. [29] apparently un-aware of the Reynolds et al. [28] study, present a simplified model for de-pressurization of a pressure vessel. As with the Reynolds et al. study, the model developed by Xia et al. assumes a constant mass flow rate and uses a lumped parameter model for determining the temperature of the vessel wall.

The blowdown effect in pressure vessels containing hydrocarbons was studied by Haque et al. [30,31]. The model they developed addresses three different regions within the vessel where free water, liquid hydrocarbons and gas preside. The model assumes spatially uniform temperature and pressure within each region. Energy, momentum and mass balances are applied to each region to develop the equations for prediction of pressure and temperature decay.

The Gas Technology Institute undertook a numerical study of fast filling of natural gas cylinders in 1994 [32]. The model developed by Kountz assumes the gas within the cylinder is at uniform temperature and pressure and has negligible kinetic energy. The model performs a control volume analysis of the cylinder and uses a lumped mass model for heat transfer to and from the cylinder wall. The author points out the difficulty in estimating the convective heat transfer coefficient between the gas and cylinder wall and suggests experimental investigations as a means of obtaining a correct value.

In 1994, Charton et al. [33] developed a model that predicts the pressure and temperature rise and fall within a reservoir that is depressurized in order to charge a larger reservoir. They initially assumed natural convection and constant surface temperature of the wall within both reservoirs but eventually determined that forced convection provides a more accurate representation of the heat transfer in the low-pressure reservoir. Instead of the lumped capacitance model and simplified cases presented by Reynolds et al. and Xia et al., the Charton et al. study solves the differential equations governing the charging and depressurization using a finite difference numeric scheme which eliminates the assumption of constant properties and mass flow rate. However, the model cannot be considered totally predictive, in order to calculate the convective heat transfer coefficient within the low-pressure

reservoir, the authors where forced to assume a Reynolds number for the flow at the walls of the cylinder. Charton et al. also assumes the walls of the two reservoirs to be isothermal due to the speed of gas transfer (from one to four seconds), and the thermal mass of the reservoirs.

In 1996, the study by Daney et al [34] modeled the filling of a gas cylinder assuming adiabatic conditions and an ideal gas. The study noted that as the initial to final pressure ratio increased without limit, the final gas temperature approached kT_i. Due to the assumption that no heat transfer occurs during filling, this model will significantly over-predict the temperature rise within the cylinder.

Similar to the Charton et al. model, a computational model developed by Perret [35] is based on the conservation of mass and energy for a control volume encompassing the test cylinder. Like the Charton et al. model, Perret's model assumes forced convection during the fill and natural convection during cool down. The Nusselt number for forced convection is derived using the equation below:

$$Nu = 0.0366\mathrm{Pr}^{1/3}\mathrm{Re}^{4/5} \tag{1-7}$$

Where the Reynolds number is computed from the average mass flux in the cross section of the cylinder. The author comments that further experimentation is necessary in order to validate the convective heat transfer coefficient between the gas and tank wall. Perret's model does not assume isothermal cylinder walls but instead solves the one dimensional conduction equation through the thickness of the cylinder wall.

A study undertaken by Dynetek and General Hydrogen [3] included a model for predicting gas temperature and pressure rise within the cylinder. The model is based on the conservation of mass and energy for a control volume encompassing the test cylinder. Little

information about the model is given but the model does assume the gas temperature within the cylinder is spatially uniform.

The study by Lincoln Composites [36] included a model based on the model of Reynolds et al [28]. The model uses experimental data to curve fit the predicted increase in gas temperature. The model suffers from the same restrictions of the Reynolds et al model and as such, must rely on curve fitting with experimental data in order to determine the rate of heat transfer from the gas to the cylinder walls. The study includes a second model for the calculation of the transient thermal response of the cylinder liner. This second model is used to determine the temperature profile of the cylinder wall throughout the fill. The model assumes the heat flux into the wall is constant throughout the fill, which is likely inaccurate during the early stages of the fill.

1.2.3.2 Experimental Studies

Haque et al. [30,31] performed experiments on two different pressure vessels in an effort to validate their computer model. The first vessel was cylindrically shaped with spherical ends. It had an inside diameter of 1.13 m and a length of 3.24 m. The second vessel was cylindrical with flat ends, an internal diameter of 0.273 m and a length of 1.524 m. Both vessels were instrumented with thermocouples to determine the temperature distribution within the vessel. The thermocouples were attached to a multi-arm spider structure radiating from a central support. 120 thermocouples were used in vessel 1 and 64 were used in vessel 2. The vessels were blown-down from an initial pressure of 150 bar.

Charton et al. [33] undertook a set of experiments to validate their model. In the experiments, a spherical receiver reservoir is filled by expanding gas from a spherical container of high-pressure gas. The receiver reservoir had a greater volume than the high-

pressure reservoir. The total fill time for the receiver varied through their experiments between 1 and 5 seconds. Due to the speed of the fill, pressure sensor and temperature sensor response time had a significant effect on the experimental results.

The Gas Technology Institute has performed numerous experimental studies of fast filling using natural gas and hydrogen [37,38]. In order to validate their model [32] they performed over 50 fast fills of type 3 and 4 cylinders at various ambient temperatures, initial fill pressures and fill rates for both hydrogen and natural gas. The experimental results were used to correlate the model parameters using regression analysis. With the correlated model they then developed a patented [25-27] fast filling algorithm which calculates the volume of the cylinder being filled by pressure rise correlations in an effort to provide a temperature compensated fill to rated mass of gas. The dispenser they used incorporates a mass flow sensor for calculating the mass of gas dispensed. During their various experiments the cylinders were instrumented with temperature sensors recording: internal gas temperature at 5 locations along the axis of the cylinder, cylinder outer surface temperatures at 5 locations and the ambient temperature within the environmental chamber used in these experiments. The ambient temperatures ranged from -15 °C to 45 °C. Their testing results showed the internal gas temperature, and cylinder outer surface temperature during the fill to be non-uniform. Results showed a temperature difference of as much as 28 °C inside the cylinder, with the coolest location being the mid-point of the centerline. On the outer cylinder wall the temperature varied by as much as 5 °C. The authors point out the challenge of obtaining a single point measurement of gas temperature on which to derive the true density of the gas [38].

In 2001, Dynetek undertook the experimental study conducted by Jeary [39] to determine the fast fill characteristics of a 34 L type 3 compressed gas cylinder. The study used three K-type thermocouples, one mounted on the inside of the aluminum liner, one mounted in a corresponding location on the outside surface of the cylinder and one inserted in the tail end of the cylinder measuring the local gas temperature. The cylinder was filled from an approximate initial pressure of 5 bar up to a final fill pressure of 338 bar in 40 seconds. The resulting increase in temperature showed a maximum local gas temperature measurement of 80.8 °C, at the tail end of the cylinder. The maximum measured local liner temperature was 73.5 °C.

Lincoln Composites (formerly General Dynamics), a manufacturer of type 4 plastic lined compressed gas cylinders, conducted a study of the fast filling of a 700 bar cylinder. The study conducted by Eihusen [36] investigated the internal gas temperatures, and liner temperatures during fast fill and cool down for various fill rates. The cylinder was a type 4 with internal volume of 111L. The cylinder was instrumented with one thermocouple to record the gas temperature at the centre of the cylinder, 2 thermocouples affixed to the liner wall and 5 thermocouples located on the outer wall, inlet and end fittings. The fill rate was controlled through a needle valve located between the test cylinder and a 850 bar storage bank. A 100 second fill from 50 to 700 bar resulted in an increase in temperature from 10 to 131.2 °C. In contrast a 500 second fill from 50 to 700 bar resulted in a gas temperature increase from 10 to 87.5 °C.

In 2003, a joint General Hydrogen and Dynetek study was undertaken by Duncan et al. [3]. The study is primarily an experimental investigation of the gas pressure and temperature rise within a Dynetek compressed gas cylinder during filling. The study

investigates the effect of cylinder size, and fill rate on the gas temperature rise during filling. Three separate experiments were undertaken. The first experiment involves the transfer of hydrogen gas from a 1200 L cylinder bank to a Dynetek model W205H350B8N test cylinder at an average fill rate of 8.7 g/s. The second experiment used the same setup but with an average fill rate of 10.6 g/s. The third experiment involves the transfer from a Dynetek model W205H350B8N cylinder into a Dynetek model M039H350G5N8N test cylinder. The fill time for the last test is approximately 10 s. For the first and second experiment the high-pressure cylinder bank is connected to the test cylinder through a thin tube with a needle valve in between. The test cylinder is instrumented with 8 thermocouples measuring the cylinder outer surface temperature, 2 thermocouples measuring the gas temperature within the cylinder at the non-fill end, and 1 pressure sensor measuring the gas pressure at the non-fill end. The study used T-type thermocouples accurate to within 0.5 °C. The thermocouples are grounded probes and have a diameter of 0.04 in. The third experiment involves the fast fill of a smaller test cylinder. Again setting the position of the needle valve between the high-pressure cylinder and test cylinder controls the mass flow rate of the gas. The high-pressure cylinder used during this test is a 205 L Dynetek model W205H350G8N. The low-pressure test cylinder used was a 39 L Dynetek model M039H350G5N8N. Each experiment is begun by manually opening a hand valve to initiate the transfer of gas. For both tests the test cylinder was filled to a pressure of 400 bar. The flow rate of hydrogen to the test cylinder is controlled through the positioning of the needle valve. The experimental results of Duncan et al. [3] showed a large variation in gas temperature at the non-fill end and cylinder outer surface temperature measurements were revealed to be non-uniform. The maximum local gas temperatures measured in the three

experiments were 94 °C, 85 °C and 110 °C respectively. The effect of increasing the fill rate increased the maximum gas temperature measured during the fill.

The European Integrated Hydrogen Project commissioned a study in 2003 conducted by Perret [35]. The study compared the results of a fast fill experiment on a 9 L composite gas cylinder with the results of a 0-D computational model. The timeframe for the experimental fill was approximately one second. The predicted and experimental measurement of the final fill temperature were within 15 K, however, due to the extremely short filling time and the response time of the temperature sensor used, the experimental and simulated temperature during the fill do not compare well. The author comments that further experimentation is necessary in order to validate the convective heat transfer coefficient between the gas and tank wall.

1.2.3.3 Instrumentation Requirements and Issues

The instrumentation of pressure vessels and in particular compressed gas cylinders is an important issue in experimental studies and deserves further treatment. Results of both the Charton et al. and Perret et al. studies [33,35] are severely affected by sensor response time. When the fill time is small, pressure sensor time response has a significant effect on experimental results. Due to the thermal mass inherent in temperature measurement, the time constant of temperature sensors is much greater than those of pressure sensors. The effect of sensor lag on temperature measurement is much greater than for pressure measurement.

Another important instrumentation factor in experimental studies is the location and number of temperature probes. For determining when the cylinder has reached rated capacity, the density of the gas must be calculated, which in turn requires knowledge of the average temperature and pressure of the gas within the cylinder. In many studies the model compares

the experimentally measured temperature to the average stagnation temperature predicted by the model (as all models to date assume uniform and stagnation conditions within the reservoir). However, those studies that placed more than one thermocouple inside the reservoir have noted the non-uniformity of gas temperature within the reservoir/cylinder during filling [3,31,38]. The only study to date to map out the temperature distribution inside a reservoir is the Haque et al. study [31].

1.2.3.4 Literature Summary

All the modeling studies conducted to date have assumed the gas temperature within the cylinder to be uniform and the velocity to be stagnant. The assumption is necessary in order to perform a control volume analysis of the cylinder or vessel that is being filled. Having assumed uniform temperature, the more advanced models attempt to predict the heat transfer from the gas in the cylinder to the cylinder walls and out to the surroundings. To do this, the model must determine the convective heat transfer coefficient between the gas and cylinder wall. While many empirical correlations exist for calculating the Nusselt number for the case of forced convection, these correlations require knowledge of the Reynolds number inside the cylinder and are specific to certain geometries. As the models treat the cylinder as one control volume the velocity profile inside the cylinder is not resolved. This makes it impossible to calculate the Reynolds number. Furthermore, the direction of flow inside the cylinder is not uniform, there exists backflow as the gas entering the cylinder reflexes off the back wall of the cylinder. Hence, in most models, the Reynolds number inside the cylinder is assumed or is a parameter used for fitting data to experimental results.

In order to accurately model the heat transfer from the gas to the cylinder, a model must discretize the space within the cylinder. By performing spatial discretization, the model

can determine the temperature and velocity profiles within the cylinder, which, in turn will allow for the calculation of the convective heat transfer at the cells along the wall. This method will allow for the calculation of the average temperature, but will also provide the temperature at numerous locations on the grid of discrete points inside the cylinder. This will allow for an appropriate comparison between the local temperature predicted by the model and the experimental measurements of local temperature.

Table 1-3 provides a comparison of the most relevant numerical studies with the work of the present study.

Only a few of the experimental studies to date have placed more than one temperature sensor within the cylinder to measure gas temperature. The only study that has placed enough temperature sensors within the vessel to provide a temperature distribution is the study of Haque et al. [31]. This study analyzed the blowdown of a large, cylinder shaped, steel pressure vessel. While this study provides insight into experimental techniques, due to the different experimental circumstances, their results are not directly useful for the analysis of the temperature distribution within a type 3 compressed gas cylinder. The Gas Technology institute study [38] found a significant spatial variability in temperature. Three thermocouples located at ¼, ½ and ¾ lengths of the centerline all read significantly different temperatures during filling. After the completion of the fill thermocouples at ¼ and ¾ lengths measured temperatures that converged to within 1 K within minutes of the end of the fill. The thermocouple located at ½ length of the centreline took 20 minutes to converge to within 5 K of the ¼ and ¾ length thermocouples. The study of Duncan et al. [3] found temperature differences as high as 10 °C between thermocouples placed at 1/3 and 2/3 of the length of the

cylinder centerline. From the end of filling it took ~ 5 minutes for these thermocouples to read a uniform temperature.

Table 1-4 provides a comparison of the most relevant experimental studies with the suggest work of the present study.

Time response of pressure and temperature sensors during filling is critical for accurate comparisons between experimental and modeled data. During filling a large increase in temperature occurs during the first 25 % of the fill time. The temperature rise is highly dependent on the fill rate. A slower fill rate and hence longer overall fill time will result in a lower rate of temperature increase. For total fill times on the order of 1 – 30 seconds the rate of temperature increase is large and fast response temperature sensors are extremely important. The rate of pressure rise can also be significant depending on the total fill time. However, generally pressure sensors respond much faster than temperature sensors and hence response time is only an issue in case of extremely fast fills, on the order of seconds.

Table 1-3: Comparison of relevant numerical studies with the present work

	Reynolds et al [28]	Kountz [32]	Charton et al [33]	Perret [35]	This Work
Modeling Method	Analytical	Finite Difference	Finite Difference	Finite Difference	Finite Volume
Assumptions					
Uniform gas temperature	Yes	Yes	Yes	Yes	No
Mass Flow Rate	Const	Fixed Orifice Calc	Fixed pipe length and size calc	Fixed Orifice Calc	Variable
Lumped Capacitance	Yes	Yes	Yes	No	No
Internal convective heat transfer coefficient	Assumed value	Assumed value	Dittus-Boelter equation	Dittus-Boelter equation	Discretize wall to calculate local h_{conv}
Reynolds Number for Nu# calculation	N/a	N/a	Assumed value	Average mass flux in cylinder	No
Heat Transfer					
Internal Convection	Const.	Const.	Forced Convection correlation	Forced Convection correlation	No correlations used
External Convection	adiabatic	Const.	Adiabatic	Const.	Const.
Conduction	No		No	Yes	Yes
Equation of State	Ideal, constant	STRAPPNG	Soave	Redlich-Kwong	Redlich-Kwong
Gas	General	Natural Gas	Helium, Deterium	Hydrogen	Hydrogen

Table 1-4: Comparison of relevant experimental studies with the present work

	Haque et al. [31]	Charton et al. [33]	Gas Technology Institute [38]	Duncan et al. [3]	This Work
Type of Pressure Vessel	Cylindrical Steel Tank	Spherical Steel Tank	Types 1, 3, and 4 cylinders	Type 3 Dynetek Cylinder	Type 3 Dynetek Cylinder
Gas	Water/Steam	Helium/Deterium	Natural Gas/Hydrogen	Hydrogen	Hydrogen
Fill method	Blowdown through fixed orifice	Uncontrolled expansion through fixed pipe	Cascade fill	Expansion through a needle valve	Controlled Constant pressure ramp
Size of Pressure Vessel	~3200 L and 89 L	4 L	190-220L	39L and 205L	74 L
Fill Time	100 - 1500 sec	~ 4 sec.	30 sec. – 600 sec.	10sec/400sec/500sec	1 min – 10 minutes
Temperature sensor					
Type	Bare wire thermocouples	0.5mm dia. Type K Thermocouple	Thermocouples – type and size were not stated	0.04 in. dia grounded probe Type T thermocouple	Exposed tip 0.5mm dia, Type T thermocouples
Number	120 in 3200L vessel and 64 in 89L vessel	1	5 gas temperatures, 5 cylinder surface temperatures	1 gas temperature, 3 outer wall	~60 thermocouples
Location of gas temperature sensors	Distributed throughout the vessel. Some thermocouples spot welded to the wall	unknown	Inlet, ¼ length, ½ length, ¾ length, and non fill end. All located along the centerline	12" cm and 24" into the non-fill end along the centerline	Distributed through half of the cylinder
Parameters investigated	Gas composition/Cylinder type/blowdown time/initial pressure	Gas/fill time/initial pressure	Cylinder type/fill time/initial pressure/ambient temperature	Fill time/cylinder size	Fill time/ /initial mass
Spatial variation in temperature	Yes	N/a	Yes	Yes	Yes

1.3 MOTIVATION FOR THIS WORK

The refuelling of a gasoline-powered vehicle sets the standard for ease, complexity, safety and duration of fuelling. In order to gain consumer acceptability, refuelling of a hydrogen-powered vehicle must meet or exceed the present gasoline technology.

The ease, complexity and safety of refuelling a hydrogen vehicle can be addressed through engineering design of the fuelling station. The quick release nozzles currently used in most hydrogen fuelling stations make refuelling easy for the consumer and in many ways less complex than the present gasoline system. The safety of refuelling focuses on ensuring no gas escapes during transfer and that the dispenser fills the compressed gas cylinder such that the temperature and pressure limits of the cylinder are never exceeded.

The time required to fill a hydrogen vehicle is an important parameter for consumer acceptability [3]. Consumers are accustomed to the present refuelling times of gasoline-powered vehicles, thus fuelling times of less than 3 minutes are desired [12].

Due to thermal material limitations of the present gas cylinder technology, the average gas temperature must be maintained within –40 to 85 °C during normal operation, which includes filling and discharging [1,2] This thermal limitation restricts the refuelling time to on the order of 3-5 minutes for a fill equivalent to 40L of gasoline. In comparison a 40L fill of gasoline from a commercial station takes approximately 1-2 minutes. Thus the motivation exists for research into the area of improved refuelling times of compressed gas cylinders for vehicular applications.

The accuracy of fill is defined by the percentage fill achieved by the dispenser (ratio of the mass of gas within the cylinder at the end of filling to the rated mass of gas at the design temperature and pressure). The accuracy of the fill has a direct affect on the range of the

vehicle since under-filling will lessen the range. Over-filling is undesirable for safety reasons thus a dispenser should fill a cylinder to as close as possible without exceeding 100% fill. The present work will help to improve the accuracy of the fill by providing a better measurement of the average temperature of the gas inside the cylinder during fuelling.

While there are many previous works that have measured and modeled the temperature rise of the gas during filling, the modeling studies to date have all assumed the gas temperature within the cylinder to be uniform temperature. This assumption leads to the necessity of further assumptions regarding the heat transfer from the gas to the cylinder walls. Until a reliable empirical formula is developed to relate the convective heat transfer coefficient to the fill parameters, these models cannot be considered totally predictive as they rely on experimental data to tune the heat transfer coefficients. On the experimental side, only a handful of studies have measured the gas temperature within the cylinder at multiple locations and none of the studies provided sufficient local measurements of temperature to define the temperature distribution within the cylinder. This research aims to address the assumption of uniform temperature by studying the gas temperature distribution within the cylinder during filling via numerical modeling and experimental measurements.

1.4 OBJECTIVES OF THIS WORK

The goal of this research will be to determine when a cylinder is filled to rated capacity using the PVT method (calculating the density of the gas based on the temperature and pressure of the gas). To meet this goal the research will focus on investigating the temperature field within a compressed gas cylinder during filling, in order to determine the average temperature of the hydrogen gas which will allow for the calculation of density based on pressure and temperature.

A computational fluid dynamics (CFD) model is created that spatially discretize the cylinder in order to predict the distribution of gas temperature. The model will take into account, compressible unsteady viscous flow, real gas effects, heat transfer to the cylinder walls and conduction through the cylinder walls to ambient. The model is validated by comparison with a set of experimental fast fills of a compressed gas cylinder instrumented with numerous temperature sensors, in an effort to measure the gas temperature distribution within the cylinder and provide an accurate estimate of the average gas temperature within the cylinder. The experimental fills will be conducted at various fill rates, and initial pressures in order to assess their impact on the gas temperature field and to validate the model for a range of filling conditions.

The validated model will help to assess the difference between the local measurements of temperature inside the cylinder and the average temperature based on the position of the local measurement. The model will also help to identify the best locations for the onboard temperature sensor such that the local measurement best represents the average gas temperature for a range of fill conditions.

1.5 OUTLINE OF THESIS

Chapter 1 presents the introduction and a literature review for this study. Included in the review is an overview of the issues involved with the three leading technologies for the storage of hydrogen onboard vehicles. This work concentrates on the use of pressurized gas as a storage method, and hence the literature review discusses in detail studies pertaining to the refuelling of compressed gas vessels. These studies are placed into the categories of modeling studies and experimental studies. The most pertinent studies are then compared with the present study as a conclusion to the chapter.

Chapter 2 utilizes the principles of computational fluid dynamics (CFD) to develop a two-dimensional model of the temperature field within the cylinder during refuelling. The model discretizes the space within the cylinder and its walls to create numerous control volumes over which the governing equations for mass, momentum, energy and turbulent parameters are solved. The results of the model are validated by comparison with a set of experimental results. The model is then used to investigate the temperature field within the cylinder identifying the locations of maximum and minimum temperature and to analyze the relationship between the average gas temperature and the local measurement of gas temperature.

Chapter 3 presents the experimental hardware, method and fills performed on a 74L type 3 compressed gas cylinder. The experimental fills are performed using the Pacific Spirit Hydrogen Fuelling Station located at the National Research Councils Institute for Fuel Cell Innovation in Vancouver Canada. Three sets of tests are performed to assess the repeatability of fill conditions and experimental measurements, the effect of initial mass/pressure and the fill rate on the temperature field.

Chapter 4 presents a summary of the work performed, and discusses the conclusions drawn and provides recommendations for future research.

1.6 REFERENCES

[1] International Standard Organization. Gaseous hydrogen and hydrogen blends land vehicule fuel tanks Part 1: General Requirements. ISO 15869. 2005.

[2] American National Standards Institute / Canadian Standards Association. Basic Requirements for Natural Gas Vehicle (NGV) Fuel Containers. ANSI/CSA NGV2-2000.

[3] Duncan M and Macfarlane S, "Fast Filling of Type 3 Hydrogen Storage Cylinders", Hydrogen and Fuel Cells Conference, Victoria, Canada, June 2003.

[4] Scott, D., "Template for Sustainability," International Journal of Hydrogen Energy, Vol. 29, No. 1, 2004, pp. 17-22.

[5] Scott, D., "Hydrogen - the case for inevitability," International Journal of Hydrogen Energy, Vol. 29, No. 3, 2004, pp. 225-227.

[6] Choudhury, R., "GM Well-to-Wheel Analysis of Energy use and Greenhouse Gas Emissions of Advanced Fuel/Vehicle Systems – A European Study," General Motors, Ottobrunn, Germany, 2002.

[7] Hohlein B, von Andrian, S., Grube, Th., and Menzer, R., "Critical assessment of power trains with fuel-cell systems and different fuels," Journal of Power Sources, Vol. 86, 2000, pp. 243-249.

[8] Ewald R., Int. J. Hydrogen Energy 23/9 (1998) 803-814.

[9] National Research Council Committee on Alternatives and Strategies for Future, The Hydrogen Economy: Opportunities, Costs, Barriers, and R&D Needs, National Academy Press, Washington, 2004

[10] James, B., Baum, G., Lomax Jr, F., Thomas, C., and Kuhn Jr, I., "Comparison of Onboard Hydrogen Storage for Fuel Cell Vehicles," Directed Technologies Inc., Contract DE-AC02-94CE50389, Jan. 1996.

[11] Zuttel A, "Hydrogen Storage Methods," Naturwissenschaften (2004), Vol. 91, 2004, pp. 157-172.

[12] Schneider, J., 2005, "Optimizing the Fuelling of Hydrogen Vehicles," The Fuel Cell Review, 2(4) pp. 15-24.

[13] Barron, R., Cryogenic Systems, 2nd ed., Oxford University Press, New York, 1985.

[14] Nandi, T. and Sarangi, S., "Performance and Optimization of Hydrogen Liquefaction Cycles," International Journal of Hydrogen Energy, Vol. 18, No. 2, 1993, pp. 131-139.

[15] Moran, M. and Shapiro HN, Fundamentals of Engineering Thermodynamics, 3rd ed., Wiley & Sons, New York, 1995.

[16] Farkas, A., Orthohydrogen, parahydrogen and heavy hydrogen, Cambridge University Press, New York, 1935.

[17] McCarty, R., Hord, J., and Roder, H., Selected Properties of Hydrogen, National Bureau of Standards Monograph 168, U.S. Government Printing Office, Washington, 1981.

[18] Gursu, S., Lordgooei, M., Sherif, S., and Veziroglu, T., "An Optimization Study of Liquid Hydrogen Boil-off Losses," International Journal of Hydrogen Energy, Vol. 17, No. 3, 1992, pp. 227-236.

[19] Zhou, L., "Progress and problems in hydrogen storage methods," Renewable and Sustainable Energy Reviews, Vol. 9, No. 4, 2005, pp. 395-408.

[20] Daimler Chrysler. Sodium Borohydride: Fuel Cell Vehicle 'Natrium' Uses Clean, Safe Technology to Provide Hydrogen on Demand. Press Release June 11 2002. 2002.

[21] Amendola, S., Sharp-Goldman, S., Janjua, M., Spencer, N., Kelly, M., Petillo, P., and Binder, M., "A safe, portable, hydrogen gas generator using aqueous borohydride solution and Ru catalyst," International Journal of Hydrogen Energy, Vol. 25, No. 10, 2000, pp. 969-975.

[22] Hart, D.. The hydrogen economy and compressed hydrogen. IMECHE Event Publications S1020/005/2004, 103-110. 2004.

[23] Blazek, C.. Mass flow meters for NGV fuelling dispensers. Freeman Rowley, P and Kriha, K. Proceedings of the American Gas Association, Operating Section 1995 , 207-214. 1995.

[24] SAE J2601. Compressed Hydrogen Vehicle Fuelling Communication Devices. Not yet published . 2006.

[25] Kountz, K., Liss, W., and Blazek, C.. Method and Apparatus for Dispensing Compressed Natural Gas. US Patent [5,752,552]. 19-5-1998.

[26] Kountz, K., Liss, W., and Blazek, C.. Automated Process and System for Dispensing Compressed Natural Gas. US Patent [5,810,058]. 1998.

[27] Kountz, K., Kriha, K., and Liss, W.. Control method for high-pressure hydrogen vehicle fuelling station dispensers. Gas Technology Institute. Application number 20050178463. 2006. USA.

[28] Reynolds, W. and Kays, W., "Blowdown and Charging Processes in a Single Gas Receiver With Heat Transfer," Transactions of the ASME, Vol. July 1958, 1958, pp. 1160-1168.

[29] Xia, J., "A Simplified Model for Depressurization of Gas-Filled Pressure Vessels," Int.Comm.Heat Mass Transfer, Vol. 20, 1993, pp. 653-664.

[30] Haque, M., "Blowdown of Pressure Vessels – I. Computer Model," Trans.IChemE, Vol. 70, Part B, 1992, pp. 3-9.

[31] Haque, M., "Blowdown of Pressure Vessels – II. Experimental Validation of Computer Model and Case Studies," Trans.IChemE, Vol. 70, Part B, 1992, pp. 10-17.

[32] Kountz, K., "Modeling the Fast Fill Process in Natural Gas Vehicles Storage Cylinders," 1994.

[33] Charton, S., "A Simplified Model for Real Gas Expansion Between Two Reservoirs Connected by a Thin Tube," Chemical Engineering Science, Vol. 51(2), 1996, pp. 295-308.

[34] Daney, D., Edeskuty, F., Daugherty, M., Prenger, F., and Hill, D., "Hydrogen vehicle fuelling station," Vol. 41, 1996, pp. 1041-1048.

[35] Perret, C., "Modelling and Simulation of the Filling of a Gaseous Hydrogen Tank under very High Pressure," DTEN/DR/2003/167, 2004.

[36] Eihusen, J., "Application of Plastic-Lined Composite Pressure Vessels For Hydrogen Storage," Lincoln Composites, 2003.

[37] Kountz, K., Liss, W., and Blazek, C., 1998, "A New Natural Gas Dispenser Control System," Proceedings of the 1998 International Gas Research Conference, pp. 135-145.

[38] Richards, M., Liss, W., and Kountz, K., "Modeling and Testing of Fast-Fill Control Algorithms for Hydrogen Fuelling," National Hydrogen Association's 14th Annual U.S.Hydrogen Conference and Hydrogen Expo USA, 2003.

[39] Jeary, B., "Fast Filling of Compressed Hydrogen Fuel Storage Cylinders," Proceedings, 11th Canadian Hydrogen Conference, Canadian Hydrogen Association, Victoria, B.C., June, 2001.

CHAPTER 2: MEASURED EFFECTS OF FILLING TIME AND INITIAL MASS ON THE TEMPERATURE DISTRIBUTION WITHIN A HYDROGEN CYLINDER DURING REFUELLING[1]

2.1 INTRODUCTION

Compressed gas cylinders represent the simplest and most mature technology for hydrogen storage. They are also the preferred near-term option for direct-hydrogen and hybrid fuel cell vehicles. Although various shapes have been explored, the on-board tank is usually cylindrical, and it can be classified by the choice of structural materials. Type 3 and type 4 cylinders are the cylinders of choice for vehicular applications because they provide the greatest volumetric and gravimetric storage densities (see Table 2-1). The liner in a type 3 or 4 cylinder provides a gas tight seal while the wrap (usually a carbon fibre) provides the structural integrity.

Cylinder Type	Description	Performance Factor (inches)
Type 1	All Steel Tank	150,000
Type 3	Aluminum Liner with Carbon Fibre Wrap	1,300,000
Type 4	Plastic Liner with Carbon Fibre Wrap	1,250,000

Table 2-1: The performance factors for different cylinder types (adapted from [1]). Cylinder performance factor is defined as burst pressure multiplied by volume, and divided by weight.

[1] A version of this chapter has been accepted for publication. Dicken C.J.B. and Merida W. (2006) "Measured Effect of Filling Time and Initial Mass on the Temperature Distribution Within a Hydrogen Cylinder During Refuelling", Journal of Power Sources.

Refuelling vehicle cylinders involves transferring high-pressure hydrogen gas from the fuelling station tanks through a dispenser into the vehicle cylinder. The dispenser controls the rate of filling, ensures safe operation, and delivers the rated mass of gas. The total time required to refuel a cylinder (t_{total}) is important for consumer acceptance and it can have significant financial consequences in commercial applications. In central refuelling applications (transit buses, lift trucks, etc.), the refuelling time increases with fleet size.

Current regulation imposes limits on the maximum average gas temperature allowed within the cylinder, and these limits also affect refuelling time. The current standards governing the use of cylinders for vehicular applications state that the average hydrogen temperature cannot exceed 358 K [2]. However, during refuelling there is a significant rise in temperature as a result of two phenomena described in greater detail in section 2.

The choices for metering high-pressure hydrogen are limited. Coriolis meters, sonic nozzle meters and turbine meters have been considered. The meters currently used in natural gas fuelling stations contribute a significant portion to the cost of the entire dispenser. The most accurate and currently best-suited meter for high-pressure applications is the coriolis flow meter. Depending on the flow ranges, these units can cost in excess of $10,000. Metering the dispensed gas via temperature and pressure measurements can enable more economical dispensers.

There have been many experimental studies of the temperature rise within a compressed gas cylinder during refuelling, [3-11] but only a few have placed more than one temperature sensor within the cylinder to measure gas temperature. The only study that has placed enough temperature sensors within the vessel to provide a temperature distribution is the study of Haque and co-workers [5, 9]. This study analyzed the blowdown of a large,

cylindrical, steel pressure vessel. While insight was gained into experimental techniques, these results are not directly useful for the analysis of the temperature distribution within a type 3 cylinder (due to different materials and experimental conditions). Researchers at the Gas Technology Institute [6] also found a significant spatial variability in temperature. Three thermocouples located at ¼, ½ and ¾ lengths of the centerline all read significantly different temperatures during filling. Towards the end of filling the thermocouples at ¼ and ¾ lengths converged to single temperature while the thermocouple at ½ length took greater than 20 minutes to converge to the same reading.

In a separate publication, we reported on a 2-dimensional axisymmetric model that predicted the gas temperature and pressure rise in a hydrogen cylinder during the fill process. The predictions were compared with preliminary experimental measurements and they agreed to within 4 K.[12]

Our objectives in the present study were: i) to monitor and record the temperature field within a type 3 compressed gas cylinders during refuelling, ii) to determine the effect of fill rate and initial pressure on the temperature field, and iii) to determine the relationship between the temperature rise and the amount of gas dispensed during a fill.

To achieve these objectives this investigation was separated into three experimental phases. The first, determined the repeatability of the fill conditions and the experimental measurements of temperature and pressure. The second investigated the effects of fill rate, and the third initial pressure on the temperature field within the cylinder, respectively. The experiments were performed at the Pacific Spirit Hydrogen Fueling Station located at the National Research Council's Institute for Fuel Cell Innovation in Vancouver, Canada.

These measurements have been used to validate numerical models [12] and are being used to identify optimal placement of a single commercial sensor to approximate the average gas temperature (as measured from an experimental sensor grid). In collaboration with our industrial partners, the data gathered in this study will also be used to elucidate the heat transfer characteristics between the cylinder materials and the hydrogen fuel.

2.2 THEORY

The thermodynamics of filling compressed gas cylinders has been the subject of most of the fast fill studies to date [3,5,7-8,13-15]. Inherent to the fill process is a significant increase in gas temperature. The temperature rise during filling is the result of the combination of two phenomena.

For hydrogen the Joule-Thomson coefficient is negative at the temperatures and pressures of filling. As a result, an isenthalpic expansion of the gas from the high-pressure tank through the dispenser throttling device and into the low-pressure cylinder results in an increase in gas temperature. The isenthalpic expansion occurs within the dispenser and the gas entering the cylinder is thus preheated.

The second phenomenon that causes a temperature rise during filling is the compression of the gas inside the cylinder. At the onset of filling, the gas inside the cylinder is compressed by the introduction of the higher-pressure gas from the fuelling station. This compression continues throughout the fill as additional gas compresses the gas already in the cylinder. The corresponding increase in temperature is often referred to as the heat of compression. A comparison of the magnitudes of these two phenomenon shows that the Joule-Thomson effect has an insignificant effect on the overall temperature rise when consideration

is given to the thermodynamics of the entire process [13]. Overall, larger dispensing rates (in kg s^{-1}) lead to larger heating rates (in K s^{-1}) that affect the accuracy of the fill. When the temperature reaches the maximum limit (358 K) the gas delivery is halted independently of the final mass dispensed. As the gas cools, the pressure inside the cylinder decreases and this leads to well known under-filling issues on board fuel cell vehicles.

A simplified analysis of the filling of a compressed gas cylinder can be performed by treating the interior of the cylinder as a single control volume. Figure 2-1shows the layout of a typical cylinder with gas entering the cylinder from an inlet at one end of the cylinder. The compression of the gas within the cylinder yields a dramatic temperature rise, which is mitigated by heat loss from the gas to the cylinder liner. Part of the heat transferred to the liner is stored within the material and part is conducted through the cylinder wall to the environment.

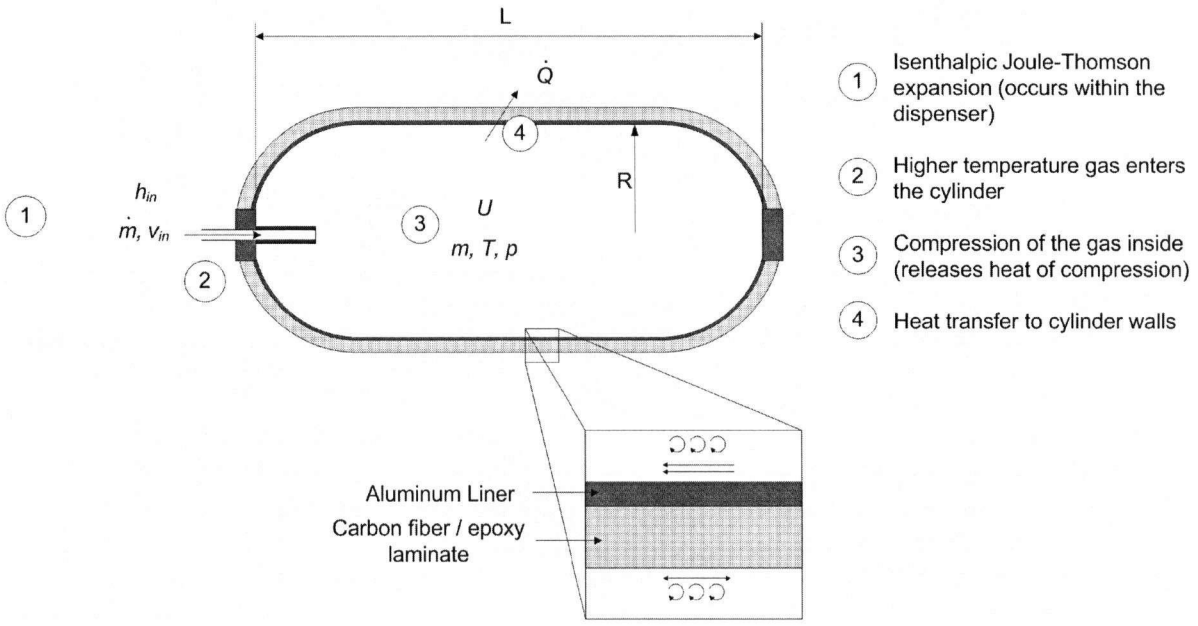

Figure 2-1: Schematic of filling of a compressed gas cylinder

A single control volume assumes the gas temperature, pressure and density are uniform within the cylinder and that stagnant conditions prevail. The conservation of energy and the conservation of mass yields:

$$\dot{m}_{in} = \frac{dm}{dt} \tag{1}$$

$$\frac{dU}{dt} = \frac{d(mu)}{dt} = u\frac{dm}{dt} + m\frac{du}{dt} = \dot{m}_{in}h_{in} - \dot{Q} \tag{2}$$

For our analysis we were interested in the increase in temperature and pressure over time. Due to the pressures achieved during filling (350 bar), and the subsequent compressibility at these high pressures (Z = 1.23 at 293K and 350 bar) a real gas equation of state is required in order to determine the properties u and h_{in} as a function of temperature, pressure and specific volume [16]. Numerous equations of state exist for accurately predicting the properties of hydrogen in the range of temperature and pressure of filling. The Redlich-Kwong equation of state (2-3) was chosen for this analysis, as it is accurate and computationally inexpensive. Equations (2-4) and (2-5) give the internal energy and enthalpy of the gas as a function of the temperature, pressure and specific volume.

$$p = \frac{R_{gas}T}{v-b} - \frac{a}{T^{1/2}v(v+b)} \tag{3}$$

$$u = \frac{3a}{2bT^{1/2}}\ln\left(\frac{v}{v+b}\right) + u_o \tag{4}$$

$$h = u - u_0 + pv - R_{gas}T + h_o \tag{5}$$

Where the subscript o denotes the ideal gas value, a and b are constants for a specific gas. Substituting equations (1), (3), (4), and (5) into equation (2) yields the equation for temperature rise of a real gas during re-fuelling:

$$\frac{dT}{dt} = \frac{\frac{\dot{m}_{in}}{m}\left(\frac{3a}{2b}\left\{\frac{\ln\left(\frac{v_{in}}{v_{in}+b}\right)}{T_{in}^{0.5}} - \frac{\ln\left(\frac{VM}{VM+mb}\right)}{T^{0.5}}\right\} + p_{in}v_{in} - R_{gas}T_{in} + T_{in}c_p - Tc_v + \frac{3a}{2T^{\frac{1}{2}}\left(\frac{VM}{m}+b\right)}\right) - \frac{\dot{Q}}{m}}{\left(c_v - \frac{3a}{4bT^{\frac{3}{2}}}\ln\left(\frac{VM}{VM+bm}\right)\right)} \quad (6)$$

The rise in temperature is dependent on the temperature of the inlet gas T_{in}, the specific volume of the inlet gas v_{in}, the initial gas temperature T, the specific heat at constant pressure c_p and constant volume c_v, the internal volume of the cylinder V, the mass of gas within the cylinder at any point in time m, the rate of mass flow into the cylinder $\dot{m}$ and the rate of heat transfer to the cylinder walls, $\dot{Q}$.

Equation (2-6) describes the physics that induce the temperature rise during filling. The difficulty in accurately predicting the temperature rise rests in determining the heat transfer to the cylinder wall. A detailed analysis of the heat transfer during filling is beyond the scope of the present study but will be addressed in a follow on study. In the present study, equation (2-6) was solved for the case of an adiabatic fill where $\dot{Q} = 0$. This solution was used to plot the adiabatic temperature rise in Figure 2-13. A fill where no heat from the gas is transferred to the cylinder walls represents a worst case scenario with the greatest increase in temperature.

2.3 *MATERIALS AND EXPERIMENTAL METHODS*

There are many variables and operating parameters that affect the temperature field within the cylinder while filling (e.g., the mass flow rate and temperature of the gas entering the cylinder, the temperature of the cylinder walls, the ambient temperature, etc). The hydrogen dispenser controls the rate of pressure rise within the cylinder, and in this manner, it controls the mass flow rate of hydrogen gas into the cylinder. The dispenser utilizes a pressure ramp rate (PRR) executed through a pressure control valve, which creates a large initial mass flow rate of hydrogen. This initial rate decreases steadily throughout the fill. The pressure ramp rate is adjustable but large ramp rates are limited by the flow restrictions inherent in the dispenser, hose and cylinder piping geometries.

In practical applications, the temperature of the gas entering the cylinder cannot be directly controlled. A typical fuelling station does not control the temperature of the gas within the large storage banks. The inlet temperature at the cylinder is affected by: i) the initial temperature of the gas in the storage banks, ii) the initial pressure of the storage banks, iii) the hydrogen mass flow rate, iv) the switching sequence of the storage banks, and v) the ambient temperature during and prior to the experiment. The pressure ramp rate and the initial pressure of the cylinder are the two control variables used in the reported experiments.

2.3.1 Experimental Test Matrix

Three different pressure ramp rates were tested to determine the effect of the fill rate on the temperature field and temperature rise within the cylinder. The pressure ramp rates tested correspond to the nominal fill times of 40, 190, and 370 seconds (simulating fill times acceptable in hydrogen refuelling applications). The experimental fills were performed at

initial pressures of 50, 75, 100, 150, and 200 bar (to simulate partially empty tanks at refuelling). The temperature of the hydrogen entering the cylinder was recorded but it was not controlled by the dispenser.

2.3.2 Repeatability

An initial set of tests were performed to investigate the repeatability of the temperature field measurements for a given set of control variables. These tests begin with the cylinder at 100 bar. The cylinder is filled to the rated mass of gas in 40 seconds. Several fills were carried out to investigate the repeatability of the inlet conditions provided by the dispenser and the temperature measurements within the cylinder.

2.3.3 Effect of Fill Rate and Initial Pressure on Temperature Field

Fast fill experiments were performed for five different initial gas pressures within the cylinder, and three different nominal fill times. The aim of the experiment was to fill the cylinder to its rated mass capacity by monitoring the amount of gas transferred through the coriolis flow meter in the dispenser. The measurement was confirmed using our model predictions and the pressure and temperature measurements in the cylinder. The conditions for each test are outlined in the test matrix in Table 2-2.

Number of tests reported					
Fill time (s)	Initial Pressure (bar)				
	50	70	100	150	200
40	2	2	4	2	2
190	1		1		1

370	1	1	1

Table 2-2: Experimental conditions.

2.4 *EXPERIMENTAL SETUP*

The experimental setup is shown schematically in Figure 2-2. The fuelling station houses high pressure compressed gas inside ground storage banks. From these banks hydrogen is fed to the dispenser where it is metered and controlled. The dispenser is connected to the test cylinder by a 350 bar, quick connect fuelling nozzle. The test cylinder is instrumented with pressure sensors to monitor the tank pressure, a temperature sensor at the inlet to monitor the gas inlet temperature, and 63 temperature sensors inside the cylinder to record the gas temperature field. A detailed description of the main components of the test setup is described in the following sections.

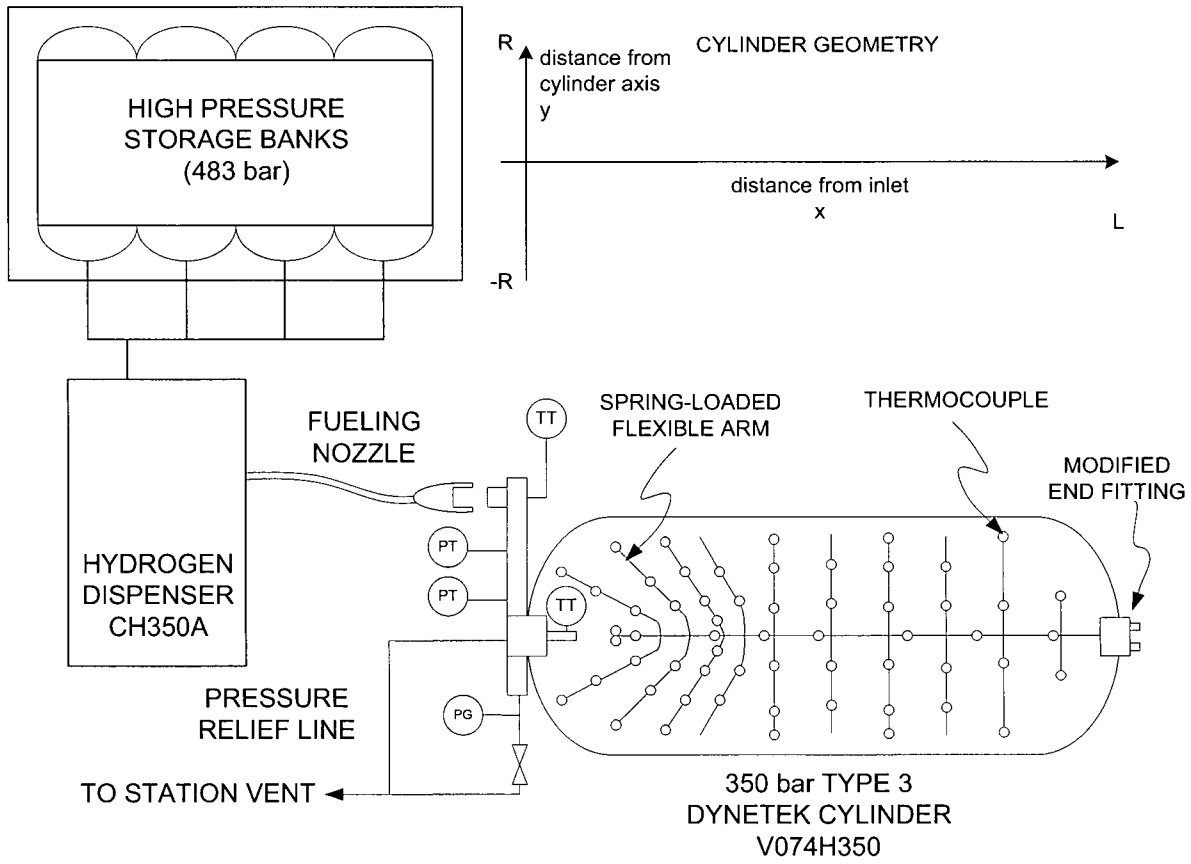

Figure 2-2: Schematic of Test Cylinder connection to the Fuelling Station

2.4.1 Test Cylinder

We used a type 3 aluminum lined, full carbon fibre wrapped cylinder for our experiments. The cylinder is manufactured by Dynetek Industries (model V074H350). It has an internal volume of 74 litres and a design pressure of 350 barg (3.51 107 Pa). At 15 °C (288 K) this pressure rating translates into 1.79 kg of stored hydrogen. The relevant geometry and the experimental tank are illustrated in Figure 2-2 and Figure 2-3. The total inner length was 90 cm while the outer diameter was 40 cm. The cylinder is equipped with a 350 bar internal tank valve block assembly (Teleflex GFI model TV-115) which is also shown in Figure 2-3. The assembly houses a 12 VDC solenoid valve, a manual shutoff valve, a pressure relief device, a pressure sensor mounted externally (PT) and a thermistor mounted internally (TT). The gas enters the cylinder through a stainless steel tube with a 5mm internal diameter and extends 82mm into the cylinder. The opposite end of the cylinder has a two-inch port, which is used as a sealed conduit for the thermocouple wires.

2.4.2 Hydrogen Dispenser

The Pacific Spirit Fueling Station is equipped with a hydrogen dispenser designed and manufactured by General Hydrogen Corporation (model CH350A). This dispenser meters and controls the rate of filling, and it is equipped with a coriolis flow meter. An electronically adjustable pressure control valve is used to set a pressure ramp rate of the gas entering the cylinder. The connection is made via a ¼ turn quick-connect nozzle. The dispenser is capable of communication with the vehicle being fuelled in order to provide a faster and more accurate fill. An electrical interface to the tank allows the dispenser to monitor the pressure within the cylinder, provides a single temperature sensor signal from within the cylinder, and

communicates the volume of the test cylinder. The volume of the cylinder is communicated through a fixed resistor, where the value of the resistor is directly proportional to the volume of the cylinder. The communication of the cylinder pressure, temperature and volume is specified in the SAE Standard J2601. This information enables accurate calculation of the initial mass of gas within the cylinder and the required mass of gas at the end of filling (based on the rated pressure, temperature and volume). The fixed communication link allows the dispenser to monitor the pressure and temperature of the gas in the cylinder throughout the fill to ensure the pressure does not exceed 1.25 times the design pressure and that the temperature of the gas does not exceed 358 K.

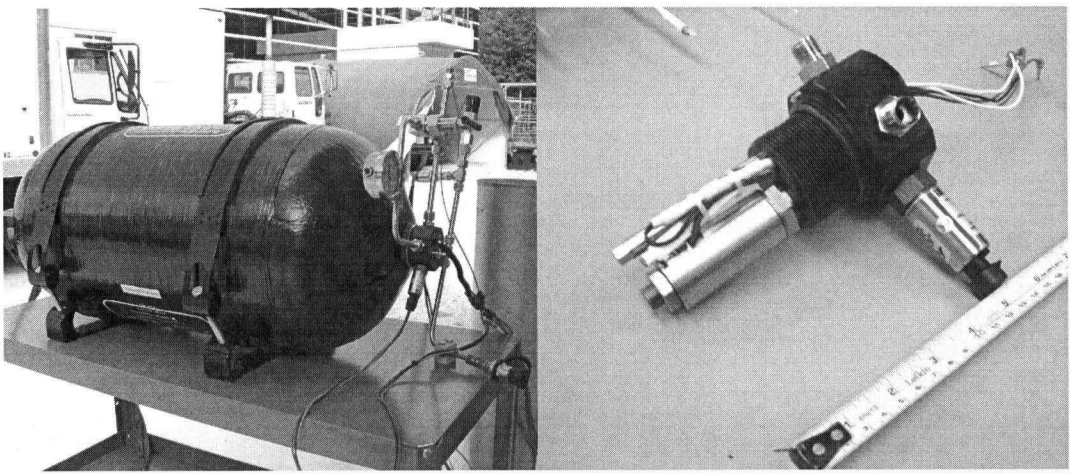

Figure 2-3: Test cylinder with inlet and vent piping (left). Cylinder inlet valve block (right).

2.4.3 Instrumentation and Data Acquisition

The thermocouples used for measuring the temperature of the gas within the cylinder were type T (copper and constantan), bare wire, with a 0.5 mm tip diameter. These fine wire thermocouples have a response time of 0.40 sec to achieve 63% of an instantaneous decrease in temperature from 427 °C to 38 °C when immersed in air moving at 60 ft/s. The thermocouples are accurate to within +/- 1 K. All sensors outputs were wired to a data

acquisition system which recorded 63 internal gas temperatures, 20 surface temperatures, and the internal and inlet pressures. All signals were logged at 10 Hz.

2.4.4 Thermocouple Locations and Support Mechanism

The thermocouples inserted into the gas cylinder are located in a grid arrangement to map out the temperature distribution. The thermocouples need to be held in position and that position must be known accurately to create plots of the temperature field. A major design constraint for the thermocouple mounting mechanism was related to the only access point (the end port which is two inches wide). The mechanism is shown in Figure 2-4: it incorporates a rigid base rod along the cylinder's centerline. Table 2-3 gives the coordinates of the thermocouples which are included in the vertical and horizontal slices. Twenty thermocouple positioning arms were attached to this rod. The arms were in turn held in position by extension springs that allow the arms to be folded to insert or remove the mechanism from the cylinder. The main rod is mounted to the modified end plug in Figure 2-3. In order to feed the electrical wires of the numerous thermocouples inside the cylinder, a custom designed end plug was fabricated. The end plug incorporates the same 2" – 12 UN thread and o-ring seal as the OEM end plug, but also included 128 sealed wire conduits (see Figure 2-5).

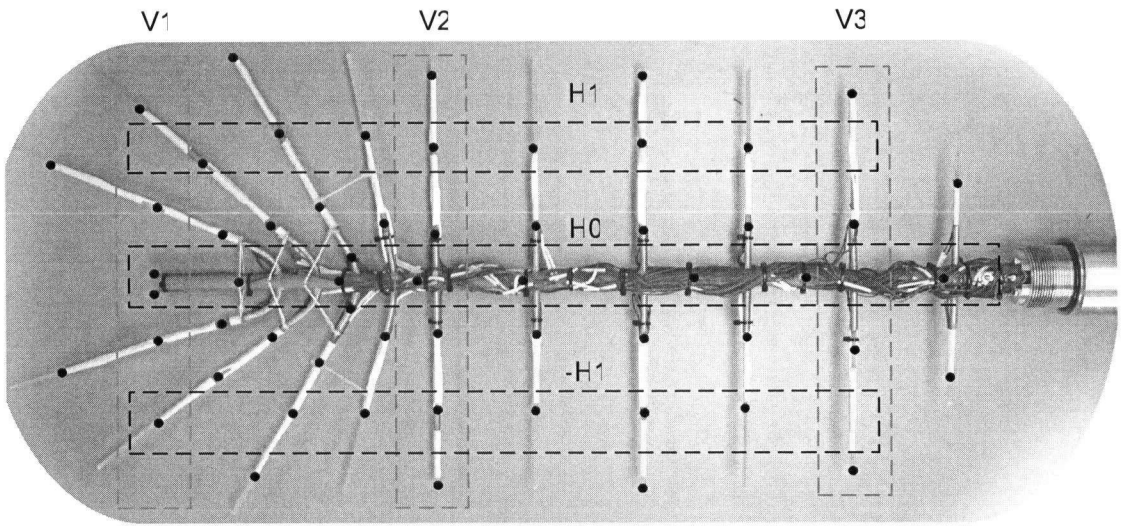

Figure 2-4: Thermocouple support mechanism. The symbols indicate the sensor positions.

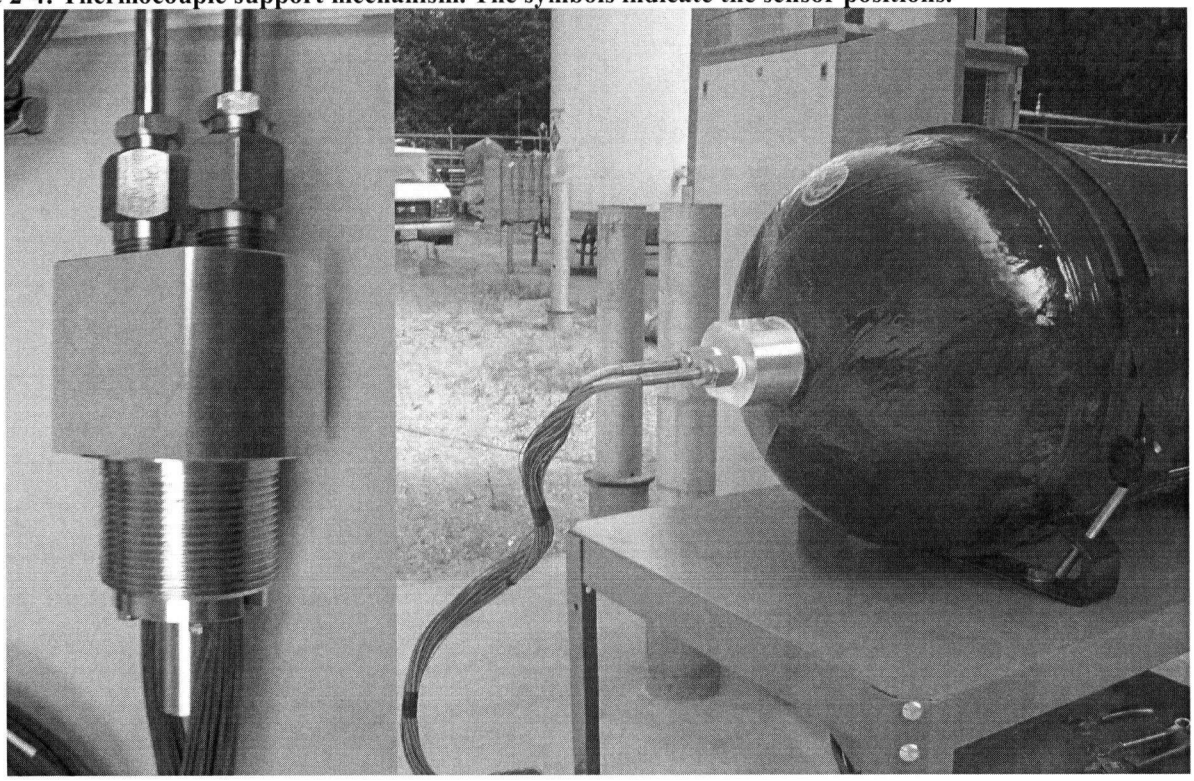

Figure 2-5: Custom designed end fitting (left). Test cylinder during testing (right).

Vertical Slices	Coordinates (x/L,y/R)	Horizontal Slices	Coordinates (x/L,y/R)
V1	(0.2,-0.28)(0.19,-0.66)(0.2,0.77)	H1	(0.11,0.54)(0.26,0.51)(0.35,0.34)

	(0.21,0.33)(0.2,0.04)(0.2,-0.04)		(0.32,0.64)(0.4,0.62)(0.45,0.57) (0.55,0.57)(0.64,0.58)(0.74,0.56)(0.93,0.43)
V2	(0.45,-0.94)(0.45,-0.61)(0.45,-0.24) (0.46,0.89)(0.45,0.57)(0.45,0.21) (0.44,0)	H0	(0.2,0.05)(0.28,0)(0.68,-0.02)(0.44,0) (0.54,-0.01)(0.36,-0.01)(0.79,0)(0.92,-0.02)
V3	(0.86,-0.89)(0.85,-0.32) (0.83,0.81)(0.84,0.33)	-H1	(0.19,-0.66)(0.31,-0.63)(0.38,-0.63)(0.45,-0.61)(0.55,-0.60)(0.65,-0.63)(0.75,-0.61)(0.95,-0.51)

Table 2-3: Coordinates of thermocouples that make up slices V1, V2, V3, H1, H0, -H1

The areas delimited by the dashed lines in Figure 2-4 correspond to vertical and horizontal slices cut through the plane of the thermocouple support mechanism inside the test cylinder. V1 is located at the inlet end of the cylinder while V3 is located at the opposite end. H1 is located in the top half of the cylinder, -H1 is located in the bottom half of the cylinder, etc.

2.5 RESULTS

2.5.1 Repeatability

The electronic dispenser provided a reproducible mechanism to perform many fill simulations with the same initial and final conditions. For example, Figure 2-6 shows the increase in temperature and pressure for three fills from a partially empty tank (100 bar nominal initial pressure), to the rated mass of gas of the cylinder (1.79 kg of H2) as measured by the dispenser. These and other experiments were used to corroborate the reproducibility of the pressure increase given the same preset pressure ramp rate. The fills where completed on separate days with ambient temperatures in the range of 15-30 °C, to simulate real operating

conditions for different climates. The results show that within this range of ambient temperatures, normalizing the results using the initial gas temperature accounts for the differences in environmental conditions.

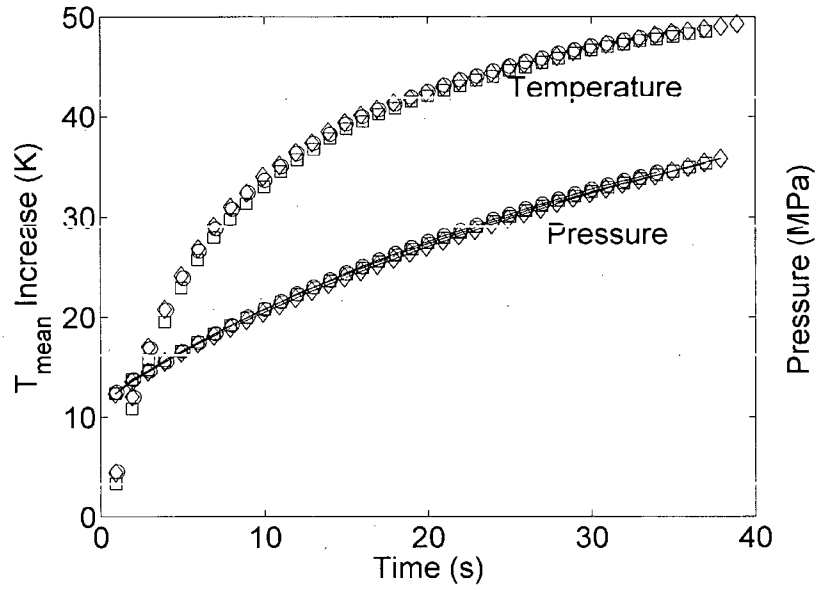

Figure 2-6: The pressure and temperature rise curves were very reproducible for the same initial and final conditions. The plots show three representative data sets (from P_i = 100 bar to the rated capacity).

2.5.2 Effect of Initial Pressure/Mass of Gas

Several fills where performed from nominal initial pressures of 50, 70, 100, 150, and 200 bar (i.e., ranging from 5×10^6 to 2×10^7 Pa). The experiments were automatically halted when the dispenser determined that the mass of gas within the cylinder had reached the rated capacity. The pressure ramp rate setting used during each fill were kept constant.

Figure 2-7 shows the volume average temperature (T_{mean}) rise during the fill normalized by the initial temperature of the gas, for initial pressures of 50, 100 and 200 bar. The volume averaged temperature (henceforth referred to as the mean temperature, T_{mean}) is calculated using equation 2-7. Where y_k is the absolute value of the vertical distance of the

thermocouple to the centreline of the cylinder, T_k is the temperature reading of the thermocouple, and A_k is an area weighting given to each thermocouple.

$$T_{mean} = \frac{\sum_{k=1}^{63} y_k T_k A_k}{\sum_{k=1}^{63} y_k A_k} \tag{7}$$

All three curves show similar features: the greatest increase in temperatures occurs at the onset of filling and the rate of temperature increase gradually diminishes throughout the fill. The fill from 50 bar initial pressure shows the greatest increase in temperature while the fill from 200 bar shows the smallest increase in temperature. Hence, filling from a higher initial pressure yields a lower overall temperature rise. This is due to a greater amount (mass) of hydrogen dispensed when started from lower pressure. Since the dispenser is programmed with set pressure ramp rates, fills starting from higher pressures are shorter as less time is needed to achieve the desired amount of mass.

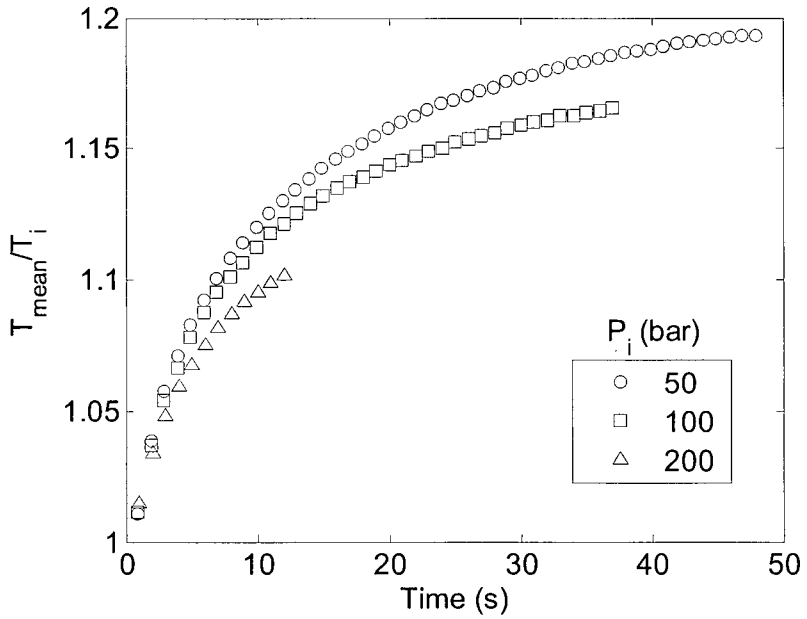

Figure 2-7: The temperature rise during fills from 50, 100, and 200 bar to the rated capacity.

Hydrogen deviates from ideal-gas behaviour at high pressures. For this reason, our model used the Redlich-Kwong equation of state for hydrogen to calculate the initial and final mass of gas within the cylinder (from the experimental measurement of pressure and temperature). The use of the volumetric average of the 63 thermocouples within the cylinder provides a much more accurate assessment of the true average gas temperature than would be attained by a single temperature probe. The effect that initial mass within the cylinder has on the final temperature of the gas is illustrated in Figure 2-8. The ratio of mean temperature to initial temperature is plotted against the ratio of final mass of gas to the initial mass of gas (the final mass is essentially the same for all fills). By normalizing both the temperature increase and the mass increase a trend is clearly shown. A point is included at the beginning of the fill (without dispensing any gas the temperature of the cylinder gas will remain the same). The relative increase in normalized temperature per unit of normalized mass dispensed decreases as the amount of gas dispensed increases. The shape of the curve can be fitted to an expression of the form:

$$\frac{T_{mean}}{T_i} = \left(A + B(m/m_i)^{1/2}\right)^C \tag{8}$$

The observed curves are very similar to the shapes predicted by the analysis of Reynolds and Kays [7]. However, explaining the physical significance of the fitted parameters, or justifying the merits of a particular model is beyond the scope of the present work. However, we note that this type of empirical expressions can be useful to characterise cylinder designs. They could also be used in practical dispensing schemes based on temperature and pressure measurement only.

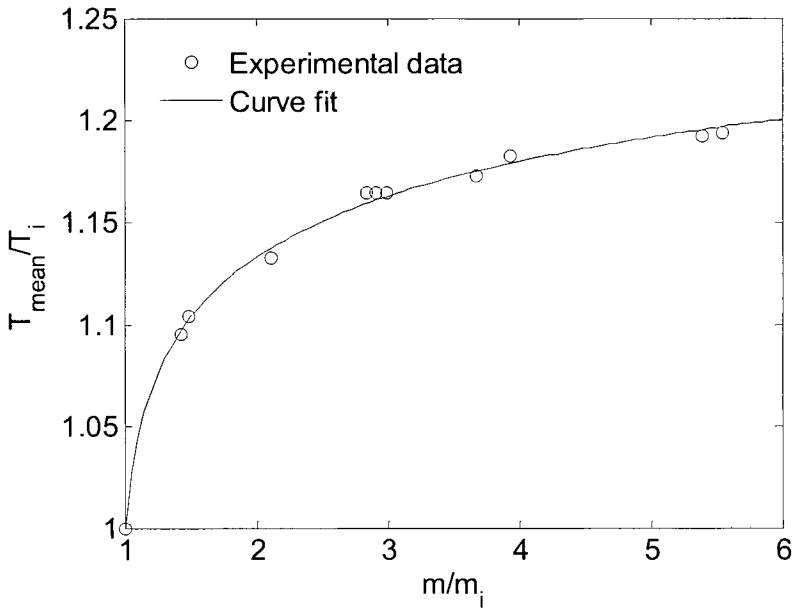

Figure 2-8: The measured normalized temperature vs. the normalized mass fits a curve given by Equation 2-7.

2.5.3 Effect of Fill Rate

Figure 2-9 plots the normalized mean temperature throughout three fills with t_{total} = 40, 190 and 370 s. All three fills where initiated from a nominal initial pressure of 100 bar and were filled to the rated capacity of the cylinder yielding a ratio of final mass to initial mass of gas of 3.0. The large temperature rise at the beginning of filling is characteristic of a large initial mass flow rate of gas into the cylinder. This is an inherent characteristic of the dispenser design and geometry. After this initial rise in temperature, each fill proceeds at a separate pressure ramp rate leading to different overall fill times. The temperature rise is greatest for the short (40 s) fill and smallest for the long (370 s) fill. The lower final temperature of longer fill times is due to the increased amount of time for heat transfer between the gas and the cylinder wall. The effect of fill time is described by plotting the final temperatures versus the

total fill time as indicated by the large circles in Figure 2-9. Shorter fill times result in significantly higher final temperatures.

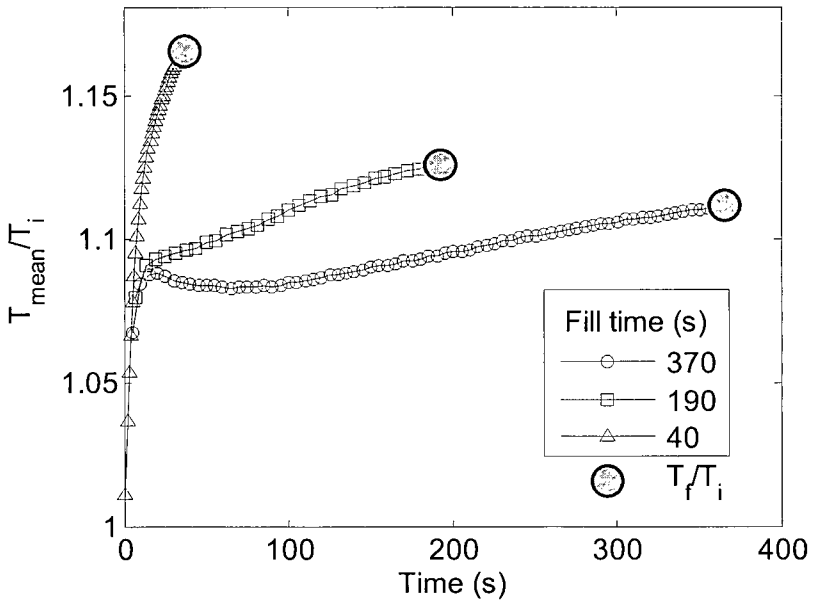

Figure 2-9: The measured normalized temperature rise for three values of t_{total} ($m_f/m_i = 3$).

To quantify the temperature variation within the cylinder we calculated the standard deviation of the 63 temperatures. A larger standard deviation implying a greater degree of temperature variation, and a lower standard deviation identifying a more uniform temperature field. Figure 2-10 shows the calculated values for σ_T for three fills. All three fills have a ratio of final to initial mass of 3.0.

The 40 s fill shows the lowest temperature variation and the greatest variation in temperature was observed during the 370 s fill. The results of Figure 2-10 lead to the conclusion that longer fill times and hence lower mass flow rate into the cylinder results in a greater temperature variation within the cylinder. This is likely the result of temperature stratification in the cylinder due to buoyancy forces which are not negligible at low flow rates.

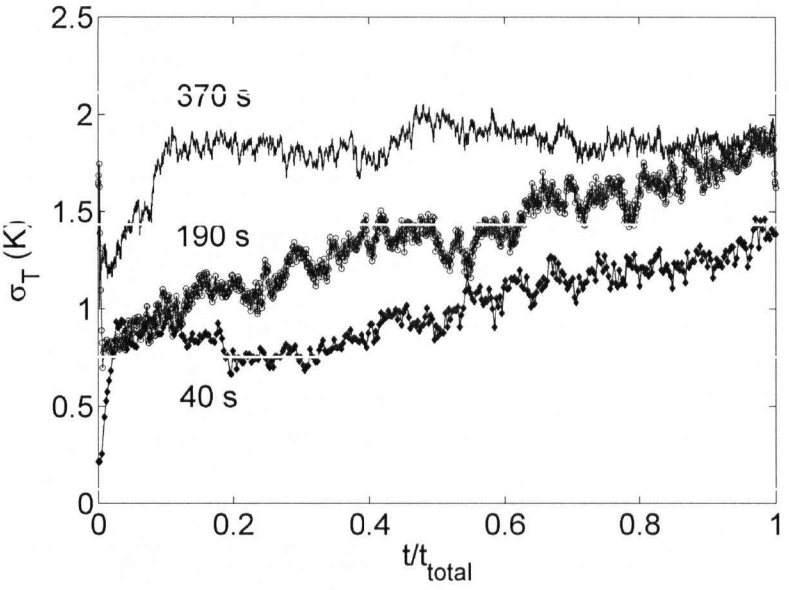

Figure 2-10: The instantaneous standard deviation in temperature over three fills.

A lower mass flow rate results in a lower gas inlet velocity and hence a lower Froude number. For a five-minute fill from 100 bar to a settled pressure of 350 bar, the Froude number of the gas will approach unity near the end of the fill. At this point the effect of the inertial forces, and the buoyancy forces on the velocity and temperature field within the cylinder become equivalent.

The fill and initial cool down stage of the 40 s fill from 100 bar to 350 bar is shown in Figure 2-11. Plotted in the figure is the standard deviation of the 63 thermocouples and the normalized mean temperature against time. Of interest, the standard deviation at the end of the fill dips down to a minimum and then quickly rises thereafter. This behaviour is the result of the gas temperature at the in cylinder inlet region rapidly approaching the mean temperature at the conclusion of filling. The increase in standard deviation thereafter is due to a greater temperature stratification as the temperature field settles out and is completely dominated by natural convection. Once the temperature field settles out, the standard deviation reaches a

maximum approximately 1 minute after the end of the fill and then decreases. The standard deviation and normalized mean temperature as the cylinder and gas within cool back down to ambient temperature is plotted in Figure 2-12. The result indicates the mean temperature of the gas decreases rapidly in the first five minutes after the end of the fill. This is thought to be the result of heat transfer from the gas to the cylinder liner which is large at the end of the fill due to a significant temperature difference between the gas and liner. Once the temperature difference between the gas and liner settles out, the rate of mean temperature change slows.

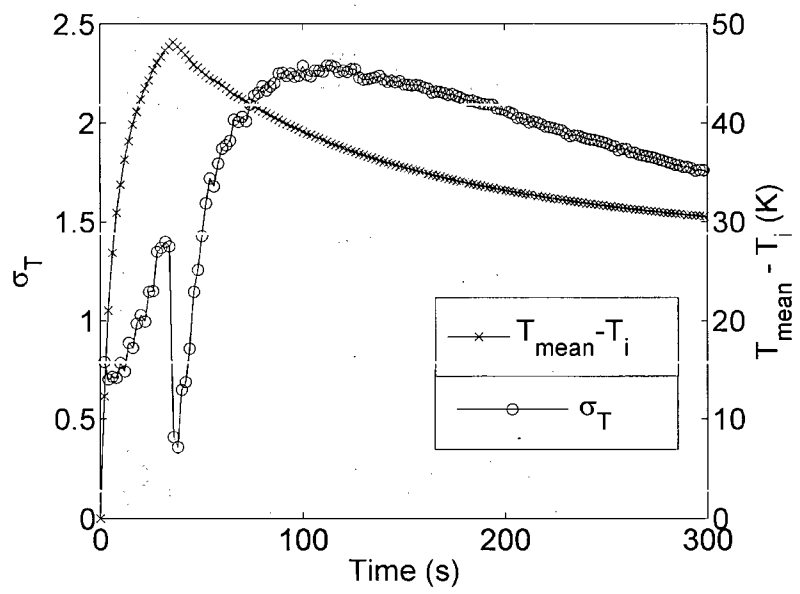

Figure 2-11: Normalized mean temperature and instantaneous standard deviation for the 40 s fill during and five minutes after the fill.

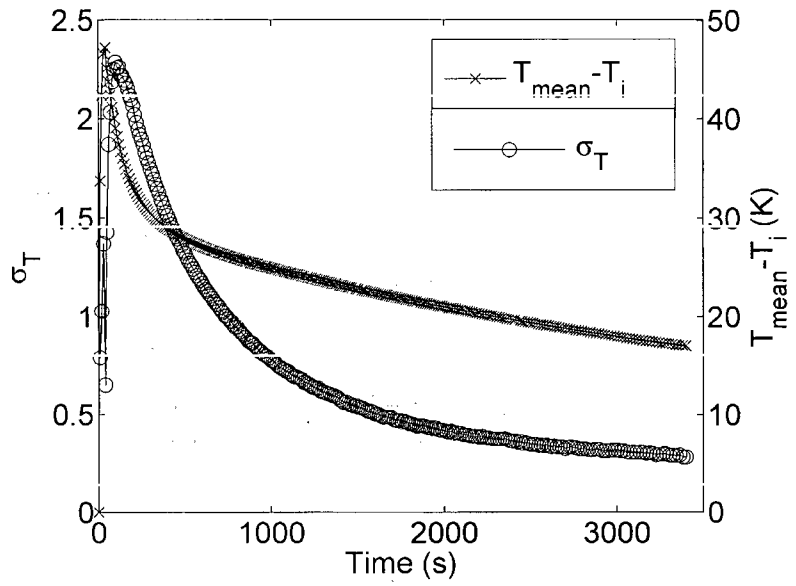

Figure 2-12: Normalized mean temperature and instantaneous standard deviation for the 40 s during the post fill cool down.

The overall effect of fill time and mass of gas dispensed is summarized in Figure 2-13 and the relevant curve fitting parameters are summarised in Table 2-4. The normalized final temperature is plotted against the normalized initial mass of gas for the three different fill times investigated in this study. Included in Figure 2-13 is a plot of the normalized temperature against the normalized mass for an adiabatic fill. The curve is the solution of equation (2-6) for the case of an adiabatic fill ($\dot{Q} = 0$). Slower fills result in a lower final temperature of gas due to the additional time available for the cylinder liner to absorb the heat of compression. For a fixed final mass, the lower the initial mass of gas the greater the final temperature will be, however, the greatest increase in temperature occurs with the initial increase in mass. No fill time is given for the adiabatic fill as the temperature rise is independent of fill time because no heat is transferred in the process. The adiabatic fill represents the maximum temperature increase during a fill. The difference between the

adiabatic fill and the 40, 190 and 370 s fills is the amount of heat transferred to the cylinder liner.

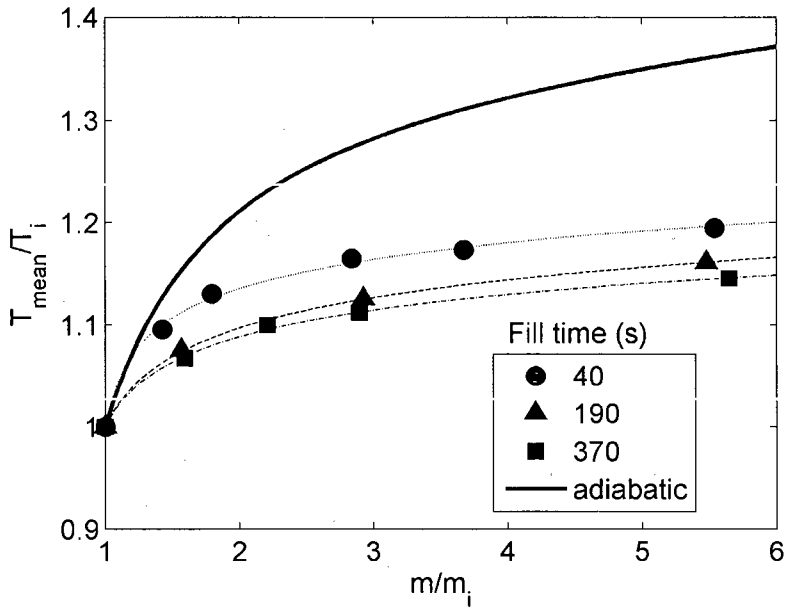

Figure 2-13: The normalized temperature vs. the normalized mass increase for three fill rates.

Fill time (s)	A	B	C
40	-35.17000	36.16000	0.04595
190	-9.50400	10.50000	0.05526
370	-10.51000	11.50000	0.04841

Table 2-4: Curve fitting coefficients for the expression in Equation 2-7.

The measured temperatures along the centreline normalized by the mean temperature at that point in time are shown in Figure 2-14. The centreline temperature within the cylinder is important because it is the most accessible location for temperature measurements in practical applications with cylindrical fuel tanks. The measured temperature along the centerline increases significantly from the inlet to the first thermocouple location. The lack of

thermocouples in the first 15% of the length of the cylinder is due to the inlet tube which extents from the cylinder valve block approximately 10 cm into the cylinder as seen in Figure 2-2. All three plots show a similar temperature profile with a rapid increase in temperature as the gas exits the inlet tube. The temperature increased from the inlet towards the opposite end where it approached the mean temperature. The temperature profile along the centerline has a similar shape in each of the three fills and throughout the duration of each fill.

Figure 2-15 is a plot of the temperature profile in three vertical planes (V1, V2, V3). The temperature is normalized using the average temperature at the time of measurement. The distance from the centreline is normalized using the inner radius of the cylinder. The curves correspond to the instantaneous temperature at $t = t_{total}/2$ for three fill rates. These curves show a dip in temperature at the centreline as the jet of the cooler gas from the inlet is directed along the axis of the cylinder. The fastest fill shows the most uniform temperature in the top and bottom half of the cylinder. The 190 and 370 s fills show a vertical stratification of temperature. The degree of stratification increases with fill time as the slowest fill shows the greatest temperature variation in the vertical direction. This result shows that buoyancy will have a significant effect on the temperature distribution within the cylinder at longer fill times.

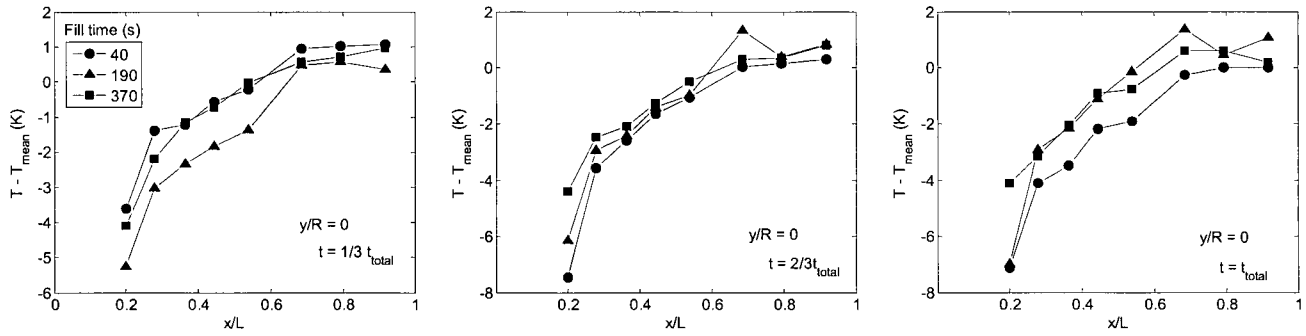

Figure 2-14: The measured temperature along the cylinder axis for $t = t_{total}/3$, $2t_{total}/3$, and t_{total} (left, middle, right, respectively).

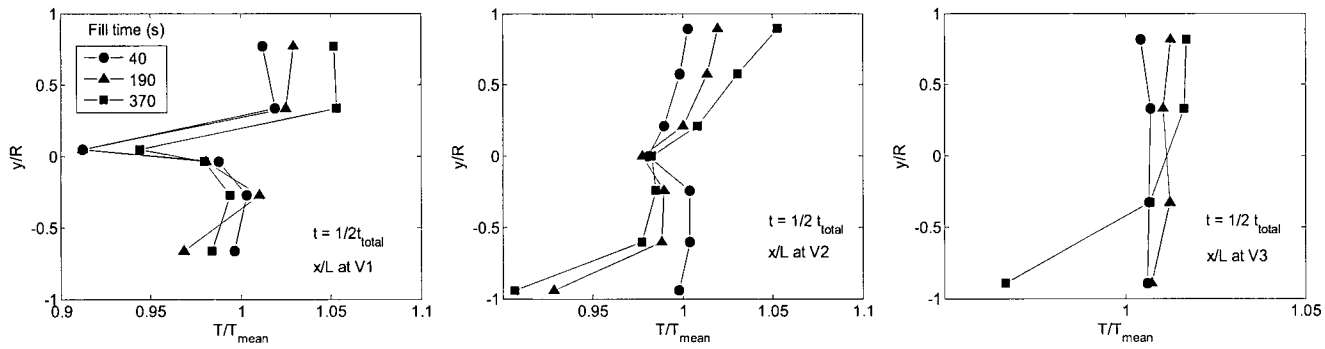

Figure 2-15: The measured temperature along the vertical planes V1, V2, V3 (left, middle, right, respectively) at $t = t_{total}/2$ for three fills.

The overall temperature distributions at $t= t_{total}/2$ through the 40 second, 190 second and 370 second fills are shown in Figure 2-16. In these plots the temperatures measured by the 63 thermocouples inside the cylinder are used to create a contour plot of the temperature field within the cylinder. The greater mass flow rate into the cylinder which occurs during a shorter fills generated temperature distributions that were essentially symmetric about the cylinder axis. We have compared this field to a 2D axially symmetric CFD model. The model predicted the shape of the temperature field accurately throughout the fill. For the slower fills, the temperature distribution became more and more stratified in the vertical direction owing to the lower gas velocity at the inlet, allowing buoyancy forces to become a significant influence on the temperature field.

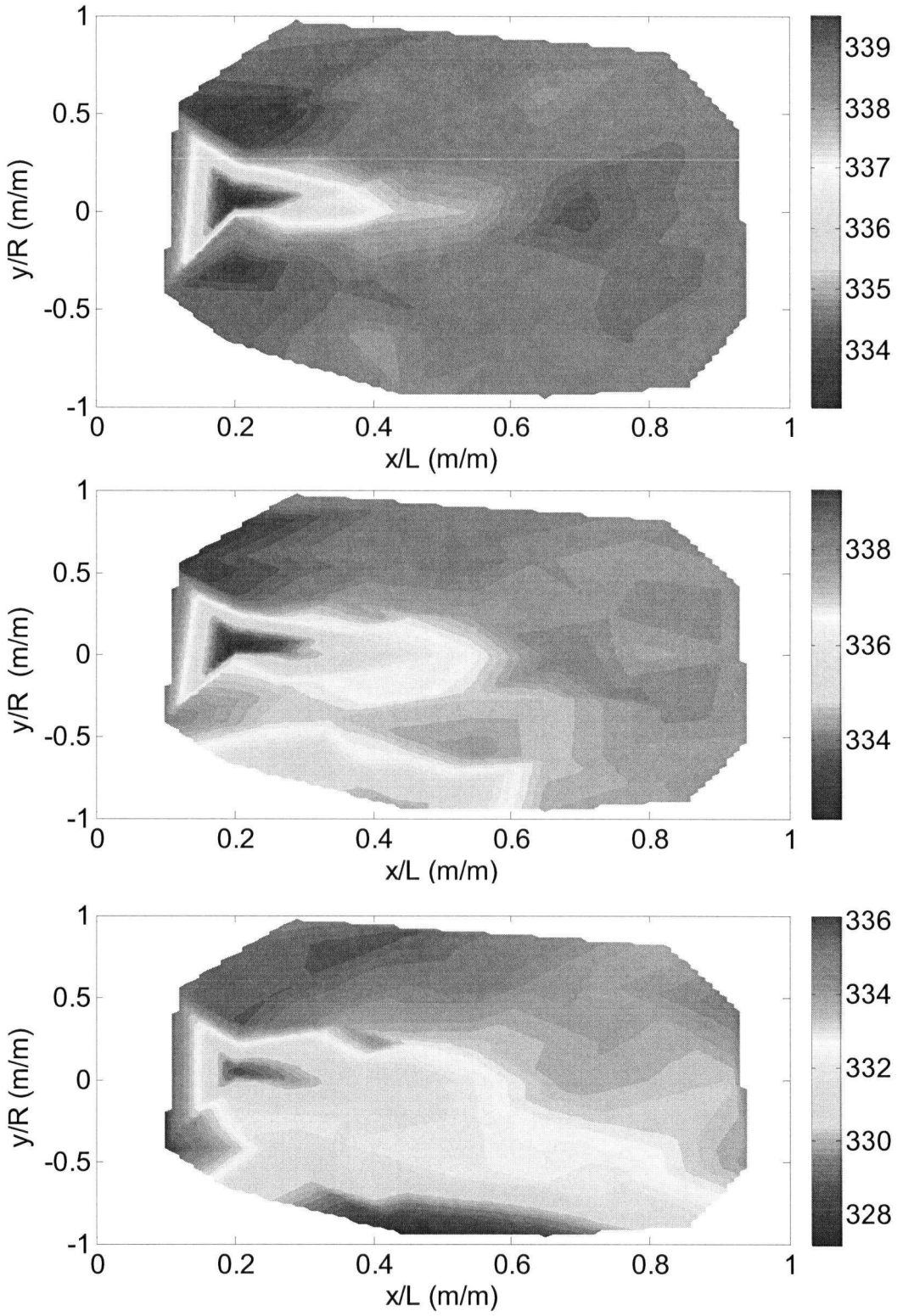

Figure 2-16: Measured temperature distribution (in K) at $t = t_{total}/2$ for t_{total} = 40, 190, and 370 s (top, middle, bottom, respectively).

Two full temperature profile series along the three vertical slices in Figure 2-3 (V1, V2, V3) are plotted in Figure 2-17. The series on the left and right correspond to the shortest and longest total fuelling times (t_{total} = 40 and 370 s) respectively. For both fill rates, the temperature profiles along V1 show a significant dip in temperature at the cylinder centerline (due to the cool inlet gas). In all three planes, the long fill has a considerable temperature stratification when compared to its shorter counterpart. As previously noted, this is the result of the greater influence of buoyancy forces during the longer fill. Neglecting the dip in temperature along the centerline, the short fill shows a nearly uniform temperature in the vertical direction throughout the fill.

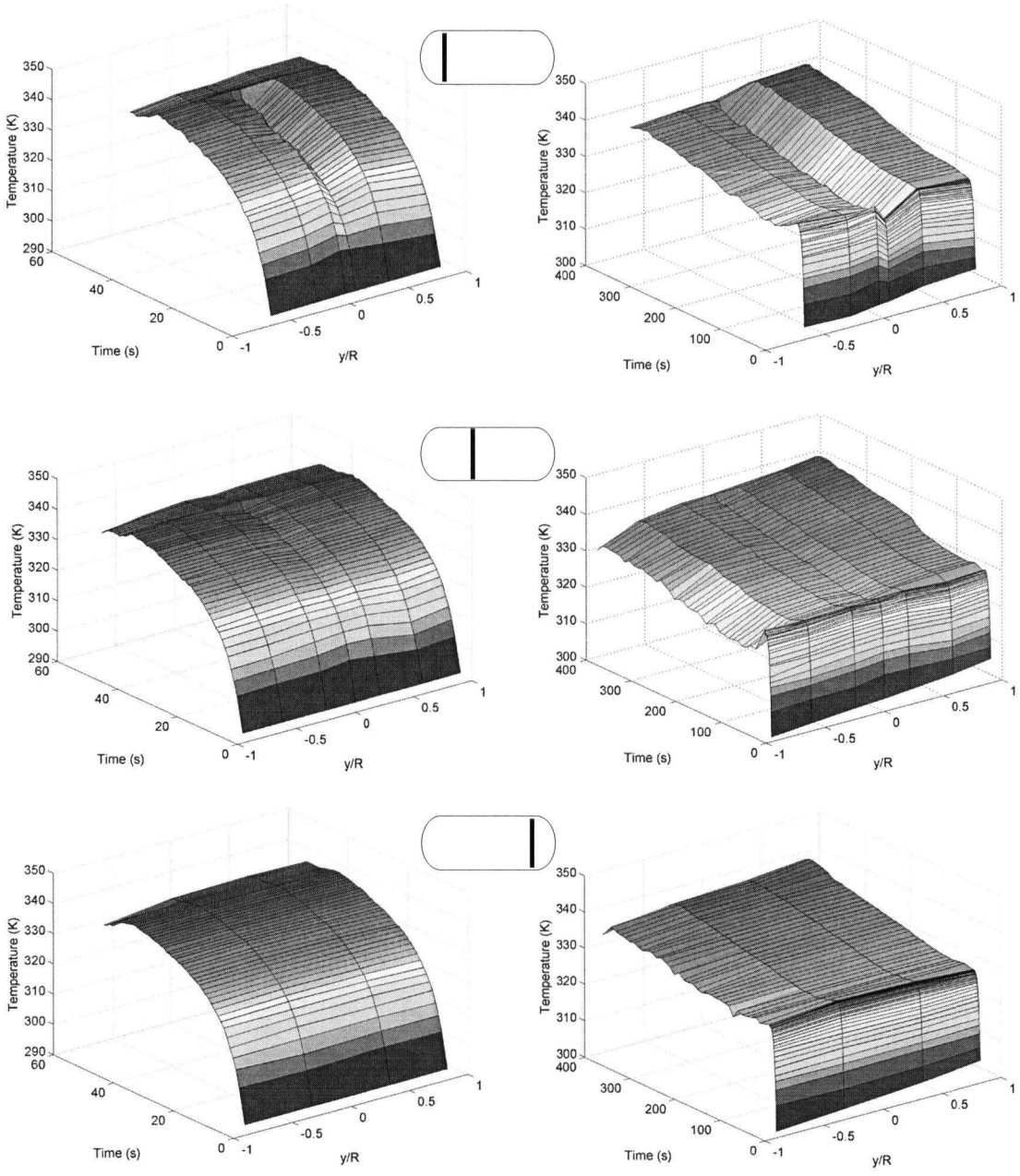

Figure 2-17: Measured temperature distribution along three vertical slices (V1, V2, V3 correspond to top, middle, and bottom) during fast and slow fills. t_{total} = 40 and 370 s (for the left and right series, respectively).

Similarly, the temperature profiles along the three horizontal slices in Figure 2-3 (H1, H0, -H1) are plotted in Figure 2-18. For the short fill the temperatures along H1 and –H1 are

essentially uniform. The longer fill shows more temperature variation along slices H1 and –H1. Figure 2-17 and Figure 2-18 include data for $t = t_{total} + 10$ s. These data illustrate the temperature field that develops immediately after the conclusion of the fill. The figures show that the temperature near the inlet of the cylinder increases towards the mean gas temperature soon after the completion of the fill. The temperature field within the cylinder quickly begins to stratify after the flow of gas into the cylinder stops, and buoyancy drives the separation of the cooler gas to the bottom of the cylinder and the hotter gas to the top of the cylinder.

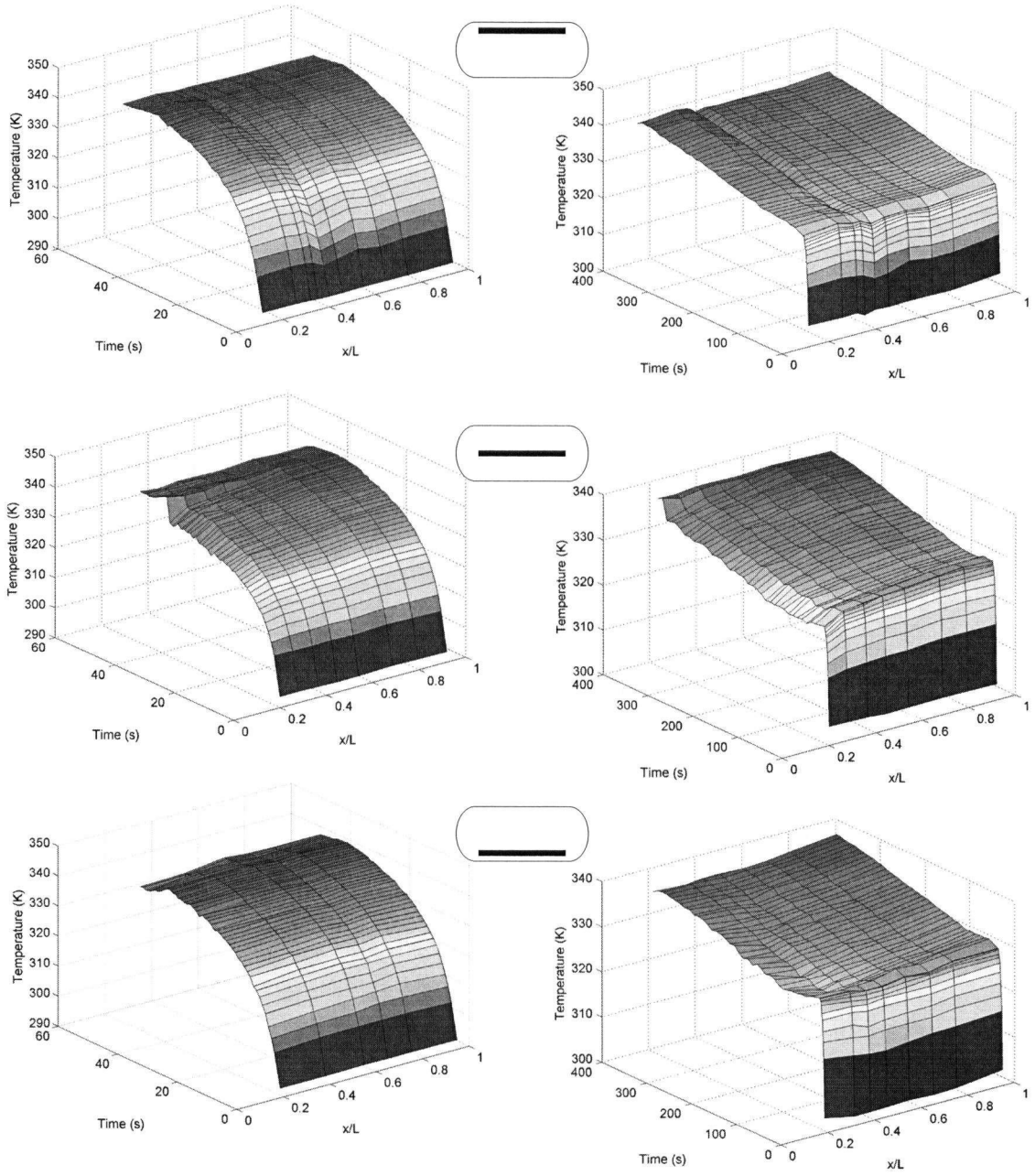

Figure 2-18: Measured temperature distribution along three horizontal slices (H1, H0, -H1 correspond to top, middle, and bottom) during fast and slow fills. t_{total} = 40 and 370 s (for the left and right series, respectively).

2.6 *CONCLUSIONS*

A 74L type 3 compressed gas cylinder was instrumented with 63 thermocouples distributed along the vertical axial plane. These sensors were used to monitor and record the temperature field inside the cylinder during numerous experimental fills. The fills were performed using the Pacific Spirit Hydrogen Fueling Station located at the National Research Councils Institute for Fuel Cell Innovation in Vancouver Canada.

The cylinder was filled from initial pressures of 50, 70, 100, 150, and 200 bar to the rated capacity of the cylinder (1.79 kg of hydrogen) in order to assess the effect of the initial mass of gas on the temperature rise during filling. The greatest rate of temperature increase occurred at the onset of filling where the ratio of the current mass of gas to the initial mass of gas was the lowest. The rate of temperature rise decreases per amount of gas dispensed as the ratio of M_f/M_i increases.

The effect of fill rate was investigated by filling the cylinder from an initial pressure of 100 bar to the rated capacity of the cylinder at fill rates corresponding to total fill times of 40, 190, and 370 seconds. The faster fills generated larger temperature changes.

The effect of fill rate on the temperature distribution of the hydrogen gas within the cylinder was demonstrated by slower fills producing a temperature field with significant stratification in the vertical direction. This stratification was attributed to the greater influence of buoyancy forces at lower gas inlet velocities. The shorter fills produced a temperature field with a large conical temperature gradient extending out from the cylinder inlet and symmetrical about the cylinder axis.

The end opposite to the gas inlet experiences an instantaneous local temperature that best reflected the mean temperature of the gas. As a result, this end of the cylinder is identified

as the optimal location for the temperature sensors aimed at metering fuel based on combined temperature and pressure measurements.

2.7 NOMENCLATURE

A	Curve fitting coefficient	
a	Redlich-Kwong constant for hydrogen	
B	Curve fitting coefficient	
b	Redlich-Kwong constant for hydrogen	
C	Curve fitting coefficient	
c_p	specific heat at constant pressure	J/molK
c_v	specific heat at constant volume	J/molK
H_j	Sensor subset for horizontal temperature planes (j =0, ±1)	
h_{in}	specific enthalpy	J/mol
L	Cylinder length	m
M	Molar Mass of Hydrogen	kg/mol
m	Mass of gas inside the cylinder	kg
m_i	Initial mass of hydrogen in the cylinder	kg
$\dot{m}$	mass flow rate	kg/s
$\dot{Q}$	heat transfer rate	W
P	Pressure	bar
P_i	Initial pressure inside the cylinder	bar
R	Cylinder radius	m
R_{gas}	Universal gas constant	J/molK
T	Temperature	K
T_i	Initial temperature inside the cylinder	K
T_{in}	Temperature of inlet gas	K
T_{mean}	Volumetric Mean temperature	K
T	time	s
U	Internal energy	J
u	specific internal energy	J/mol
V_i	Sensor subset for vertical temperature planes (i =1, 2, 3)	
v_{in}	specific volume of inlet gas	m^3/mol
V	internal volume of the cylinder	m^3
x	Distance from cylinder inlet	m
y	Vertical distance from cylinder axis	m

2.8 REFERENCES

[1] James, B., G. Baum, and F. Lomax, Comparison of Onboard Hydrogen Storage for Fuel Cell Vehicles. *Directed Technologies Inc., Contract DE-AC02-94CE50389*, (1996).

[2] ISO, Gaseous Hydrogen and Hydrogen Blends. Land Vehicule Fuel Tanks Part 1: General Requirements (ISO 15869). *International Standard Organization*, (2005).

[3] Charton, S., V. Blet, and J.P. Corriou, A Simplified Model for Real Gas Expansion between Two Reservoirs Connected by a Thin Tube. *Chemical Engineering Science*, 51(2), (1996) 295-308.

[4] Daney, D. E., F. J. Edeskuty, and M. A. Daugherty, Hydrogen Vehicle Fueling Station. *Advances in Cryogenic Engineering*, 41, (1996) 1041-1048.

[5] Haque, M. A., M. Richardson, and G. Saville, Blowdown of Pressure Vessels - I. Computer Model. *Trans.IChemE*, 70(Part B), (1992) 3-9.

[6] Kountz, K., W. Liss, and C. Blazek, A New Natural Gas Dispenser Control System. *Proceedings of the 1998 International Gas Research Conference*, (1998) 135-145.

[7] Reynolds, W. C. and W. M. Kays, Blowdown and Charging Processes in a Single Gas Receiver with Heat Transfer. *Transactions of the ASME*, (July), (1958) 1160-1168.

[8] Xia, J., A Simplified Model for Depressurization of Gas-Filled Pressure Vessels. *Int. Comm. Heat Mass Transfer*, 20, (1993) 653-664.

[9] Haque, M. A., M. Richardson, and G. Saville, Blowdown of Pressure Vessels - II. Experimental Validation of Computer Model and Case Studies. *Trans.IChemE*, 70(Part B), (1992) 10-17.

[10] Newhouse, N., Fast Filling of NGV Fuel Containers. *SAE Technical Paper Series 1999-01-3739*, (2005).

[11] Schneider, J., Optimizing the Fuelling of Hydrogen Vehicles. *The Fuel Cell Review*, 2(4), (2005) 15-24.

[12] Dicken, C.J.B. and W. Mérida, Transient Temperature Distribution in a Type 3 Hydrogen Cylinder upon Refuelling. *Submitted to. ASME Journal of Heat Transfer*, (2006).

[13] Jeary, B., Fast Filling of Compressed Hydrogen Fuel Storage Cylinders, *Proceedings of the 11th Canadian Hydrogen Conference,* (2001)

[14] Kountz, K., Modeling the Fast Fill Process in Natural Gas Vehicles Storage Cylinders, *207th American Chemical Society Meeting,*, (1994)

[15] Richards, M., Liss, W., Kountz, K., Kriha, K., Modeling and Testing of Fast-Fill Control Algorithms for Hydrogen Fueling, *National Hydrogen Association's 14th Annual U.S. Hydrogen Conference and Hydrogen Expo USA*, (2003)

[16] Annamalai, K., Puri, I.K., Advanced Thermodynamics Engineering, CRC Press, 2002

CHAPTER 3: TRANSIENT TEMPERATURE DISTRIBUTION WITHIN A HYDROGEN CYLINDER DURING REFUELLING[1]

3.1 INTRODUCTION

Compressed gas is currently the leading technology for storing hydrogen on board vehicles. This storage method utilizes a cylinder packaged within the vehicle to store the hydrogen at pressures of 350 bar (new designs at 700 bar are now in commercial production). There are four different types of compressed gas cylinders, however for transportation applications where weight minimization is crucial the two predominant cylinders are type 3 and type 4. Both types of cylinder are composed of a liner and laminate. The liner is a thin layer of material, which provides a gas tight seal, the laminate is a epoxy laden carbon-fibre wrap which provides strength. Type 3 cylinders use an Aluminum liner where as type 4 cylinders utilize a plastic liner.

Refuelling of the vehicle cylinder involves transferring high-pressure hydrogen gas from the hydrogen fuelling station tanks through a dispenser into the vehicle cylinder. The role of the dispenser is to control the rate of filling, ensure a safe fill, and to fill the cylinder to the rated mass of gas.

[1] A version of this chapter has been submitted for publication. Dicken C.J.B. and Merida W. (2006) "Transient Temperature Distribution Within a Hydrogen Cylinder During Refuelling", Journal of Heat Transfer.

The present standards governing compressed gas cylinders for vehicular applications limit the gas temperature within the cylinder to a maximum of 358 K and limit the gas pressure to a maximum of 1.25 times the design pressure (for a 350 bar cylinder the maximum fill pressure is 438 bar) of the cylinder [1, 2]. The practical refuelling times for compressed gas cylinders are limited by the maximum temperature requirement.

The accuracy of the fill is defined in terms of the ratio of mass of gas at the completion of filling to the rated mass of gas for the cylinder model. The temperature limitations of the cylinder also affect the accuracy of the fill. When a fill reaches the 358 K limitation the fill is stopped regardless of the mass of gas dispensed. This leads to under filling of the vehicle cylinder.

While much work has been done to measure and model the temperature rise of the gas during filling [3-17], the modeling studies to date have all assumed uniform temperature within the cylinder. The assumption is necessary in order to perform a control volume analysis of the cylinder or vessel that is being filled. Having assumed uniform temperature, the more advanced models attempt to predict the heat transfer from the gas in the cylinder to the cylinder walls and out to the surroundings. To do this, the model must determine the convective heat transfer coefficient between the gas and cylinder wall. While many empirical correlations exist for calculating the Nusselt number for the case of forced convection, these correlations require knowledge of the local Reynolds number inside the cylinder. The models treat the cylinder as a single control volume and as a result the velocity profile inside the cylinder is not resolved. This makes it impossible to calculate the local Reynolds number. Furthermore, the direction of flow inside the cylinder is not uniform, there exists backflow as

the gas entering the cylinder reflects off the back wall of the cylinder. Hence, in most models, the Reynolds number inside the cylinder is assumed or is a parameter used for fitting data to experimental results.

In order to accurately model the heat transfer from the gas to the cylinder, a model must discretize the space within the cylinder. By performing spatial discretization, the model can determine the temperature and velocity profiles within the cylinder, which in turn will allow for the calculation of the convective heat transfer at the cells along the wall. This method allows for the calculation of the average temperature, but also provides the temperature at numerous locations on the grid of discrete points inside the cylinder. Thus affording an appropriate comparison between the local temperature predicted by the model and the experimental measurements of local temperature.

Only a few of the experimental studies to date have placed more than one temperature sensor within the cylinder to measure gas temperature. The only study that has placed enough temperature sensors within the vessel to provide a temperature distribution is the study of Haque et al. [13]. This study analyzed the blowdown of a large, cylinder shaped, steel pressure vessel. While this study provides insight into experimental techniques, due to the different geometry, gas and fill rates, their results are not directly useful for the analysis of the temperature distribution within a type 3 compressed gas cylinder. The Gas Technology institute study [11] found a significant spatial variability in temperature. Three thermocouples located at ¼, ½ and ¾ lengths of the centerline all read significantly different temperatures during filling (up to 30 K difference). Towards the end of filling the thermocouples at ¼ and ¾ lengths converged to single temperature where as the thermocouple at ½ length took greater than 20 minutes to converge to the same reading as the ¼ and ¾ length thermocouples. The

study of Duncan et al. [5] found temperature differences as high as 10 K between thermocouples placed at 1/3 and 2/3 of the length of the cylinder centerline. From the end of filling it took ~ 5 minutes for these thermocouples to read a uniform temperature.

Our study challenges the assumption of uniform temperature by studying the gas temperature distribution within the cylinder during filling. The goal of this study is to investigate the temperature field within a compressed gas cylinder during filling, in order to determine the average temperature of the hydrogen gas which will allow for the calculation of density based on pressure and temperature.

A computational fluid dynamics (CFD) model has been developed that spatially discretizes the cylinder in order to predict the distribution of gas temperature. The model considered, compressible unsteady viscous flow, real gas effects, heat transfer to the cylinder walls and conduction through the cylinder walls to ambient. The model was validated by comparison with a set of experimental fast fills of a compressed gas cylinder instrumented with 63 thermocouples distributed throughout the cylinder in an effort to measure the gas temperature distribution within the cylinder and provide an accurate estimate of the average gas temperature within the cylinder.

The validated model assesses the difference between the local measurements of temperature inside the cylinder and the average temperature based on the position of the local measurement. The model also helps to identify the best locations for the onboard temperature sensor such that the local measurement best represents the average gas temperature for a range of fill conditions. A validated model will also serve to provide insight into the heat transfer processes which occur during filling.

3.2 *THEORY*

Inherent to the fill process is a significant increase in gas temperature. The temperature rise during filling is the result of the combination of two phenomena. Hydrogen has a negative Joule-Thomson coefficient at the temperatures and pressures of filling. Hence an isenthalpic expansion of the gas from the high-pressure tank through the dispenser throttling device into the low-pressure cylinder results in an increase in hydrogen temperature. It is important to emphasize that the isenthalpic expansion occurs within the dispenser and the result is a higher gas temperature entering the cylinder.

The second phenomenon that causes a temperature rise during filling is the compression of the gas inside the cylinder. At the start of filling the gas is compressed by the introduction of the higher-pressure gas from the fuelling station. This is repeated throughout the fill as the addition of gas into the cylinder compresses the gas already in the cylinder. When gas is compressed it will increase in temperature. The increase in temperature is often referred to as the heat of compression.

A comparison of the magnitudes of these two phenomenon shows that the Joule-Thomson effect has an insignificant effect on the overall temperature rise when consideration is given to the thermodynamics of the entire process [14].

The temperature rise is mitigated through heat transfer from the gas to the cylinder walls. The physics of the fill process are illustrated in Figure 3-1.

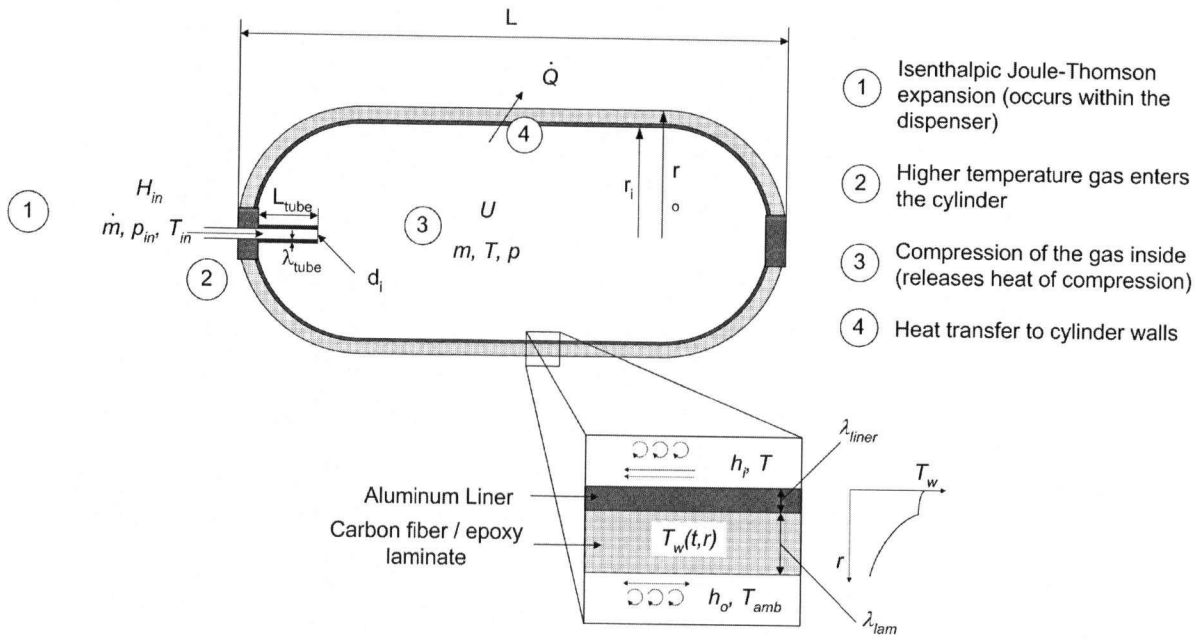

Figure 3-1: Schematic of filling a compressed gas cylinder

3.2.1 Dimensional Analysis

A dimensional analysis of the flow entering the cylinder provides insight into the nature of the flow field. In this study, a 74L, 350 bar cylinder is used for testing. The rated mass of gas of the cylinder at 350 bar and 15 °C is 1.79 kg of hydrogen gas. The flow rate required to fill a cylinder with an initial pressure of 100 bar to the rated mass of gas depends on the desired fill time. For this analysis we assume a lower and upper bound on fill time of 40 seconds and 5 min respectively. The Reynolds number at the inlet can be determined using equation 3-1 below.

$$\mathrm{Re}_i = \frac{\dot{m} d_i}{A_i \mu_i} \tag{3-1}$$

Where d_i is the diameter of the inlet, A_i is the cross-sectional area of the inlet, $\dot{m}$ is the average mass flow rate of hydrogen, and μ is the viscosity of the gas. While the viscosity of the gas will vary throughout the fill depending on the density and temperature of the gas at the

inlet, the average Reynolds number at the inlet is on the order of 10^5. This is well within the turbulent flow regime and hence the flow at the inlet is considered turbulent.

Another important dimensional parameter for this analysis is the Froude number. This dimensional parameter relates the inertial and gravitational forces acting on the fluid. The Froude number is defined by equation 3-2.

$$Fr_i = \frac{u_i}{\sqrt{2gr_i}} \tag{3-2}$$

Where u_i is the velocity of the gas at the inlet, g is the acceleration due to gravity and $2r_i$ is used as the vertical length scale. The vertical length scale is defined by the inside diameter of the cylinder. The velocity of the gas at the inlet will vary throughout the fill. At the onset of filling the velocity of the hydrogen gas at the inlet quickly reaches its peak (within the first few seconds) and then declines slowly as the density of the gas inside the cylinder increases. It is important to note that the dispenser controls the filling rate and hence the velocity of the gas at the inlet never reaches the sonic point. The Mach number at the inlet is defined by equation 3-3.

$$Ma = \frac{u_i}{c_s} = \frac{\dot{m}}{c_s \rho_i A_i} \tag{3-3}$$

Where $\dot{m}$ is the average mass flow rate of hydrogen gas, c_s is the speed of sound of the gas, ρ_i is the density of the gas at the inlet and A_i is the cross sectional area of the inlet. The initial and final inlet Mach numbers for the case of a 40 second and 5 minute fill are shown in Table 3-1.

	40 second fill	5 minute fill
Start of Fill	0.140	0.02
End of Fill	0.036	0.005

Table 3-1: Inlet Mach numbers for 40s and 5min fill.

The inlet is the location of highest velocity within the cylinder and hence based on the results listed in Table 3-1, the flow everywhere within the cylinder can be considered subsonic.

With u_i determined from the Mach number, the Froude number can be calculated using equation 3-2. The resultant Reynolds and Froude numbers are summarized in Table 3-2.

	40 second fill		5 minute fill	
	Re_i	Fr_i	Re_i	Fr_i
Start of Fill	8.2×10^5	99	1.1×10^5	13
End of Fill	7.23×10^5	34	1.0×10^5	4

Table 3-2: Summary of Re and Fr numbers for a 40 second and 5 minute fill.

For a 40 second fill the Reynolds number indicates the flow is turbulent and that the effect of gravity on the flow is small in comparison to the inertial forces. For the 5-minute fill the flow is also turbulent throughout filling however, towards the end of the fill the effect of gravity on the flow field will become significant.

3.2.2 Model Development

The goal of the two dimensional model is to predict the temperature distribution within a compressed gas cylinder during filling. To this end the model utilizes the principles of computational fluid dynamics (CFD) to discretize the space within the cylinder and its walls,

creating numerous control volumes. The governing equations are solved over the boundaries of the control volumes to determine the characteristics of the hydrogen flow.

A model capable of predicting the temperature field within a compressed gas cylinder during refuelling can be used to determine the local "hot spots" inside the cylinder and will be able to analyze the relationship between the average gas temperature and local points of gas temperature measurements. A validated model will also help to determine the difference between the gas temperature and the liner and laminate temperatures of the cylinder. This last point is important because, at present the thermal properties of the cylinder walls limit the speed with which a cylinder can be refuelled.

The model assumes the flow within the cylinder to be axisymmetric with respect to the centerline of the cylinder. In essence, assuming the effect of gravity and buoyancy forces to be negligible when compared to the magnitude of the gas velocity entering the cylinder. It is important to note that this assumption is only valid while the cylinder is being filled. At the completion of filling gravity and buoyancy forces will significantly affect flow within the cylinder. Further to the dimensional analysis performed above, the longer the fill time, the greater the relative effect of gravitational forces on the flow field inside the cylinder. Hence the longer the fill time the less suitable the assumption of axisymmetric flow. For this reason the model was run for the case of a forty second fill.

For the purposes of this model, the liner and laminate that make up the cylinder walls are assumed to be isotropic. In actuality the thermal conductivity of the carbon fibre wrap is anisotropic due to the nature of the wrapping. Radiation heat transfer between the hydrogen gas and cylinder walls is assumed to be negligible due to the small temperature difference between the gas and liner surface.

The model is split into two computational domains. The first is the fluid domain within the cylinder, which is filled with hydrogen gas. The second domain is the cylinder wall and inlet tube. The wall is split into the liner and laminate. The geometry and shape of both domains are given in Figure 3-1. The dimensions used for the model are supplied in Table 3-3. The liner and laminate thickness along the length of the cylinder is assumed to be uniform.

Table 3-3: Cylinder Dimensions

Dimension	Description	Value	Unit
L	Length of the cylinder	0.893	[m]
r_i	Inner radius of the cylinder	0.179	[m]
r_o	Outer radius of the cylinder	0.198	[m]
λ_{liner}	Liner thickness (assumed to be uniform throughout)	0.004	[m]
λ_{lam}	Laminate thickness (assumed to be uniform throughout)	0.015	[m]
d_{inlet}	Inside diameter of the gas inlet tube	0.005	[m]
λ_{tube}	Wall thickness of the gas inlet tube	0.002	[m]
L_{tube}	Length of the tube protruding into the cylinder	0.082	[m]

The flow within the cylinder, and heat transfer through the walls, vary with time; hence all governing equations must be solved in their unsteady form. While the heat of compression dominates the increase in temperature during filling, viscous effects are important for accurately determining the convective heat transfer from the gas to the cylinder liner. Due to the high gas velocities at the inlet and due to the fundamental problem of density

varying with time, the model incorporates compressibility effects. A real gas equation of state is used instead of the ideal gas law due to the high density of the gas at the pressures of filling. As seen in the preceding section the flow at the inlet is turbulent throughout the fill and hence the model solves the Reynolds averaged governing equations using a turbulence model for closure of the turbulent viscosity term.

Applying the conservation of mass to the fluid region of the model and applying Reynolds averaging techniques yields the first governing equation for a finite volume.

$$\frac{\partial}{\partial t}\bar{\rho}+\frac{\partial}{\partial x_i}\left(\bar{\rho}\tilde{u}\right)=0 \tag{3-4}$$

Where $\bar{\rho}$ is the ensemble average of density, and $\tilde{v}$ is the Favre average of velocity. The law of conservation of momentum yields the equations below.

$$\frac{\partial}{\partial t}\left(\overline{\rho}\tilde{u}_i\right)+\frac{\partial}{\partial x_j}\left(\overline{\rho}\tilde{u}_i\tilde{u}_j\right)=-\frac{\partial \overline{p}}{\partial x_i}+\frac{\partial}{\partial x_j}\left(\overline{\tau}_{ij}-\overline{\rho u_i' u_j'}\right) \tag{3-5}$$

$$\tau_{ij}=-\frac{2}{3}\mu\varepsilon_{ij}\frac{\partial u_k}{\partial x_k}+\mu\left(\frac{\partial u_i}{\partial x_j}+\frac{\partial u_j}{\partial x_i}\right) \tag{3-6}$$

The term $-\overline{\rho u_i' u_j'}$ is an unclosed term and will be modeled using the k-ε model described below. Applying the conservation of energy produces the equations below.

$$\frac{\partial}{\partial t}\left(\overline{\rho}\tilde{H}\right)+\frac{\partial}{\partial x_j}\left(\overline{\rho}\tilde{H}\tilde{u}_j\right)=-\frac{\partial \overline{p}}{\partial t}+\frac{\partial}{\partial x_j}\left(-\overline{q}_j-\overline{\rho h' u_j'}+\tilde{u}_i\overline{\tau}_{ij}+\overline{u_i'\tau_{ij}}\right) \tag{3-7}$$

$$q_j=-k\frac{\partial T}{\partial x_j} \tag{3-8}$$

$$H=h+\frac{1}{2}u_i u_i \tag{3-9}$$

The terms $\left(-\overline{\rho h' u_j'} - \overline{u_i' \tau_{ij}}\right)$ are the unclosed terms, which will be modeled with the k-e turbulence model. In addition to the governing equations for mass, momentum and energy, two more governing equations are required to describe the turbulence within the flow.

Many turbulence models exist for obtaining closure for the governing equations. The flow field developed within the cylinder is dominated by the structure of the turbulent jet of gas protruding from the cylinder inlet. Compressible turbulent gas jets have been studied extensively as they exist in many practical fluid dynamics problems. The standard k-ε model has been used in many studies of transient gas jets. Due to the assumption of isotropy inherent in the standard k-ε model the results for transient gas jets tend to over-predict the spreading rate [18-20]. Adjusting the coefficients of the k-ε model corrects for this over-prediction [18].

The standard k-ε turbulence model [21] uses two parameters to describe the turbulence of the fluid. The turbulence kinetic energy, *k*, and the rate of turbulent energy dissipation, ε, are defined as follows:

$$k_t \equiv \frac{1}{2}\overline{u_i u_i} \tag{3-10}$$

$$\varepsilon_t = \upsilon \overline{\frac{\partial u_i}{\partial x_j}\frac{\partial u_i}{\partial x_j}} \tag{3-11}$$

The transport equations for the turbulent kinetic energy and its dissipation rate are as follows [22]:

$$\frac{\partial}{\partial t}(\rho k_t) + \frac{\partial}{\partial x_i}(\rho k_t u_i) = \frac{\partial}{\partial x_j}\left[\left(\mu + \frac{\mu_t}{\sigma_k}\right)\frac{\partial k_t}{\partial x_j}\right] - \rho\overline{u_i' u_j'}\frac{\partial u_j}{\partial x_i} - \rho\varepsilon - 2\rho\varepsilon\frac{k_t}{c_s^2} \tag{3-12}$$

$$\frac{\partial}{\partial t}(\rho \varepsilon_t) + \frac{\partial}{\partial x_i}(\rho \varepsilon_t u_i) = \frac{\partial}{\partial x_j}\left[\left(\mu + \frac{\mu_t}{\sigma_\varepsilon}\right)\frac{\partial \varepsilon_t}{\partial x_j}\right] + C_{1\varepsilon}\frac{\varepsilon_t}{k}\left(-\rho\overline{u_i' u_j'}\frac{\partial u_j}{\partial x_i}\right) - C_{2\varepsilon}\rho\frac{\varepsilon_t^2}{k} \tag{3-13}$$

The k-ε model brings closure to the Reynolds averaged conservation of momentum by eliminating the term $-\overline{\rho u_i' u_j'}$ in equation 3-5 and replacing the μ in equation 3-6 by μ_t.

Where,

$$\mu_t = \rho C_\mu \frac{k_t^2}{\varepsilon_t} \tag{3-14}$$

The closure for the Reynolds averaged energy equation 3-7 is gained by eliminating the term $\left(-\overline{\rho h' u_j'} - \overline{u_i' \tau_{ij}}\right)$ and replacing the λ in equation 3-8 with λ_{eff}, and replacing μ in equation 3-6 with μ_{eff}. Where,

$$\lambda_{eff} = \lambda + \frac{c_p \mu_t}{\mathrm{Pr}_t} \tag{3-15}$$

$$\mu_{eff} = \mu + \mu_t \tag{3-16}$$

The value of the constants used in the k-e model are modified slightly as suggested by Ouellette et al. in [18]. The values are presented in the Table 3-4.

Table 3-4: Value of constants used in the k-ε model

Constant	Value
$C_{1\varepsilon}$	1.52
$C_{2\varepsilon}$	1.92
C_μ	0.09

Within the domain of the cylinder walls the conservation of mass and momentum do not apply as the material is solid. The conservation of energy within the cylinder wall takes the form:

$$\frac{\partial}{\partial t}(\rho_w h_w) = k_w \frac{\partial^2 T_w}{\partial x_j^2} \tag{3-17}$$

The heat transfer between the hydrogen gas and the cylinder liner is dominated by turbulent convection. The model employs a log law of the wall for mean temperature in the turbulent region of the thermal boundary layer and a linear conduction sub layer [22].

To integrate the compressibility effects of high-pressure hydrogen the model using the Redlich-Kwong real gas equation of state [23],

$$p = \frac{RT}{(v-b)} - \frac{a}{T^{\frac{1}{2}}(v(v+b))} \tag{3-18}$$

Where p denotes the gas pressure, R the universal gas constant, T is the temperature of the gas, and v is the molar specific volume. The terms a and b are constants related to the critical properties of the material through the equations:

$$a = 0.08664 \frac{R^2 T_c^{2.5}}{p_c} \tag{3-19}$$

$$b = 0.4275 \frac{RT_c}{p_c} \tag{3-20}$$

The subscript c denotes the value of the property at the critical point.

While many real gas equations of state exist for hydrogen, the Redlich-Kwong equation was chosen as it provides acceptable accuracy in the ranges of temperature and pressure in this study, and is computationally inexpensive. Other more accurate equations exist but require far more computation, which will severely limit the speed of the overall model.

The CFD software Fluent 6.2 was used to develop the model. Since Fluent does not include a real gas library for hydrogen a significant part of this work was to derive a real gas

model for hydrogen. This required creating and compiling a "user defined function" in Fluent to calculate all of the thermodynamic property data required by the solver. The approach of [23] is followed in deriving the equations for the thermodynamic properties of hydrogen based on the Redlich-Kwong equation of state. Table 3-5 summarizes the equations derived for calculating the thermodynamic properties of hydrogen.

Table 3-5: Equations for calculating Thermodynamic Property data based on the Redlich-Kwong Equation of State

Property	Equation	
h	$h = \frac{3a}{2bT^{\frac{1}{2}}}\ln\left(\frac{v}{v+b}\right) + \frac{RTv}{v-b} - \frac{a}{T^{\frac{1}{2}}(v+b)} - RT + \int_{T_{ref}}^{T} c_p dT + h_{ref}$	(3-21)
ρ	Solve cubic equation: $v^3 - \frac{RT}{p}v^2 + \left(\frac{a}{pT^{\frac{1}{2}}} - b\frac{RT}{p} - b^2\right)v - \frac{ab}{pT^{\frac{1}{2}}} = 0$ $\rho = \frac{1}{v}$	(3-22)
c_p [24]	$c_p = p\left(\frac{\partial v}{\partial T}\right)_p - R - \frac{3a}{4bT^{\frac{3}{2}}}\ln\left(\frac{v}{v+b}\right) + \frac{3a}{2T^{\frac{1}{2}}v(v+b)}\left(\frac{\partial v}{\partial T}\right)_p + R\sum_{k=1}^{17} N_k^{i_k}$	(3-23)
S	$S = \frac{a}{2bT^{\frac{3}{2}}}\ln\left(\frac{v}{v+b}\right) - R\ln\left(\frac{v}{v-b}\right) - R\ln\left(\frac{\rho T}{\rho_{ref}T_{ref}}\right) + \int_{T_{ref}}^{T}\left(\sum_{k=1}^{17} N_k T^{i_k-1}\right)dT + S_{ref}$	(3-24)
a	$a = v\sqrt{\frac{c_p}{R - c_p}\left(\frac{\partial v}{\partial p}\right)_T}$	(3-25)

μ	$\mu = 6.3e-7\sqrt{2.018}\left(\frac{p_c}{101325}\right)^{\frac{2}{3}}\left(T_c^{-0.1667}\right)\left(\frac{\left(\frac{T}{T_c}\right)^{\frac{3}{2}}}{\frac{T}{T_c}+0.8}\right)$	(3-26)
λ	$\lambda = \left(c_p + 1.25R\right)\mu$	(3-27)
$\left(\frac{\partial v}{\partial p}\right)_T$	$\left(\frac{\partial v}{\partial p}\right)_T = \frac{1}{\left[\frac{a}{T^{\frac{1}{2}}}\left(\frac{1}{v^2(v+b)}+\frac{1}{v(v+b)^2}\right)-\frac{RT}{(v-b)^2}\right]}$	(3-28)
$\left(\frac{\partial v}{\partial T}\right)_p$	$\left(\frac{\partial v}{\partial T}\right)_p = -\left(\frac{R}{v-b}+\frac{a}{2T^{\frac{3}{2}}v(v+b)}\right)\left(\frac{\partial v}{\partial p}\right)_T$	(3-29)
$\left(\frac{\partial \rho}{\partial T}\right)_p$	$\left(\frac{\partial \rho}{\partial T}\right)_p = -\rho^2\left(\frac{\partial v}{\partial T}\right)_p$	(3-30)
$\left(\frac{\partial \rho}{\partial p}\right)_T$	$\left(\frac{\partial \rho}{\partial p}\right)_T = -\rho^2\left(\frac{\partial v}{\partial p}\right)_T$	(3-31)
$\left(\frac{\partial h}{\partial T}\right)_p$	$\left(\frac{\partial h}{\partial T}\right)_p = c_p$	(3-32)
$\left(\frac{\partial h}{\partial p}\right)_T$	$\left(\frac{\partial h}{\partial p}\right)_T = \left[v - T\left(\frac{\partial v}{\partial T}\right)_p\right]$	(3-33)

The constants used for evaluating the specific heat at constant pressure where taken from [24].

The numerics involved in the model are managed by the commercial CFD software - Fluent. The model does not solve the governing equations directly in the form presented. Fluent uses the finite volume method, which converts the governing equations to their integral form before solving them for each control volume within the computational grid. Once the governing equations are converted to their integral form, the model discretizes the governing equations by using Taylor series expansion to approximate the derivatives present in the governing equations. This process only approximates the derivatives and hence there is a numerical truncation error associated with the approximation. Using higher order discretization schemes minimizes this error since the error is proportional to the order of the scheme (i.e. a first order scheme has error of the order (Δx) where as a second order scheme has error of the order $(\Delta x)^2$). To improve accuracy, the model uses second order (the highest order available within Fluent) discretization in both space and time.

The model uses the Fluent coupled solver with the implicit formulation, axisymmetric in space and unsteady in time. Within each time step, convergence is judged by analyzing the mass flow rate of gas entering the cylinder, the total heat transferred to the cylinder walls and the mass averaged temperature of the gas within the cylinder. The solution for each time step is converged when these three parameters meet to a single value for each within 4 significant digits.

3.2.3 Boundary and Initial Conditions

The model boundary conditions are assessed at the cylinder inlet, inside wall and outside wall of the cylinder. At the inlet, a pressure boundary condition is used. This boundary condition is varied with time to match the increase in pressure at the inlet throughout a fill. At

the inlet, the flow direction is assumed to be uniform in the direction of the cylinder axis. Since the energy equation is solved in the model, a total temperature boundary condition is used at the inlet. The total temperature represents the temperature of the gas at stagnation conditions. This boundary condition is also varied with time to represent experimental inlet conditions throughout the fill.

At the inside wall of the cylinder a non-slip boundary condition is used to solve the conservation of mass, momentum, turbulent kinetic energy and dissipation rate. There is no boundary condition for the energy equation at the inner wall. Instead the energy equation for the gas inside the cylinder (3-7) is coupled to the energy equation for the cylinder walls (3-17).

At the outer wall a constant heat transfer coefficient thermal boundary condition is used to determine the heat transfer between the cylinder wall and the environment. The ambient temperature is assumed to be constant throughout the fill.

The initial conditions for the model are defined by the initial temperature and pressure of the gas within the cylinder. The cylinder walls are assumed to be the same temperature as the gas. The pressure and temperature of the gas are assumed to be uniform within the space of the cylinder.

3.2.4 Computational Grid

The computational grid used for the model is shown in Figure 3-2. The grid is a combination of structured and unstructured mesh. The inlet area is mapped with a high-resolution structured mesh as this is the area where the highest gas velocities will occur. The walls are also discretized with a structured mesh in order to ensure enough computational nodes through the cylinder wall. The bulk gas region is then meshed with an unstructured grid.

The grid resolution at the wall is left coarse as the wall functions built into fluent will be used to compute the boundary layer flow parameters.

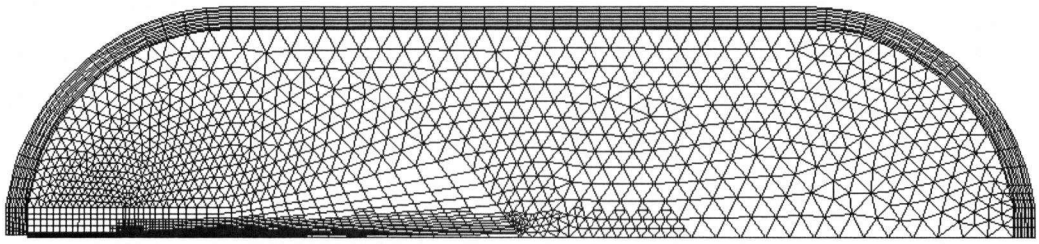

Figure 3-2: Computational grid used for modeling the compressed gas cylinder

3.3 EXPERIMENTAL MATERIALS AND METHODS

The model is to be validated by comparison with experimental results. A compressed gas cylinder was instrumented with 63 thermocouples to measure the temperature distribution inside the cylinder during refuelling. The thermocouples were held in position by a specially designed insert with spring-loaded arms. The cylinder was filled using the Pacific Spirit Fuelling station located at the National Research Council of Canada's Institute for Fuel Cell Innovation. The fuelling station stores hydrogen at 450 bar and transfers the hydrogen to the cylinder using a General Hydrogen CH350A dispenser.

The compressed gas cylinder used in these experiments is a Dynetek type 3 model V074H350. The cylinder has an internal volume of 74 litres and an external diameter and length of 39.9cm and 90cm respectively. The test setup of the fuelling station, dispenser, and test cylinder is detailed in Figure 2-3. The test cylinder is instrumented with two pressure sensors for monitoring the tank pressure and inlet pressure, a thermocouple for monitoring the inlet temperature of the gas and 63 thermocouples supported inside the cylinder, which measure the hydrogen gas temperature at numerous locations within the cylinder. The thermocouples used where type T with an accuracy of +/- 1 K.

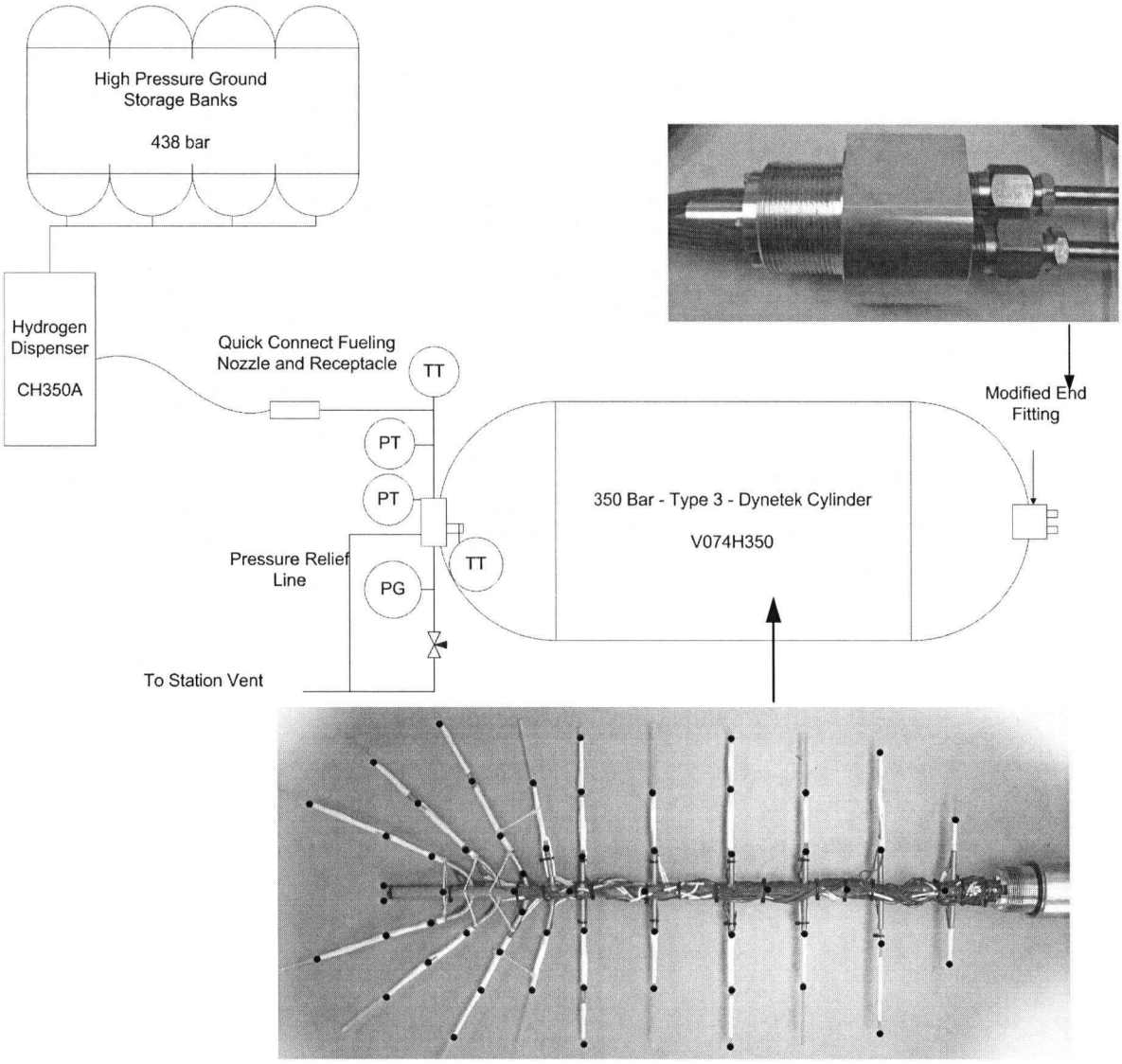

Figure 3-3: Schematic of the test setup including ground storage, dispenser and test cylinder.

3.4 RESULTS

3.4.1 Repeatability of Experimental Fills

Many fills were performed with the experimental setup, two representative fills, here after referred to as fill 1a and 1b, were performed under the initial and fill conditions listed in Table 3-6. The change in average hydrogen gas temperature within the cylinder and increase

in pressure during the fill are plotted in Figure 3-4 and Figure 3-5. The greatest increase in temperature occurs at the start of filling. This is because at the rate of increase in mass compared to the current mass is greatest at the start of filling. The Joule-Thomson effect is also greatest at the onset of filling where the pressure drop across the throttling device is greatest. The shape of the temperature increase is in agreement with previous studies of the filling of compressed gas cylinders [3-6, 8, 9, 11-17]. The results show that fill 1a and 1b produce virtually identical increases in average temperature and pressure. This is due to the excellent repeatability provided by the electronically controlled CH350A dispenser.

Table 3-6: Initial Conditions for Fill 1a and 1b

Fill 1a	Value	Fill 1b	Value
Initial Temperature	293.4 K	Initial Temperature	299.4 K
Initial Pressure	93.6 barg	Initial Pressure	93.1 barg
Initial Mass	0.540 kg	Initial Mass of H2	0.5273 kg
Nominal Pressure Ramp Rate	415 bar/min	Nominal Pressure Ramp Rate	415 bar/min

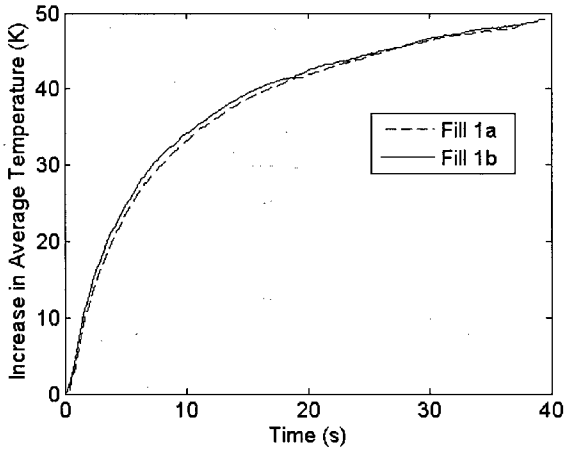

Figure 3-4: The relative increase in average temperature within the cylinder during test 1a and 1b.

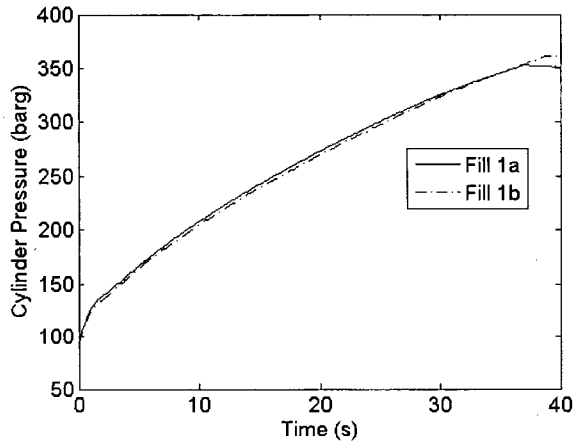

Figure 3-5: Increase in cylinder pressure during fill 1a and 1b.

In order to validate the numerical model, the initial conditions along with the temperature and pressure inlet boundary conditions measured during fill 1a where input into the model. The model was then run to produce a simulated fill. A detailed list of the initial conditions, boundary conditions and material properties used to numerically simulate fill 1a are listed in Table 3-7.

Table 3-7: Initial Conditions for Fill 1a and 1b

Boundary Condition	Value	Unit
Ambient temperature	293.4	[K]
Convective heat transfer coefficient between the cylinder outer surface and the ambient air	10	[W/m^{2}K]
Gas inlet pressure ramp rate	See Figure 3-6	[bar]
Gas inlet temperature	See Figure 3-6	[K]
Initial Condition		
Gas pressure	93	[barg]
Gas temperature	293.4	[K]
Material Properties		
Aluminum Liner		
Thermal conductivity	167	[W/mK]
Density	900	[kg/m^3]
Specific Heat	2730	[J/kgK]
Carbon-fibre/epoxy laminate		
Thermal conductivity	1.0	[W/mK]
Density	938	[Kg/m^3]
Specific Heat	1494	[J/kgK]

The inlet pressure and temperature boundary conditions are taken directly from the results of fill 1a. Figure 3-6 shows the inlet temperature and pressure measured just before the inlet to the cylinder during fill 1b. These results were curve fitted and input into the Fluent model. The sudden increase in inlet temperature at the start of the fill is the result of the compression of the gas inside of the fill line prior to forcing open the tank solenoid valve. The second increase in temperature thereafter is the result of the Joule Thomson heating which is

greatest at the start of the fill and declines as the pressure of the test cylinder and ground storage cylinders approach equilibrium.

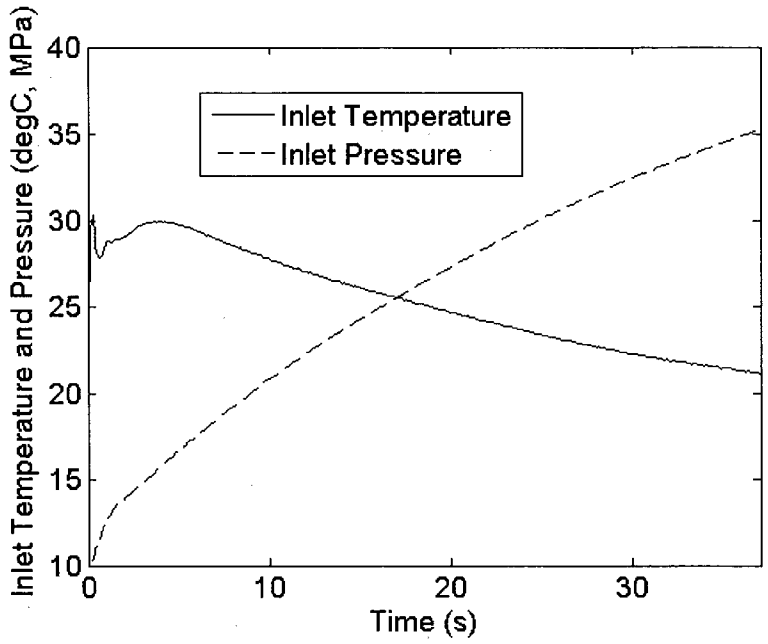

Figure 3-6: Inlet gas temperature and pressure measured during fill 1b.

3.4.2 Comparison of Experimental and Model Results

The comparison of the rise in average gas temperature during the model and experiment fill is the main method used for validating the model. Figure 3-7 shows the average gas temperature of the hydrogen gas for the modeled and experimental case. The model and experimental results are in agreement. Quantitatively, the maximum difference between the model and experimental results is 4K. The largest difference between model and experiment occurs at the end of filling as the model slightly under predicts the heat transfer throughout the fill. Qualitatively the model correctly predicts the shape of the curve where there is a rapid rise in temperature at the onset of filling when the rate of compression of the gas is greatest and the thermal mass of the gas within the cylinder is at its lowest. In order to correctly predict the temperature rise, the model must be able to accurately simulate the heat

transfer between the gas and the inner wall of the cylinder. This result thus shows that the CFD model accurately predicts the heat transfer during filling.

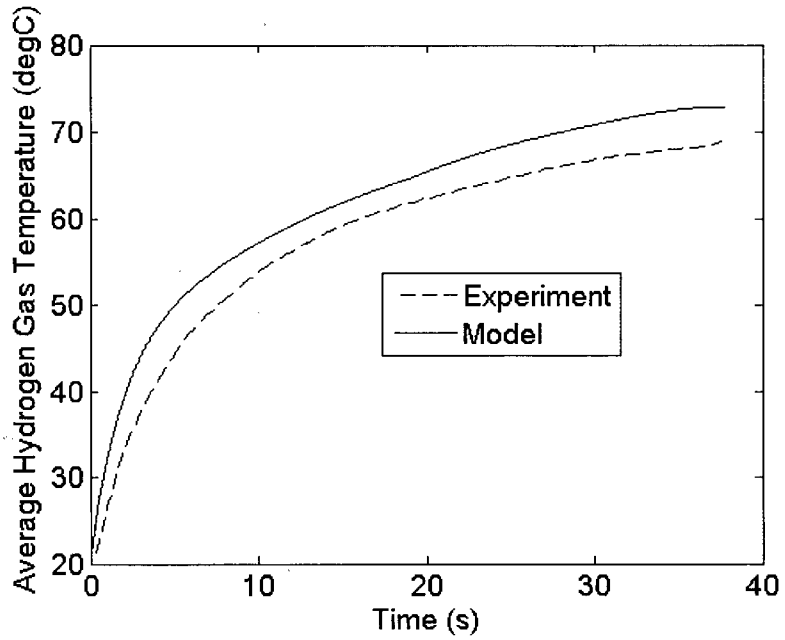

Figure 3-7: Average Temperature Rise during filling

Using the Redlich-Kwong equation of state to solve for the density of the hydrogen at the end of the fill, the 4K difference in temperature between the model and experiment, results in the model over estimating the density by 1%.

A secondary means of model validation is the comparison of the model predicted gas temperature field and experimental measurements of the temperature field within the cylinder. Figure 3-8, Figure 3-9, Figure 3-10 and Figure 3-11 show the model predicted temperature distribution throughout the cylinder at 5, 15, 25 seconds and at the end of the fill. Figure 3-12, Figure 3-13, Figure 3-14, and Figure 3-15 show the temperature distribution measured by the 63 thermocouples mounted within the cylinder at 5, 15, 25 seconds and at the end of the fill. The model results predict the maximum temperature within the cylinder to be located at the fill end, surrounding the inlet. In general the experimental temperature fields confirm this

prediction. Both the model and experiment predict a significant temperature gradient protruding from the cylinder inlet. The model predicts a larger variation in temperature because it includes the cylinder inlet where incoming gas is at a much lower temperature. During the experiment the closest thermocouple to the inlet was ~ 7 cm from the inlet along the centreline of the cylinder. Between the inlet and the location of the first thermocouple the temperature of the gas increases considerably. Away from the inlet plume the variation of the temperature field of the bulk gas is within 3 K.

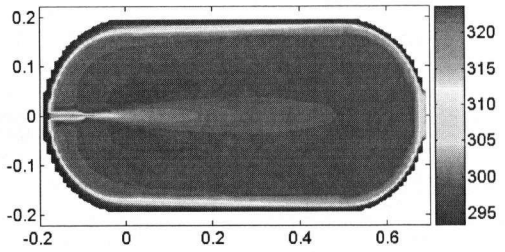

Figure 3-8: Model predicted temperature distribution within the cylinder at time 5s. Average Temperature = 323.2 K

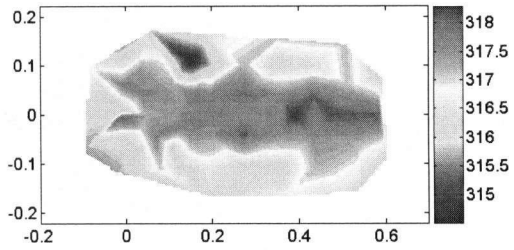

Figure 3-9: Experimental temperature distribution within the cylinder at time 5s. Average Temperature = 317.6 K

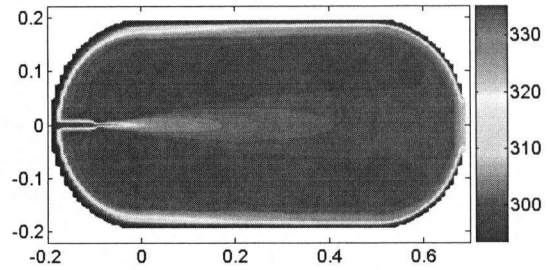

Figure 3-10: Model predicted temperature distribution within the cylinder at time 15s. Average Temperature = 335 K

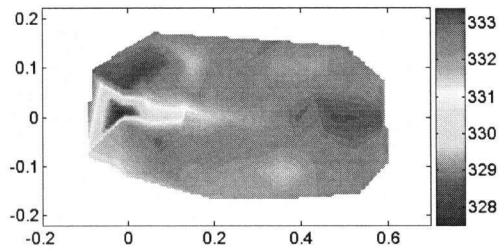

Figure 3-11: Experimental temperature distribution within the cylinder at time 15s. Average Temperature = 332.4 K

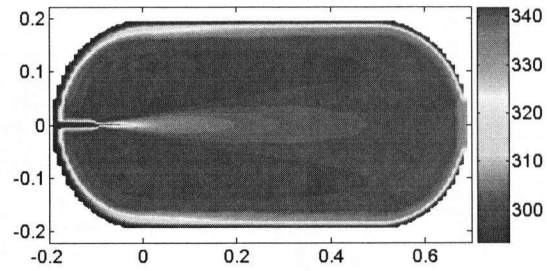

Figure 3-12: Model predicted temperature distribution within the cylinder at time 25s. Average Temperature = 341.8 K

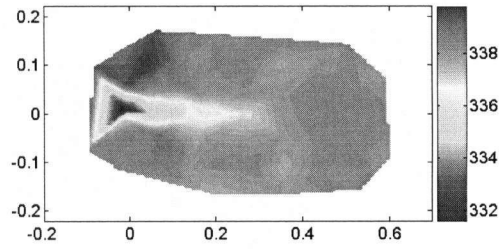

Figure 3-13: Experimental temperature distribution within the cylinder at time 25s. Average Temperature = 338.1 K

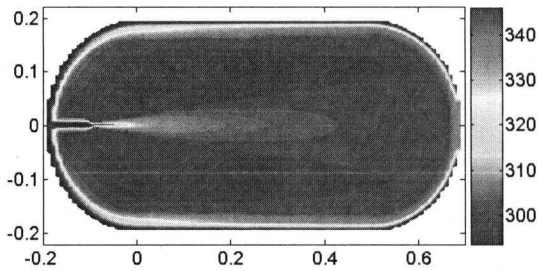

Figure 3-14: Model predicted temperature distribution within the cylinder at the end of the fill. Average Temperature = 346 K

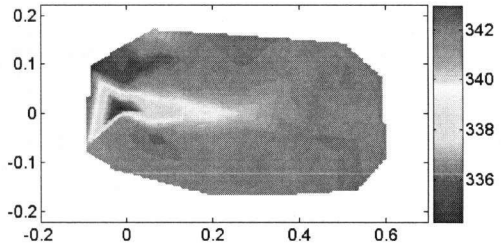

Figure 3-15: Experimental temperature distribution within the cylinder at the end of the fill. Average Temperature = 342 K

The small variation in gas temperature in the bulk makes this region ideal for placing a sole temperature sensor whereby the temperature measured would best reflect the average temperature of the gas within the cylinder. While the bulk region may be ideal for accuracy it is difficult to access the region with a sensor. Most cylinders have accessible ports at either end making the centreline the easiest place to locate a sensor. Figure 3-16 plots the model prediction of the temperature of the gas along the normalized centreline of the cylinder at four different time steps through the fill. The model thus predicts a significant temperature gradient from the initial expansion of the inlet gas jet at 0.11 to the midpoint of the centreline. From the midpoint to the tail end of the cylinder the temperature along the centreline increases slowly towards the average temperature of the gas near the end point of the cylinder. This makes the insertion of a temperature probe through the end port of the cylinder an ideal location for both accuracy and accessibility.

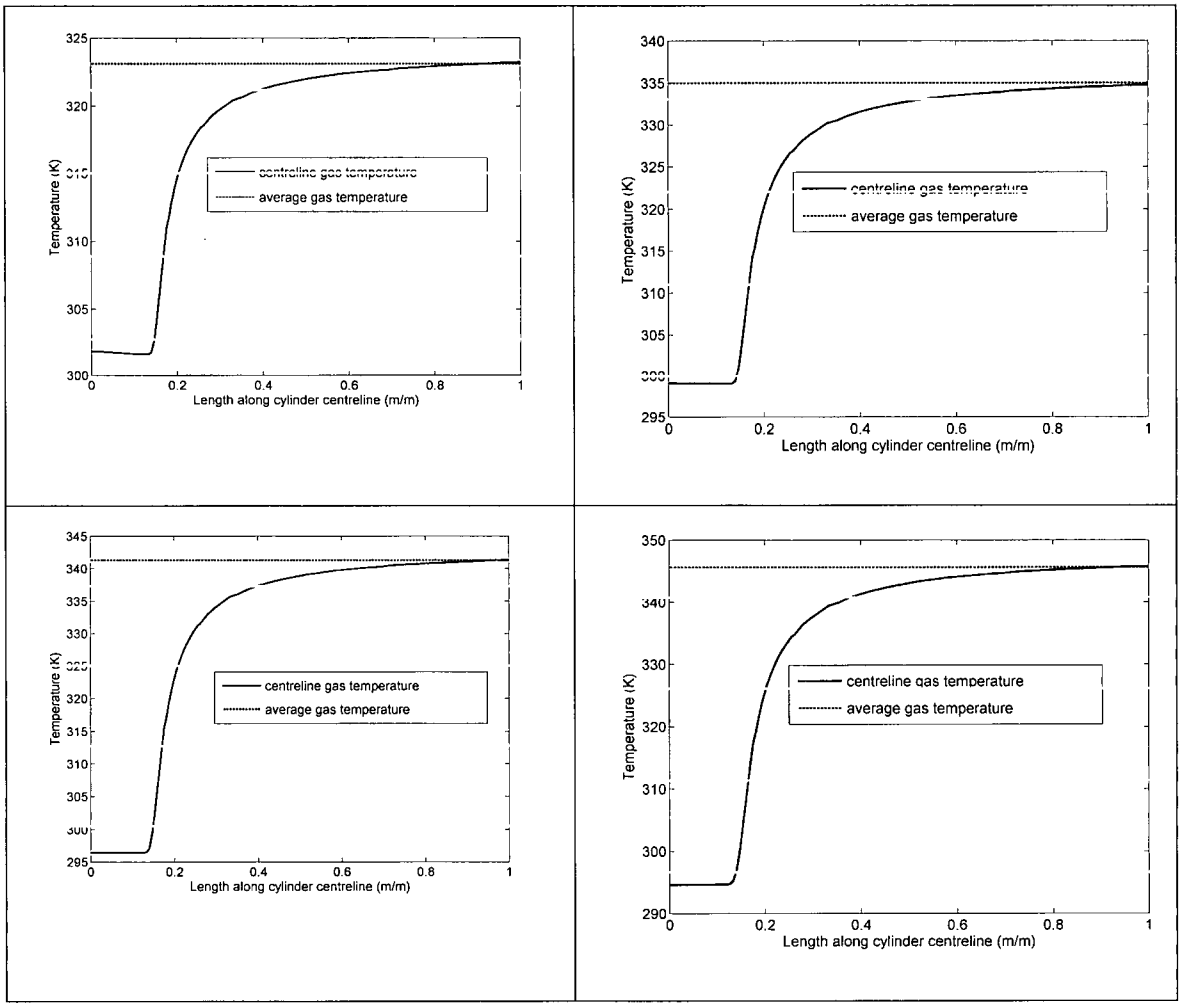

Figure 3-16: Model predicted temperature along the centerline of the cylinder at 5s (top left), 15s (top right), 25s (bottom left), and the end of the fill (bottom right).

3.5 CONCLUSIONS

A two dimensional axis-symmetric CFD model of the filling of a compressed gas cylinder has been developed and compared to experimental measurements. The model is able to predict the final average temperature of the gas at the conclusion of the fill within 4K of the experimental result. The temperature distributions at 15 seconds, 25 seconds and at the end of the fill along with the experimental measurements confirm: the minimum temperature is located at the gas inlet, and there exists a large temperature gradient at the inlet of the cylinder. The temperature in the bulk region of gas surrounding the inlet is much more uniform and

provides the best location for a single temperature sensor to monitor the average temperature of the gas throughout the fill.

3.6 NOMENCLATURE

A	Area [m^2]
a	constant of the Redlich Kwong equation of state
b	constant of the Redlich Kwong equation of state
$C_{1\varepsilon}$	constant of the k-e model
$C_{2\varepsilon}$	constant of the k-e model
C_{μ}	constant of the k-e model
c_p	specific heat capacity [J/molK]
c_s	speed of sound in hydrogen [m/s]
d	diameter [m]
Fr	Froude number
g	gravitational acceleration 9.81 [m/s^2]
H	Total Enthalpy [J]
h	specific enthalpy [J/mol]
$h_{conv,avg}$	mean convective heat transfer coefficient, inner surface [W/m^2K]
$h_{conv,in}$	local convective heat transfer coefficient, inner surface [W/m^2K]
$h_{conv,out}$	local convective heat transfer coefficient, outer surface [W/m^2K]
i_k	set of 17 constants for the specific heat capacity of hydrogen
k	thermal conductivity [W/mK]
k_{eff}	effective thermal conductivity [W/mK]
k_t	turbulent kinetic energy [m^2/s^2]
L	Length of the cylinder [m]
L_{tube}	Length of tube protruding from inlet [m]
m	mass [kg]
$\dot{m}$	mass flow rate [kg/s]

Ma	Mach number
N_k	set of 17 constants for the specific heat capacity of hydrogen
p	pressure [Pa]
p_c	hydrogen critical pressure [Pa]
Pr_t	turbulent Prandlt number
$\dot{Q}$	Total heat transfer rate [W]
q	heat transfer [J]
R	universal gas constant [J/molK]
Re	Reynolds number
r_i	inner radius of test cylinder [m]
r_o	outer radius of test cylinder [m]
T	Temperature [K]
T_c	hydrogen critical temperature [K]
t	time [s]
U	Internal Energy [J]
u	velocity [m/s]
v	specific volume [m^3/mol]
x	distance [m]
Greek	
ε_{ij}	unit tensor
ε_t	turbulent rate of dissipation [m^2/s^3]
λ_{lam}	laminate thickness [m]
λ_{liner}	liner thickness [m]
λ_{tube}	tube thickness [m]
λ_w	total wall thickness [m]
μ	viscosity [Pa s]
μ_{eff}	effective viscosity [Pa s]
μ_t	turbulent viscosity [Pa s]
ρ	density [kg/m^3]
σ_k	constant of k-ε model = 1.0

σ_ε	constant of k- ε model = 1.3
τ_{ij}	stress tensor
υ	kinematic viscosity [m^2/s]
Subscripts	
i	x-direction
j	y-direction
k	z-direction
in	inlet
ref	reference state
w	wall
Superscripts	
~	Favre average
-	ensemble average
′	turbulent fluctuating component

3.7 REFERENCES

[1] International Standard Organization, 2005, "Gaseous Hydrogen and Hydrogen Blends Land Vehicule Fuel Tanks Part 1: General Requirements," ISO 15869.

[2] International Standard Organization, 2005, "Gas Cylinders High Pressure Cylinders for the on-Board Storage of Natural Gas as a Fuel for Automotive Vehicles," ISO 11439.

[3] Charton, S., Blet, V., and Corriou, J. P., 1996, "A Simplified Model for Real Gas Expansion between Two Reservoirs Connected by a Thin Tube," Chemical Engineering Science, 51(2), pp. 295-308.

[4] Daney, D. E., Edeskuty, F. J., and Daugherty, M. A., 1996, "Hydrogen Vehicle Fueling Station," Advances in Cryogenic Engineering, 41, pp. 1041-1048.

[5] Duncan, M., and Macfarlane, S., 2003, "Fast Filling of Type 3 Hydrogen Storage Cylinders," Submitted to the Hydrogen and Fuel Cells Conference, June, 2003.

[6] Eihusen, J.A., 2003, "Application of Plastic-Lined Composite Pressure Vessels For Hydrogen Storage," General Dynamics Armament and Technical Products, http://www.lincolncomposites.com/media.html.

[7] Haque, M. A., Richardson, M., and Saville, G., 1992, "Blowdown of Pressure Vessels - I. Computer Model," Trans.IChemE, 70(Part B) pp. 3-9.

[8] Kountz, K., 1994, "Modeling the Fast Fill Process in Natural Gas Vehicles Storage Cylinders," 207th American Chemical Society Meeting, March, 1994.

[9] Perret, C., 2004, "Modelling and Simulation of the Filling of a Gaseous Hydrogen Tank under very High Pressure," European Integrated Hydrogen Project Phase II, WP 3.2, DTEN/DR/2003/167, January 2004.

[10] Reynolds, W. C., and Kays, W. M., 1958, "Blowdown and Charging Processes in a Single Gas Receiver with Heat Transfer," Transactions of the ASME, July, pp. 1160-1168.

[11] Richards, M., Liss, W., and Kountz, K., 2003, "Modeling and Testing of Fast-Fill Control Algorithms for Hydrogen Fueling," National Hydrogen Association's 14th Annual U.S.Hydrogen Conference and Hydrogen Expo USA, March 2003.

[12] Xia, J., 1993, "A Simplified Model for Depressurization of Gas-Filled Pressure Vessels," Int.Comm.Heat Mass Transfer, 20, pp. 653-664.

[13] Haque, M. A., Richardson, M., and Saville, G., 1992, "Blowdown of Pressure Vessels - II. Experimental Validation of Computer Model and Case Studies," Trans.IChemE, 70, Part B, pp. 10-17.

[14] Jeary, B., 2001, "Fast Filling of Compressed Hydrogen Fuel Storage Cylinders," Proceedings, 11th Canadian Hydrogen Conference, Anonymous Canadian Hydrogen Association, Victoria, B.C., June, 2001.

[15] Newhouse, N., 2005, "Fast Filling of NGV Fuel Containers," SAE Technical Paper Series 1999-01-3739, 1999.

[16] Schneider, J., 2005, "Optimizing the Fuelling of Hydrogen Vehicles," The Fuel Cell Review, 2(4), pp. 15-24.

[17] Kountz, K., Liss, W., and Blazek, C., 1998, "A New Natural Gas Dispenser Control System," Proceedings of the 1998 International Gas Research Conference, Aug. 1998, pp. 135-145.

[18] Ouellette, P., Hill, and PG, 2000, "Turbulent Transient Gas Injections," Journal of Fluids Engineering, 122, pp. 743-753.

[19] Pope, S. B., 1978, "An Explanation of the Turbulent Round-Jet/Plane-Jet Abnormality," Technical Note, AIAA J., 16(3), pp. 279.

[20] Magi, V., Iyer, V., and Abraham, 2001, "The k-e Model and Computed Spreading in Round and Plane Jets," Numerical Heat Transfer, Part A, 40, pp. 317-334.

[21] Launder, B.E., and Spalding, D.B., 1972, "Lectures in Mathematical Models of Turbulence," Academic Press, London.

[22] Fluent Inc, 2005, "Fluent 6.2 User's Guide,".

[23] Annamalai, K., and Puri, I.K., 2002, "Advanced Thermodynamics Engineering," CRC Press, London, Chap 7.

[24] Jacobsen, R.T., Penoncello, S.G., and Lemmon, E.W., 1997, "Thermodynamic Properties of Cryogenic Fluids," Plenum Press, New York, Chap 3.

CHAPTER 4: CONCLUSIONS

4.1 SUMMARY OF THE PRESENT WORK

The main objective of this research was to investigate the temperature field within a compressed gas cylinder during refuelling. The approach taken to elucidate the temperature field was to develop a two dimensional axisymmetric model of the fill and to instrument a gas cylinder with 63 thermocouples to monitor and record the temperature field during actual experimental fills.

The CFD model developed in Chapter 2 includes the effects of compressible unsteady viscous flow within the boundaries of the cylinder. Real gas effects, heat transfer to the cylinder walls and conduction through the cylinder wall are included in the scope of the model. Validation of the model is achieved by comparison with a set of experimental fast fills. The model predicts the final average temperature of the gas at the conclusion of the fill within 4K of the experimental result. The temperature field is shown to be dominated by a conical region of high temperature gradient emanating from the gas inlet. The bulk region of gas surrounding the conical region is shown to be much more uniform in temperature and is determined to be the ideal location for a single temperature sensor to monitor the average temperature of the gas throughout the fill.

In order to experimentally determine the temperature distribution, a type 3, 74L compressed hydrogen cylinder was instrumented with 63 thermocouples. Two sets of experimental fills where performed to determine the effect of initial mass and fill rate on the temperature field and the overall temperature rise during the fill. The fills were performed using the Pacific Spirit Hydrogen Fueling Station located at the National Research Councils

Institute for Fuel Cell Innovation in Vancouver Canada. The results showed that the overall temperature rise was highly depended on the ratio of final to initial mass of gas within the cylinder. The greatest rate of temperature rise occurred at the beginning of the fill when the ratio of final mass of gas to the initial mass of gas is the lowest. As the ratio increased the rate of temperature rise decreased. Fill rate had a significant affect on the temperature field. Slower fills where shown to produce significant vertical temperature stratification within the cylinder owing to the increased role of buoyancy forces at lower gas inlet velocities. As predicted by the CFD model, shorter fills produced a temperature field with a large conical temperature gradient extending out from the cylinder inlet and was symmetrical about the cylinder axis.

The end opposite to the gas inlet experiences an instantaneous local temperature that best reflected the mean temperature of the gas. As a result, a temperature sensor inserted two inches into the non fill end of the cylinder along the centreline is identified as the optimal location for the temperature sensors aimed at metering fuel based on combined temperature and pressure measurements.

4.2 CONTRIBUTION TO THE FIELD

The study presented in this work is the first rigorous investigation into the temperature field inside a compressed gas cylinder during the refuelling process. This study determines the effect of fill rate/time on the temperature field within the cylinder and identifies the role of buoyancy forces for longer duration fills. The results of this study have also determined the effect of the ratio of initial to final mass of gas on the overall temperature rise. This represents the first study to present the effect of initial mass instead of the initial pressure.

The optimal location of a single temperature sensor within the cylinder to best represent the average temperature of the gas has been identified. From the results of the

numerical and experimental results, the centreline at the non fill end is identified as the optimal location of a single temperature sensor that best reflects the average gas temperature.

The experimental and modeling results gathered will help to explain the heat transfer which occurs during filling. The amount of heat transferred to the cylinder is directly related to the speed of the fill which is of great significance to industry. The validated model can be used to investigate the heat transfer that occurs within the cylinder.

The study is the first to derive a single equation for the rate of temperature rise due to the filling of a cylinder with a real gas. Analysis of this equation helps to identify the drivers for the rate of temperature increase.

The method used in this study to assess the effect of initial mass and fill rate on overall temperature rise can be used to characterize different cylinder types and sizes. These methods can be extended to other parameters that affect temperature rise (inlet temperature, ambient temperature, etc.).

4.3 RECOMMENDATIONS

The results presented in this study represent a significant step forward in the understanding of the temperature field and temperature rise during the filling of gas cylinders. The following studies are proposed to develop a further understanding of the fill process and how to achieve faster fills:

- Implementing a dispenser control system based on the principle of measuring temperature and pressure to determine when the cylinder has reached rated capacity.
- Investigate the effect of other fill parameters on the overall temperature rise.
- Instrument a cylinder to measure the rate of heat transfer to the cylinder wall. The study should investigate the affect of various fill parameters on the rate of heat transfer

with the goal of such a study being the establishment of an expression for the rate heat transfer in terms of measurable fill parameters.

- Development of a simplified model incorporating an accurate heat transfer relation for engineering/industry calculations of temperature rise based on several fill parameters.
- Utilizing modeling and experimental techniques to determining the liner and laminate temperature of the cylinder during and post filling to help establish a safe maximum gas temperature.

APPENDIX A – CODE FOR REAL GAS MODEL IN FLUENT

```
/************************************************************/
/* User-Defined Function: Redlich-Kwong Equation of State    */
/*                for Real Gas Modeling                     */
/*                                                          */
/*  Author: Chris Dicken                                    */
/*  Date: November 2005                                     */
/*                                                          */
/*                                                          */
/************************************************************/

#include <udf.h>
#include <stdio.h>
#include <ctype.h>
#include <stdarg.h>

/* The variables below need to be set for a particular gas */
/* Hydrogen */
/* REAL GAS EQUATION OF STATE MODEL - BASIC VARIABLES */

#define RGASU UNIVERSAL_GAS_CONSTANT
#define PI   3.141592654

#define MWT   2.0159
#define PCRIT 1.3152e6
#define TCRIT 33.19

/* REFERENCE STATE */

#define P_REF 1000.0
#define T_REF 273.15
#define RHO_REF 8.87676e-4
#define Ho_REF 3572754.0   /*J/kg*/
#define So_REF 71181.0     /*J/kgK*/


static int  (*usersMessage)(char *,...);
static void (*usersError)(char *,...);

/* Static variables associated with Redlich-Kwong Model */

static double rgas, a0, b0, cpT_int_ref, cp_over_T_int_ref;
```

```
/* IDEAL GAS SPECIFIC HEAT CURVE FIT */

static double N_k[17];
static double lk[16];
static double N_k_pow[16];


DEFINE_ON_DEMAND(I_do_nothing)
{
 /* this is a dummy function to allow us */
 /* to use the compiled UDFs utility    */
}

/*---------------------------------------------------------------*/
/* FUNCTION: RKEOS_error                                         */
/*---------------------------------------------------------------*/

void RKEOS_error(int err, char *f, char *msg)
{
  if (err)
    usersError("RKEOS_error (%d) from function: %s\n%s\n",err,f,msg);
}

/*---------------------------------------------------------------*/
/* FUNCTION: RKEOS_Setup                                         */
/*---------------------------------------------------------------*/

void RKEOS_Setup(Domain *domain, char *filename,
            int (*messagefunc)(char *format, ...),
            void (*errorfunc)(char *format, ...))
{

  rgas = RGASU/MWT;
  a0 = 0.42747*rgas*rgas*pow(TCRIT,2.5)/PCRIT;
  b0 = 0.08664*rgas*TCRIT/PCRIT;
  cpT_int_ref = -81271688.0;
  cp_over_T_int_ref = 4923851.0;
  N_k[0] = 1.215521517;
  N_k[1] = -3.63967627;
  N_k[2] = 4.33752654;
  N_k[3] = -2.308581738;
  N_k[4] = -3.86809271;
  N_k[5] = 8.824013566;
  N_k[6] = -7.858708525;
  N_k[7] = 7.248020909;
  N_k[8] = -1.842680629;
```

```
N_k[9] = 2.18015504;
N_k[10] = -1.305182;
N_k[11] = 2.1003175220;
N_k[12] = 2.3911604280;
N_k[13] = -1.824054653;
N_k[14] = 5.614956073;
N_k[15] = -7.3803310130;
N_k[16] = 6.63577552;
N_k_pow[0] = 10.0;
N_k_pow[1] = 9.0;
N_k_pow[2] = 8.0;
N_k_pow[3] = 7.0;
N_k_pow[4] = 3.0;
N_k_pow[5] = 4.0;
N_k_pow[6] = 3.0;
N_k_pow[7] = 2.0;
N_k_pow[8] = 2.0;
N_k_pow[9] = 1.0;
N_k_pow[10] = 0.0;
N_k_pow[11] = -2.0;
N_k_pow[12] = -3.0;
N_k_pow[13] = -4.0;
N_k_pow[14] = -6.0;
N_k_pow[15] = -8.0;
N_k_pow[16] = -12.0;
Ik[0] = -7.0;
Ik[1] = -6.0;
Ik[2] = -5.0;
Ik[3] = -4.0;
Ik[4] = -3.0;
Ik[5] = -2.0 ;
Ik[6] = -1.0;
Ik[7] = 0.0;
Ik[8] = 0.5;
Ik[9] = 1.0;
Ik[10] = 1.5;
Ik[11] = 2.0;
Ik[12] = 2.5;
Ik[13] = 3.0;
Ik[14] = 3.5;
Ik[15] = 4.0;
Ik[16] = 5.0;


usersMessage = messagefunc;
usersError = errorfunc;
```

```
  usersMessage("\nLoading Redlich-Kwong Library: %s\n", filename);
  usersMessage("\nHydrogen Properties\n");
  usersMessage("\nN_k16 = %f",N_k[16]);
  usersMessage("\nN_k_pow16 = %f",N_k_pow[16]);
  usersMessage("\nIk16 = %f",Ik[16]);
}

/*---------------------------------------------------------------*/
/* FUNCTION: RKEOS_pressure                                      */
/*         Returns pressure given T and density                  */
/*---------------------------------------------------------------*/

double RKEOS_pressure(double temp, double density)
{
  double v = 1./density;

  return rgas*temp/(v-b0)-a0/(pow(temp,0.5)*v*(v+b0));
}

/*---------------------------------------------------------------*/
/* FUNCTION: RKEOS_spvol                                         */
/*         Returns specific volume given T and P                 */
/*---------------------------------------------------------------*/

double RKEOS_spvol(double temp, double press)
{
  double a1,a2,a3,a4;
  double vv,vv1,vv2,vv3;
  double f,g,h,i,j,j2,k,L,M,N,P;

  a1 = 1.0;
  a2 = -rgas*temp/press;
  a3 = (a0/(press*pow(temp,0.5)) - b0*rgas*temp/press - pow(b0,2.0));
  a4 = -a0*b0/(press*pow(temp,0.5));

  /* Solve cubic equation for specific volume */

  f = ((3*a3/a1) - (a2*a2/(a1*a1)))/3;
  g = ((2*a2*a2*a2/(a1*a1*a1)) - (9*a2*a3/(a1*a1)) + 27*a4/a1)/27;
  h = (g*g/4) + (f*f*f/27);
  i = pow(((g*g/4)-h),0.5);
  j = pow(i,0.333333);
  if (-g/2/i > 1.0) {
        j2 = 1.0;
  } else {
        j2 = -g/2/i;
```

```
  }
  k = acos(j2);
  L = -1.0*j;
  M = cos(k/3);
  N = 1.7321*sin(k/3);
  P = -1*(a2/3/a1);
  vv1 = 2*j*cos(k/3) - (a2/3/a1);
  vv2 = L*(M+N)+P;
  vv3 = L*(M-N)+P;
  vv = vv1;

  return vv;
}

/*---------------------------------------------------------------*/
/* FUNCTION: RKEOS_density                                       */
/*        Returns density given T and P                          */
/*---------------------------------------------------------------*/

double RKEOS_density(double temp, double press, double yi[])
{
  return 1./RKEOS_spvol(temp, press); /* (Kg/m^3) */
}

/*---------------------------------------------------------------*/
/* FUNCTION: RKEOS_dvdp                                          */
/*        Returns dv/dp given T and P                            */
/*---------------------------------------------------------------*/

double RKEOS_dvdp(double temp, double density)
{
  double a1,a2,v,press,dvdp;

  press = RKEOS_pressure(temp, density);
  v = 1./density;

  a1 = -rgas*temp/pow((v-b0),2.0);
  a2 = a0/pow(temp,0.5)*(1/(v*v*(v+b0)) + 1/(v*(v+b0)*(v+b0)));
  dvdp = 1/(a1+a2);
  return dvdp;
}

/*---------------------------------------------------------------*/
/* FUNCTION: RKEOS_dvdt                                          */
/*        Returns dv/dT given T and P                            */
/*---------------------------------------------------------------*/
```

```
double RKEOS_dvdt(double temp, double density)
{
  double dpdT,dvdp,v,press;

  press = RKEOS_pressure(temp, density);
  v = 1./density;
  dvdp = RKEOS_dvdp(temp, density);

  dpdT = rgas/(v-b0) + a0/(2*pow(temp,1.5)*v*(v+b0));

  return -dpdT*dvdp;
}

/*---------------------------------------------------------------*/
/* FUNCTION: RKEOS_Cp_ideal_gas                                  */
/*        Returns ideal gas specific heat given T                */
/*---------------------------------------------------------------*/

double RKEOS_Cp_ideal_gas(double temp)
{
  int k = 0;
  double cp = 0.0;

  for (k=0 ; k <= 16 ; k++)
        {
          cp = cp + N_k[k]*pow(temp,Ik[k])*pow(10,N_k_pow[k]);
        }

  cp = cp*rgas;

  return cp;
}

/*---------------------------------------------------------------*/
/* FUNCTION: RKEOS_Int_CpdT_ideal_gas                            */
/*        Returns integral (cp dT)   */
/*---------------------------------------------------------------*/

double RKEOS_Int_CpdT_ideal_gas(double temp)
{
  int k = 0;
  double cpT = 0.0;

  for (k=0 ; k <= 5 ; k++)
        {
```

```
        cpT = cpT + N_k[k]*pow(temp,(Ik[k]+1.0))/(Ik[k]+1.0)*pow(10,N_k_pow[k]);
      }

  cpT = cpT + N_k[6]*log(temp)*pow(10,N_k_pow[k]);

  for (k=7 ; k <= 16 ; k++)
      {
        cpT = cpT + N_k[k]*pow(temp,(Ik[k]+1.0))/(Ik[k]+1.0)*pow(10,N_k_pow[k]);
      }

  cpT = cpT*rgas;

  return cpT;
}

/*-------------------------------------------------------------*/
/* FUNCTION: RKEOS_Int_Cp_over_TdT_ideal_gas                   */
/*        Returns integral (cp dT)   */
/*-------------------------------------------------------------*/

double RKEOS_Int_Cp_over_TdT_ideal_gas(double temp)
{
  int k = 0;
  double cp_over_T = 0.0;

  for (k=0 ; k <= 6 ; k++)
      {
        cp_over_T = cp_over_T + N_k[k]*pow(temp,Ik[k])/Ik[k]*pow(10,N_k_pow[k]);
      }

  cp_over_T = cp_over_T + N_k[7]*log(temp)*pow(10,N_k_pow[k]);

  for (k=8 ; k <= 16 ; k++)
      {
        cp_over_T = cp_over_T + N_k[k]*pow(temp,Ik[k])/Ik[k]*pow(10,N_k_pow[k]);
      }

  cp_over_T = cp_over_T*rgas;

  return cp_over_T;
}
/*-------------------------------------------------------------*/
/* FUNCTION: RKEOS_H_ideal_gas                                 */
/*        Returns ideal gas specific enthalpy given T     */
/*-------------------------------------------------------------*/
```

```
double RKEOS_H_ideal_gas(double temp)
{
  return RKEOS_Int_CpdT_ideal_gas(temp) - cpT_int_ref + Ho_REF;
}

/*---------------------------------------------------------------*/
/* FUNCTION: RKEOS_specific_heat                                 */
/*         Returns specific heat given T and rho                 */
/*---------------------------------------------------------------*/

double RKEOS_specific_heat(double temp, double density, double yi[])
{
  double delta_Cp,press,v,dvdt;

  press = RKEOS_pressure(temp, density);
  v = 1./density;
  dvdt = RKEOS_dvdt(temp, density);

  delta_Cp = press*dvdt - rgas -3*a0/4/b0/pow(temp,1.5)*log(v/(v+b0)) +
3*a0/2/pow(temp,0.5)/v/(v+b0)*dvdt;
  delta_Cp = 0;
  return RKEOS_Cp_ideal_gas(temp)+delta_Cp;  /* (J/Kg/K) */
}

/*---------------------------------------------------------------*/
/* FUNCTION: RKEOS_enthalpy                                      */
/*         Returns specific enthalpy given T and rho             */
/*---------------------------------------------------------------*/

double RKEOS_enthalpy(double temp, double density, double yi[])
{
  double delta_h, v;

  v = 1./density;
  delta_h = 1.5*a0/b0/pow(temp,0.5)*log(v/(v+b0)) + rgas*temp*v/(v-b0) -
a0/(v+b0)/pow(temp,0.5) - rgas*temp;

  return RKEOS_H_ideal_gas(temp)+delta_h;  /* (J/Kg) */
}

/*---------------------------------------------------------------*/
/* FUNCTION: RKEOS_entropy                                       */
/*         Returns entropy given T and rho                       */
/*---------------------------------------------------------------*/

double RKEOS_entropy(double temp, double density, double yi[])
```

```
{
  double delta_s1,delta_s2,v,cp_integral;

  cp_integral = RKEOS_Int_Cp_over_TdT_ideal_gas(temp) - cp_over_T_int_ref + So_REF;

  v = 1./density;

  delta_s1 = -rgas*log(density*temp/(RHO_REF*T_REF));
  delta_s2 = -rgas*log(v/(v-b0)) + a0/2/b0/pow(temp,1.5)*log(v/(v+b0));

  return cp_integral+delta_s1+delta_s2; /* (J/Kg/K) */
}

/*---------------------------------------------------------------*/
/* FUNCTION: RKEOS_mw                                            */
/*        Returns molecular weight                               */
/*---------------------------------------------------------------*/

double RKEOS_mw(double yi[])
{
  return MWT; /* (Kg/Kmol) */
}

/*---------------------------------------------------------------*/
/* FUNCTION: RKEOS_speed_of_sound                                */
/*        Returns s.o.s given T and rho                          */
/*---------------------------------------------------------------*/

double RKEOS_speed_of_sound(double temp, double density, double yi[])
{
  double cp = RKEOS_specific_heat(temp, density, yi);
  double dvdp = RKEOS_dvdp(temp, density);
  double v = 1./density;

  return sqrt(cp/((rgas-cp)*dvdp))*v;  /* m/s */
}

/*---------------------------------------------------------------*/
/* FUNCTION: RKEOS_rho_t                                         */
/*---------------------------------------------------------------*/

double RKEOS_rho_t(double temp, double density, double yi[])
{
  return -density*density*RKEOS_dvdt(temp, density);
}
```

```
/*-----------------------------------------------------------*/
/* FUNCTION: RKEOS_rho_p                                     */
/*-----------------------------------------------------------*/

double RKEOS_rho_p(double temp, double density, double yi[])
{
  return -density*density*RKEOS_dvdp(temp, density);
}


/*-----------------------------------------------------------*/
/* FUNCTION: RKEOS_enthalpy_t                                */
/*-----------------------------------------------------------*/

double RKEOS_enthalpy_t(double temp, double density, double yi[])
{
  return RKEOS_specific_heat(temp, density, yi);
}

/*-----------------------------------------------------------*/
/* FUNCTION: RKEOS_enthalpy_p                                */
/*-----------------------------------------------------------*/

double RKEOS_enthalpy_p(double temp, double density, double yi[])
{
  double v = 1./density;
  double dvdt = RKEOS_dvdt(temp, density);

  return v-temp*dvdt;
}

/*-----------------------------------------------------------*/
/* FUNCTION: RKEOS_viscosity                                 */
/*-----------------------------------------------------------*/

double RKEOS_viscosity(double temp, double density, double yi[])
{
  double tr, tc, pcatm, mu;

  tr = temp/TCRIT;
  tc = TCRIT;
  pcatm = PCRIT/101325.;

  mu = 6.3e-7*sqrt(MWT)*pow(pcatm,0.6666)/pow(tc,0.16666)
     *(pow(tr,1.5)/(tr+0.8));
```

```
  return mu;
}

/*-----------------------------------------------------------*/
/* FUNCTION: RKEOS_thermal_conductivity                      */
/*-----------------------------------------------------------*/
double RKEOS_thermal_conductivity(double temp, double density,
                                  double yi[])
{
  double cp, mu;

  cp = RKEOS_Cp_ideal_gas(temp);
  mu = RKEOS_viscosity(temp, density, yi);

  return (cp+1.25*rgas)*mu;
}

/* Export Real Gas Functions to Solver */
UDF_EXPORT RGAS_Functions RealGasFunctionList =
{
  RKEOS_Setup,            /* initialize          */
  RKEOS_density,          /* density             */
  RKEOS_enthalpy,         /* enthalpy            */
  RKEOS_entropy,          /* entropy             */
  RKEOS_specific_heat,    /* specific_heat       */
  RKEOS_mw,               /* molecular_weight    */
  RKEOS_speed_of_sound,   /* speed_of_sound      */
  RKEOS_viscosity,        /* viscosity           */
  RKEOS_thermal_conductivity, /* thermal_conductivity */
  RKEOS_rho_t,            /* drho/dT |const p    */
  RKEOS_rho_p,            /* drho/dp |const T    */
  RKEOS_enthalpy_t,       /* dh/dT |const p      */
  RKEOS_enthalpy_p        /* dh/dp |const T      */
};
```

APPENDIX B – ENGINEERING DRAWINGS

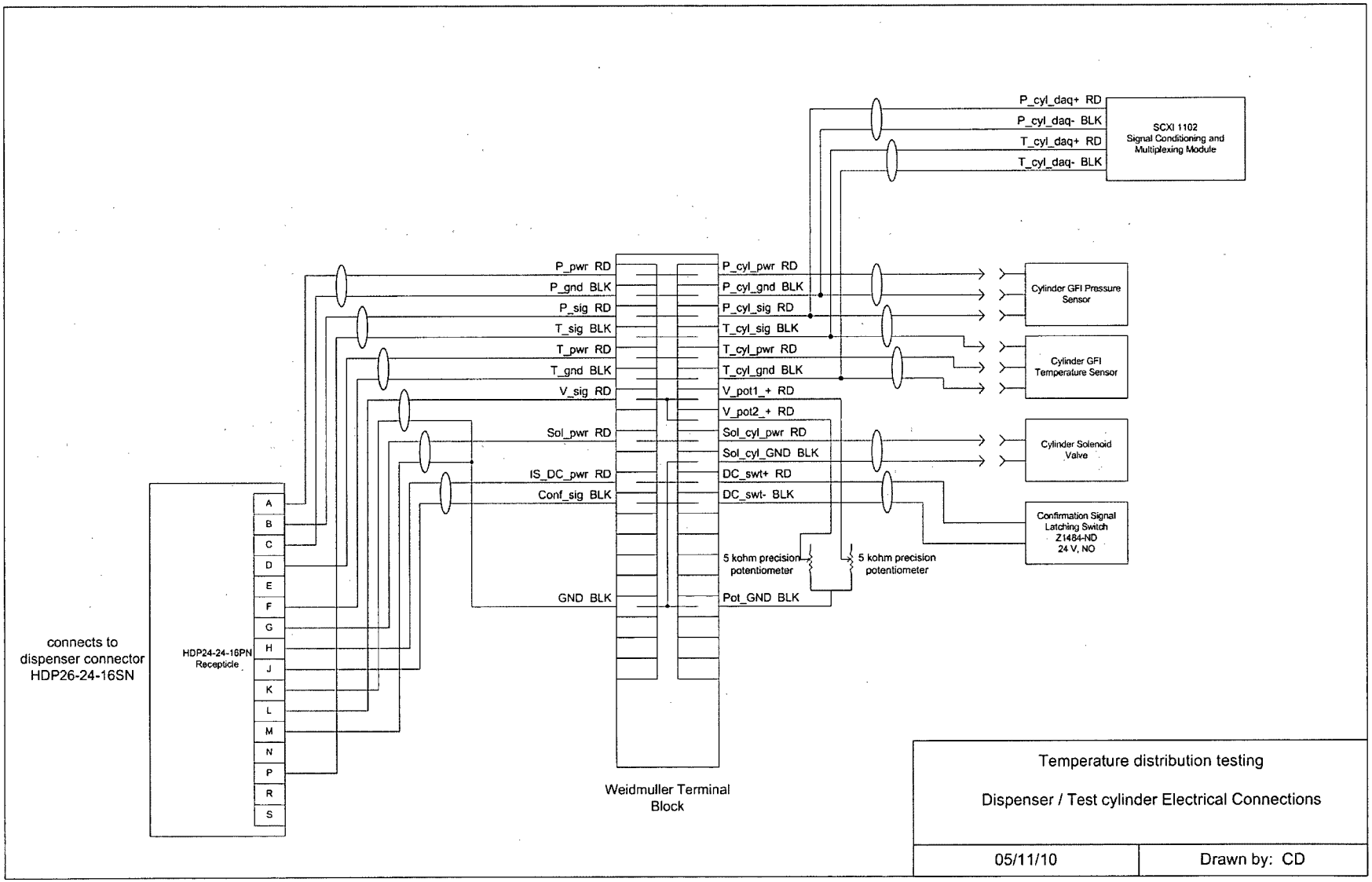
P_cyl_daq+ RD
P_cyl_daq- BLK
T_cyl_daq+ RD
T_cyl_daq- BLK
SCXI 1102
Signal Conditioning and
Multiplexing Module
P_pwr RD
P_gnd BLK
P_sig RD
T_sig BLK
T_pwr RD
T_gnd BLK
V_sig RD
Sol_pwr RD
IS_DC_pwr RD
Conf_sig BLK
GND BLK
P_cyl_pwr RD
P_cyl_gnd BLK
P_cyl_sig RD
T_cyl_sig BLK
T_cyl_pwr RD
T_cyl_gnd BLK
V_pot1_+ RD
V_pot2_+ RD
Sol_cyl_pwr RD
Sol_cyl_GND BLK
DC_swt+ RD
DC_swt- BLK
Pot_GND BLK
Cylinder GFI Pressure Sensor
Cylinder GFI Temperature Sensor
Cylinder Solenoid Valve
Confirmation Signal Latching Switch Z1484-ND 24 V, NO
5 kohm precision potentiometer
5 kohm precision potentiometer
connects to dispenser connector HDP26-24-16SN
HDP24-24-16PN Recepticle
A
B
C
D
E
F
G
H
J
K
L
M
N
P
R
S
Weidmuller Terminal Block
Temperature distribution testing
Dispenser / Test cylinder Electrical Connections
05/11/10
Drawn by: CD

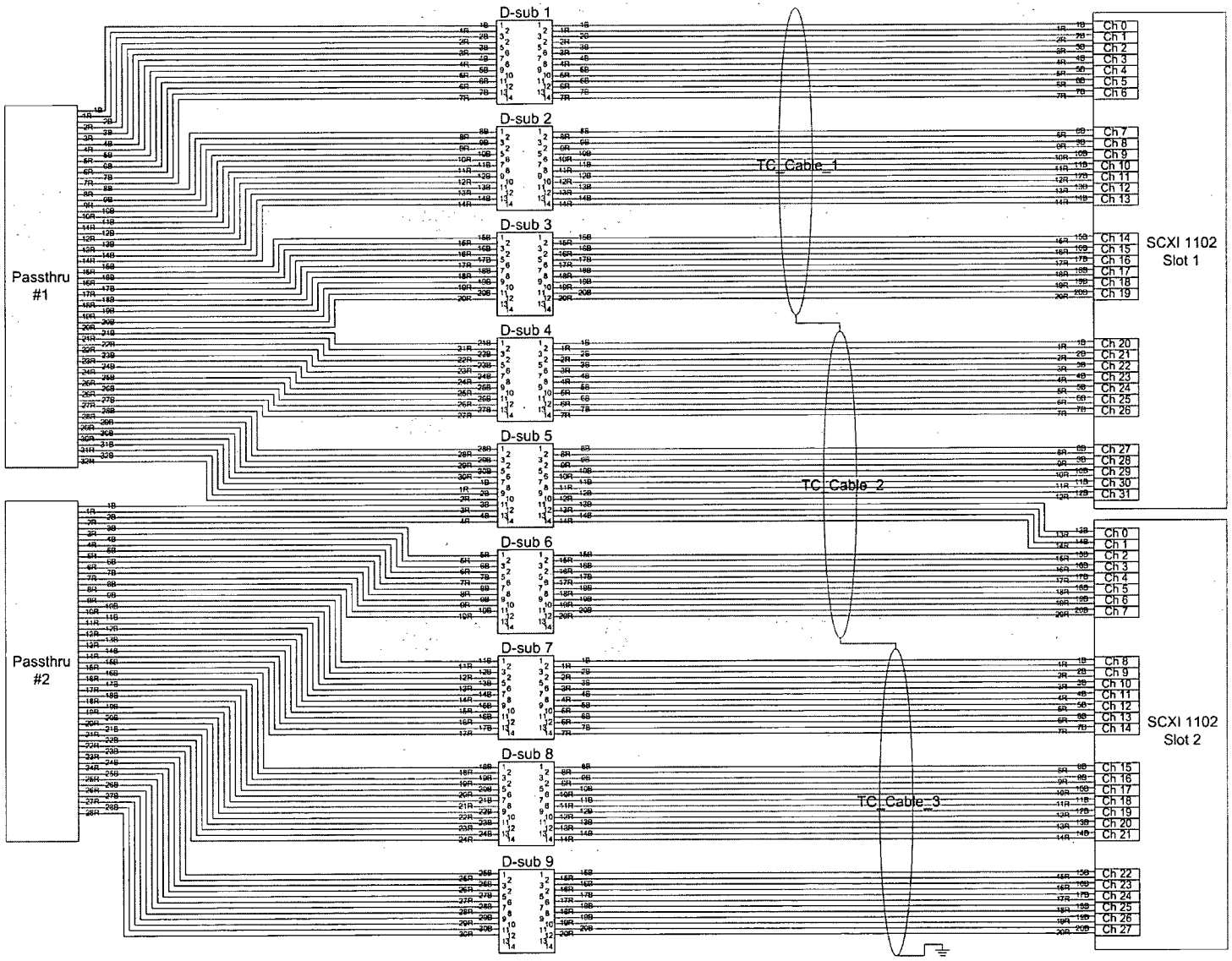
D-sub 1
D-sub 2
D-sub 3
D-sub 4
D-sub 5
D-sub 6
D-sub 7
D-sub 8
D-sub 9
Passthru #1
Passthru #2
TC_Cable_1
TC_Cable_2
TC_Cable_3
SCXI 1102 Slot 1
SCXI 1102 Slot 2
Ch 0
Ch 1
Ch 2
Ch 3
Ch 4
Ch 5
Ch 6
Ch 7
Ch 8
Ch 9
Ch 10
Ch 11
Ch 12
Ch 13
Ch 14
Ch 15
Ch 16
Ch 17
Ch 18
Ch 19
Ch 20
Ch 21
Ch 22
Ch 23
Ch 24
Ch 25
Ch 26
Ch 27
Ch 28
Ch 29
Ch 30
Ch 31

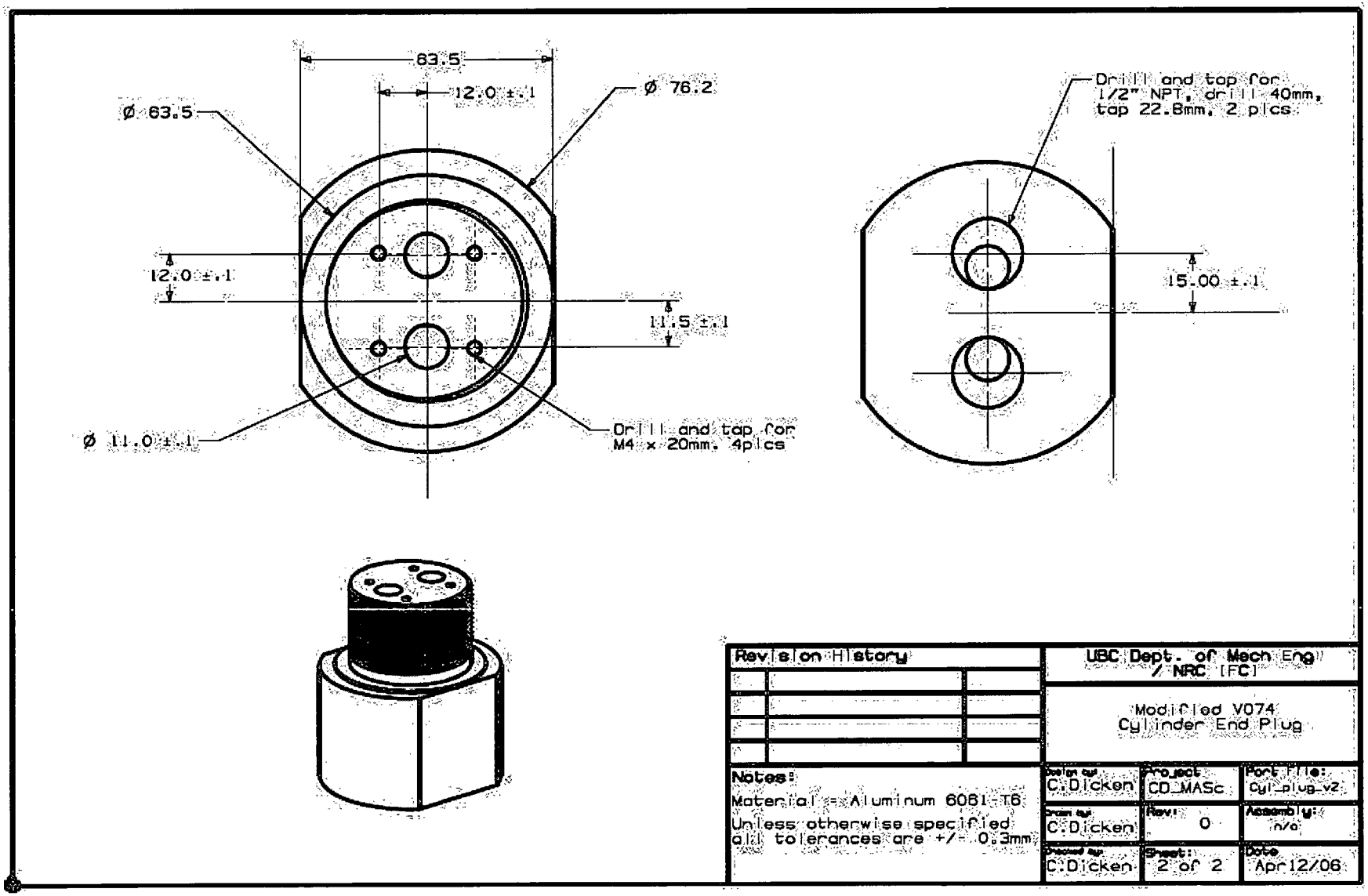
83.5
12.0 ± .1
Ø 63.5
Ø 76.2
12.0 ± .1
11.5 ± .1
Ø 11.0 ± .1
Drill and tap for
M4 x 20mm, 4plcs
Drill and tap for
1/2" NPT, drill 40mm,
tap 22.8mm, 2 plcs
15.00 ± .1
Revision History
UBC Dept. of Mech Eng
/ NRC [FC]
Modified V074
Cylinder End Plug
Notes:
Material = Aluminum 6061-T6
Unless otherwise specified
all tolerances are +/- 0.3mm
Drawn by
C.Dicken
Project
CD_MASc
Part File:
Cyl_plug_v2
Drawn by
C.Dicken
Rev:
0
Assembly:
n/a
Checked by
C.Dicken
Sheet:
2 of 2
Date
Apr12/06

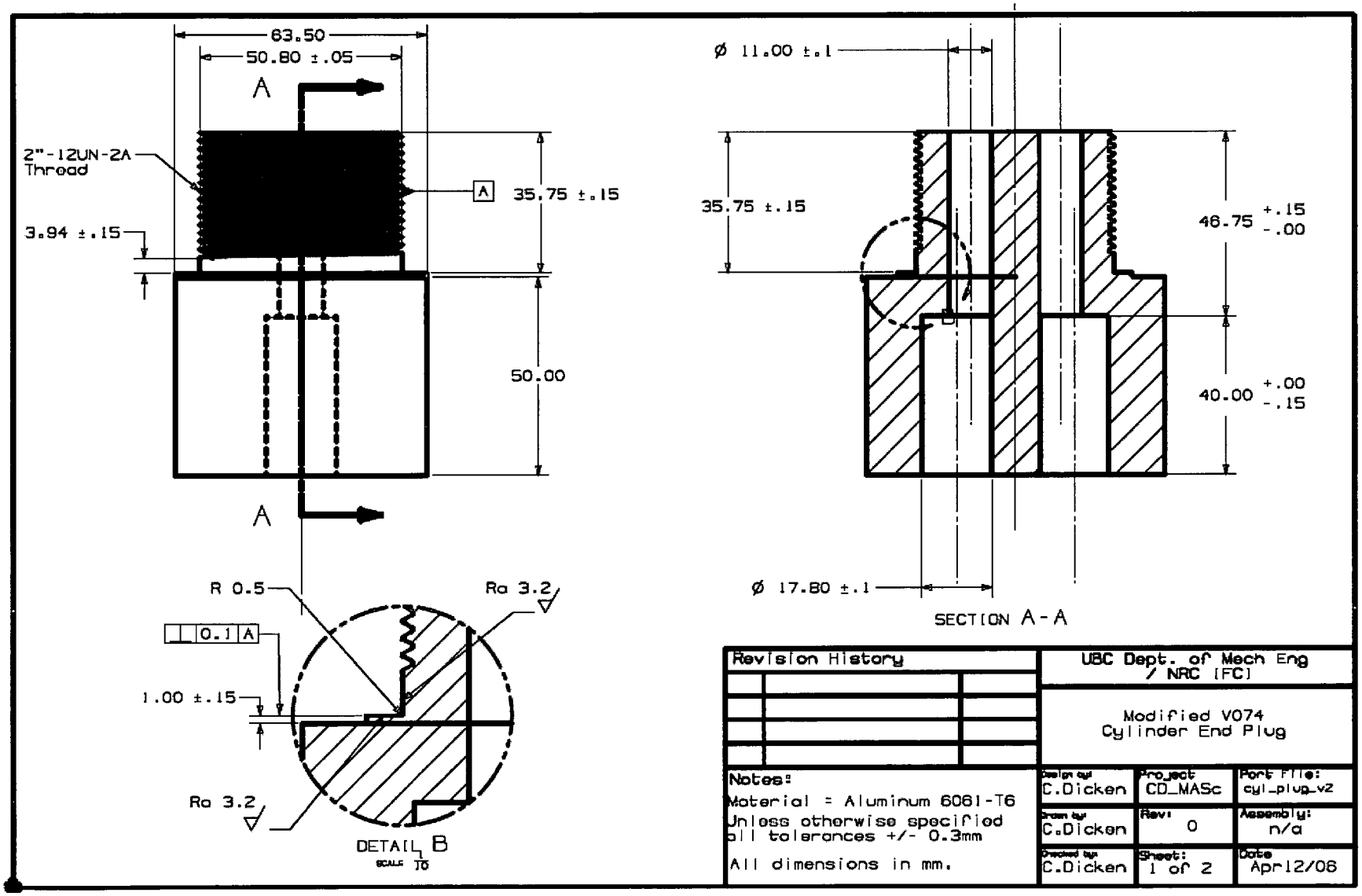
63.50
50.80 ±.05
A
2"-12UN-2A
Thread
A
35.75 ±.15
3.94 ±.15
50.00
A
R 0.5
Ra 3.2
0.1 A
1.00 ±.15
Ra 3.2
DETAIL B
SCALE 10
Ø 11.00 ±.1
35.75 ±.15
46.75 +.15 -.00
40.00 +.00 -.15
Ø 17.80 ±.1
SECTION A-A
Revision History
UBC Dept. of Mech Eng / NRC [FC]
Modified V074
Cylinder End Plug
Notes:
Material = Aluminum 6061-T6
Unless otherwise specified all tolerances +/- 0.3mm
All dimensions in mm.
Design by: C.Dicken
Project: CD_MASc
Part File: cyl_plug_v2
Drawn by: C.Dicken
Rev: 0
Assembly: n/a
Checked by: C.Dicken
Sheet: 1 of 2
Date: Apr12/06